Studies on the Load Range of an HCCI Engine using In-Cylinder Pressure, Ion Current and Optical Diagnostics

Vressner, Andreas

2007

Studies on the Load Range of an HCCI Engine using In-Cylinder Pressure, Ion Current and Optical Diagnostics

Andreas Vressner

Doctoral Thesis

Division of Combustion Engines
Department of Energy Sciences
Faculty of Engineering
Lund University

LUND UNIVERSITY

To my family

ISBN 978-91-628-7333-2
ISRN LUTMDN/TMHP—07/1056—SE
ISSN 0282-1990

Division of Combustion Engines
Department of Energy Sciences
Faculty of Engineering
Lund University
P.O. Box 118
SE-22100 Lund
Sweden

Printed in Sweden by Media-Tryck, Lund, November 2007

List of Papers

Paper 1.
Pressure Oscillations During Rapid HCCI Combustion
SAE Technical Paper 2003-01-3217
By Andreas Vressner, Andreas Lundin, Magnus Christensen, Per Tunestål & Bengt Johansson
Presented by Andreas Vressner at the SAE Powertrain & Fluid Systems Conference & Exhibition, Pittsburgh, PA , USA, October 2003
Approved for SAE Transactions in 2003

Paper 2.
Ion Current Sensing for HCCI Combustion Feedback
SAE Technical Paper 2003-01-3216
By Petter Strandh, Magnus Christensen, Johan Bengtsson, Rolf Johansson, Andreas Vressner, Per Tunestål & Bengt Johansson
Presented by Petter Strandh at the SAE Powertrain & Fluid Systems Conference & Exhibition, Pittsburgh, PA , USA, October 2003

Paper 3.
Multiple Point Ion Current Diagnostics in an HCCI Engine
SAE Technical Paper 2004-01-0934
By Andreas Vressner, Petter Strandh, Anders Hultqvist, Per Tunestål & Bengt Johansson
Presented by Andreas Vressner at the SAE World Congress, Detroit, MI, USA, March 2004
Approved for SAE Transactions in 2004

Paper 4.
Fuel Effects on Ion Current in an HCCI Engine
SAE Technical Paper 2005-01-2093
By Andreas Vressner, Anders Hultqvist, Per Tunestål, Bengt Johansson & Ryo Hasegawa
Presented by Andreas Vressner at the SAE Brasil Fuels & Lubricants Meeting, Rio De Janeiro, Brazil, May 2005
Approved for SAE Transactions in 2005

Paper 5.
Optical Diagnostics of Laser-Induced and Spark Plug-Assisted HCCI Combustion
SAE Technical Paper 2005-01-0129
By Martin Weinrotter, Ernst Wintner, Kurt Iskra and Theo Neger, Jimmy Olofsson, Hans Seyfried, Marcus Aldén, Max Lackner, Franz Winter, Andreas Vressner, Anders Hultqvist & Bengt Johansson
Presented by Martin Weinrotter at the SAE World Congress, Detroit, MI, USA, April 2005
Approved for SAE Transactions in 2005

Paper 6.
Visualization of Laser Assisted HCCI Combustion with Natural Gas as Fuel
Fisita/JSAE Technical Paper F2006P206
By Andreas Vressner, Anders Hultqvist, Bengt Johansson, Martin Weinrotter, Ernst Wintner, Kurt Iskra & Theo Neger
Presented by Andreas Vressner at the FISITA World Automotive Congress, Yokohama, Japan, October 2006

Paper 7.
Study on Combustion Chamber Geometry Effects in an HCCI Engine using High-Speed Cycle-Resolved Chemiluminescence Imaging
SAE Technical Paper 2007-01-0217
By Andreas Vressner, Anders Hultqvist & Bengt Johansson
Presented by Andreas Vressner at the SAE World Congress, Detroit, MI, USA, April 2007.

Paper 8.
High-Speed PLIF Imaging for Investigation of Turbulence Effects on Heat Release Rates in HCCI Combustion
SAE Technical Paper 2007-01-0213
By Hans Seyfried, Jimmy Olofsson, Johan Sjöholm, Mattias Richter, Marcus Aldén, Andreas Vressner, Anders Hultqvist & Bengt Johansson
Presented by Johan Sjöholm at the SAE World Congress, Detroit, MI, USA, April 2007

Paper 9.
Effect of Turbulence on HCCI Combustion
SAE Technical Paper 2007-01-0183
By Rixin Yu, Xue Song Bai, Andreas Vressner, Anders Hultqvist, Bengt Johansson, Hans Seyfried, Jimmy Olofsson, Johan Sjöholm, Mattias Richter & Marcus Aldén
Presented by Andreas Vressner at the SAE World Congress, Detroit, MI, USA, April 2007

Paper 10.
Combustion Chamber Geometry Effects on the Performance of an Ethanol Fueled HCCI Engine
SAE Technical Paper Draft 08SFL-0290
By Andreas Vressner, Rolf Egnell & Bengt Johansson
To be published at the SAE 2008 International Powertrains, Fuels and Lubricants Congress

Other Publications

High-Speed LIF Imaging for Cycle-Resolved Formaldehyde Visualization in HCCI Combustion
SAE Technical Paper 2005-01-0641
By Jimmy Olofsson, Hans Seyfried, Mattias Richter, Marcus Aldén, Andreas Vressner, Anders Hultqvist, Bengt Johansson & Karine Lombaert
Presented by Hans Seyfried at the SAE World Congress, Detroit, MI, USA, April 2005
Approved for SAE Transactions in 2005

Cycle Resolved Wall Temperature Measurements Using Laser Induced Phosphorescence in an HCCI Engine
SAE Technical Paper 2005-01-3870
By Gustaf Särner, Mattias Richter and Marcus Aldén, Andreas Vressner & Bengt Johansson
Presented by Mattias Richter at the Powertrain & Fluid Systems Conference & Exhibition, San Antonio, TX, USA, October 2005

Combustion Chamber Wall Temperature Measurement and Modelling During Transient HCCI Operation
SAE Technical Paper 2005-01-3731
Carl Wilhelmsson, Andreas Vressner, Per Tunestål, Bengt Johansson, Gustaf Särner & Marcus Aldén
Presented by Carl Wilhelmsson at the Powertrain & Fluid Systems Conference & Exhibition, San Antonio, TX, USA, October 2005

NOx and N2O Formation in HCCI Engines
SAE Technical Paper 2005-01-0126
By Per Amnéus, Fabian Mauss, Markus Kraft, Andreas Vressner & Bengt Johansson
Presented by Per Amnéus at the SAE World Congress, Detroit, MI, USA, April 2005

Quantification of the Formaldehyde Emissions from Different HCCI Engines Running on a Range of Fuels
SAE Technical Paper 2005-01-3724
By Mikael Lemel, Anders Hultqvist, Andreas Vressner, Henrik Nordgren, Håkan Persson & Bengt Johansson
Presented by Anders Hultqvist at the Powertrain & Fluid Systems Conference & Exhibition, San Antonio, TX, USA, October 2005

Abstract

Internal combustion engines are continuously developed towards decreased hazardous emissions and lower fuel consumption. The homogeneous charge compression ignition (HCCI) engine is a promising concept which combines the best features of the Diesel engine and the spark ignition (SI) engine. The efficiency is in the range of the Diesel engine and the emissions are low and comparable to the emissions from an SI engine with catalyst. No flame propagation is present in the HCCI engine; instead the whole charge is gradually consumed at several locations simultaneously. The resulting pressure rise rate is therefore high which means that the engine has to be run lean or diluted with burned gases in order not to stress the mechanical parts of the engine or produce excessive noise. Due to the lean and diluted mixtures the combustion temperature is low and fairly uniform. This results in low emissions of NO_x and PM but if the temperature is too low emissions of unburned hydrocarbons and carbon monoxide (CO) increase. Furthermore, the pressure rise rate limits HCCI combustion to low or part load and is therefore to be combined with either Diesel or SI operation at higher loads.

In this thesis different diagnostic methods have been used to study the HCCI combustion process at different engine loads. Combustion diagnostics have been performed using cylinder pressure and ion current measurement as well as optical techniques such as chemiluminescence imaging. By pressure measurement the overall combustion behaviour in the cylinder can be studied. By ion current measurement local conditions in small volumes can be studied. This is of interest since there are differences in temperature and relative air/fuel ratio between different locations in the combustion chamber. Locations with higher temperature or richer mixtures ignite first and this affects the ongoing combustion cycle. Pressure diagnostics is accurate but expensive as feedback method of the ongoing combustion process. Ion current diagnostics is cheap but due to the low temperature nature of HCCI combustion it is only usable at higher engine loads and thus the method is not an option for low load or idle conditions. Different fuels will provoke ion current differently for the selected compression ratio, initial charge temperature, measuring location and relative air/fuel ratio.

If the initial charge temperature is too low, partial or total misfire might occur. At these running conditions spark or laser assistance can be used to increase the charge temperature prior to auto ignition. This advances the combustion phasing, thus minimizing the risk of misfire. This is also interesting for control purposes since it is possible to control the HCCI combustion phasing by changing the spark or laser ignition timing. When running laser assisted HCCI, flame propagation is present from the laser ignition location and, as the pressure and temperature increase, auto ignition occurs. This operation is a mixed mode of flame propagation and auto ignition.

Lastly the effect of combustion chamber geometry on HCCI combustion rate was studied. A square bowl in piston geometry compared to Disc geometry showed the possibility to extend the maximum load limit due to decreased pressure rise rates but at the cost of decreased engine efficiency. Chemiluminescence and LIF imaging as well as LES showed stratified combustion behaviour unusual for HCCI operation which normally is a more homogeneously distributed combustion process.

Acknowledgement

There are many people I would like to thank for helping me accomplish this work. It is not possible to include all of them here but none are forgotten.

Firstly I would like to thank my financial sponsors in the Centre of Competence for Combustion Processes (KCFP) in Sweden. Numerous companies are members of this centre as well as governmental agencies. Thanks for my salary! The first person to mention is my head supervisor, professor *Bengt Johansson*, who has supported me through my entire time at the combustion engine division giving me numerous ideas on problem solving and suggestions for future work. I would also like to thank my co-supervisors *Anders Hultqvist* and *Rolf Egnell* for long hours of proofreading papers. Special thanks are required for associate professor *Per Tunestål,* the signal processing and statistical expert. I will never forget your contributions.

None of this work would be possible without the talented technicians at the department. *Bertil Andersson* has helped me putting the engine together again after numerous breakdowns including sweeping broken quartz glass of the floor in the laboratory. Your achievements are astonishing! *Tom Hademark* has helped me when the time was already up, a fast man so to say. *Kjell Jonholm* has provided me with shiny parts. *Bert Berglund* has helped installing the new engine which I will never have time to run. Electrician *Tommy Pedersen* has been keeping the power up in the laboratory. *Jan-Erik Everitt* has kept the emissions systems from hell alive at all times. *Krister Olsson* also deserves a special thank you for keeping all five computers in the control room running.

My previous and present office mates also deserve a special thank you. My old office mates who are now finished PhDs, *Göran Haraldsson* and *Jari Hyvönen*, have taught me a lot regarding scientific work and how to combine family life with PhD studies. I would like to thank *Petter Strandh* for helping me with the initial ion current measurements. The new guys *Sasa Trajkovic*, *Vittorio Manente*, *Hans Aulin* and *Thomas Johansson* have together with *Magnus Lewander, Mehrzad Kaiadi* and *Claes-Göran Zander* contributed to a good atmosphere, nice company with many laughters and interesting discussions. I would like to thank *Sasa* for all the help with the puffing, leaking whining non-working… yeah, you know what I mean. *Vittorio,* the worlds fastest Italian, you amaze me with your stories but I never get tired listening to them. *Hans*, thank you for the ride in the ever so cool Lotus. *Thomas* does not own a single item which he has not tuned in some way. Thanks for all the interesting discussions on racing engines and ideas on new tuning projects, I hope to get one of them cranking soon! *Magnus Lewander* has taught me the important differences between DVD and Blue-Ray technology. *Mehrzad*, you just simply make me laugh! *Claes-Göran* is a tough bastard, not letting me know all the secrets of Scania, but you are a good guy anyway. I would like to thank *Magnus Andersson* for improving my English language and nice company in Rio de Janeiro. Can you imagine a better place to present a paper?! *Carl Wilhelmsson* and *Håkan Persson* deserve a special thank you. You are nice friends and we share a lot of memories from conference trips and other things. I would like to thank, *Carl* for introducing me into the world of performance motorcycles and Japanese culture, *Håkan* for long discussions on optical diagnostics and of course, BMW engine tuning. *Leif* I would like to thank for providing me with high quantities of quartz glass and for arranging those nice after work events at the pub. *Uwe Horn* has taught me how to consume fuel rapidly when you need it the most like on a bridge between Detroit and Windsor... *Kent Ekholm*, *Ulf Aronsson* and *Clement Chartier* turned out to be really good at drinking beer. I would also like to welcome our newest PhD students, *Helena Persson, Noriyuki Takada* and *Patrick Borgqvist* to the division.

The collaboration with the combustion physics department at Lund Institute of Technology has been very fruitful. The people I have been working with are first and foremost *Jimmy Olofsson* and *Hans Seyfried*. We have been throwing curses at the experimental equipment and tearing our hair but it has been a great time. Thank you! *Johan Sjöholm* and *Gustaf Särner* have also been involved in the special work regarding optical engine diagnostics.

My Austrian mates *Martin Weinrotter*, *Kurt Iskra* and *Max Lackner* have been visiting us for a total of three months conducting the laser ignition experiments. It was great fun! I hope to visit you in Austria some time in the future!

Professor *Xue Song Bai* at the fluid dynamics department I would like to thank for explaining to me the ever so complex but intriguing world of turbulent combustion. *Rixin Yu* I would like to thank for providing me with nice colour plots. The collaboration has been interesting and fruitful.

Lastly but not least I would like to thank my family, parents and parents in law, my wife *Sofie* and my children *Joakim* and *Mina* for putting up with me during the long working ours finishing experiments, papers and theses. You are the inspiration of my life!

Nomenclature

ABDC	After Bottom Dead Centre
A/D	Analog to Digital
AFR	Air/Fuel Ratio
ATAC	Active Thermo-Atmosphere Combustion
ATDC	After Top Dead Centre
B	Cylinder Bore
BBDC	Before Bottom Dead Centre
BDC	Bottom Dead Centre
BMEP	Brake Mean Effective Pressure
BTDC	Before Top Dead Centre
C	Speed of Sound
C_{pt}	Pressure Transducer Sensitivity Compensation
C_p	Specific Heat at Constant Pressure
C_v	Specific Heat at Constant Volume
CA2	Crank Angle for 2% Burned Mass Fraction
CA10	Crank Angle for 10% Burned Mass Fraction
CA50	Crank Angle for 50% Burned Mass Fraction
CA90	Crank Angle for 90% Burned Mass Fraction
CAD	Crank Angle Degree
CAI	Controlled Auto-Ignition
CCD	Charge-Coupled Device (Image Sensor)
CFD	Computational Fluid Dynamics
CI	Compression Ignition (Diesel Cycle)
CIHC	Compression-Ignited Homogeneous Charge
CLD	Chemiluminescence Detector
CO	Carbon Monoxide
CO_2	Carbon Dioxide
COV	Coefficient of Variation
CR	Compression Ratio
DC	Direct Current
DI	Direct Injection
dQ	Heat Release Derivative
dP	Pressure Derivative
EGR	Exhaust Gas Recirculation
EVC	Exhaust Valve Closing
EVO	Exhaust Valve Opening
FEM	Finite Element Method
FID	Flame Ionization Detector
FTM	Fast Thermal Management
FuelMEP	Fuel Mean Effective Pressure
GDI	Gasoline Direct Injection
h	Heat Transfer Coefficient
HC	Hydrocarbon (Unburned)
HCCI	Homogeneous Charge Compression Ignition
HCDC	Homogeneous Charge Diesel Combustion
HR	Heat Release
HS	High Swirl
HTR	High Temperature Reactions

IMEP	Indicated Mean Effective Pressure
$IMEP_{gross}$	IMEP calculated over the compression and expansion strokes only
$IMEP_{net}$	IMEP calculated over the entire cycle
Ion50	Crank angle for 50% of maximum ion current amplitude.
ISHR	Initial Slow Heat Release
IVC	Inlet Valve Closing
IVO	Inlet Valve Opening
KHz	Kilo Hertz
l	Connecting Rod Length
LDV	Laser Doppler Velocimetry
LES	Large Eddy Simulations
LIF	Laser Induced Fluorescence
LIP	Laser Induced Phosphorescence
LS	Low Swirl
LTC	Low Temperature Combustion
LTR	Low Temperature Reactions
MHz	Mega Hertz
MK	Modulated Kinetics
MU	Mechanical Unit
N_2	Nitrogen
NA	Naturally Aspirated
NDIR	Non Dispersive Infrared Analyzer
NO	Nitrogen Oxide
NO_x	Nitrogen Oxides
NVO	Negative Valve Overlap
O_2	Oxygen
O_3	Ozone
P	Pressure
PAH	Polycyclic Aromatic Hydrocarbon
pC	Pico Coulomb
PCCI	Premixed Controlled Compression Ignition
PCI	Premixed Compression – Ignited
P_{in}	Inlet Manifold Pressure
PLIF	Planar Laser Induced Fluorescence
PM	Particulate Matter
PPC	Partially Premixed Combustion
PREDIC	PREmixed lean DIesel Combustion
PRF35	Primary Reference Fuel with octane number 35
PRF50	Primary Reference Fuel with octane number 50
PRF80	Primary Reference Fuel with octane number 80
PSD	Power Spectral Density
Q_{lhv}	Lower Heating Value of Fuel
Q_{hr}	Heat Release
QHTMEP	Heat Transfer Mean Effective Pressure
QMEP	Heat Release Mean Effective Pressure
RANS	Reynolds Averaged Navier Stokes
ROHR	Rate of Heat Release
RPM	Revolutions per Minute
S	Stroke
S_{ca}	Charge Amplifier Scale

S_p	Mean Piston Speed
SAE	Society of Automotive Engineers
SCR	Selective Catalytic Reduction
SI	Spark Ignition
SO_2	Sulphur Dioxide
SOC	Start of Combustion
SOI	Start of Injection
Std	Standard Deviation
T	Temperature
T_{ca}	Charge Amplifier Sensitivity Compensation
T_{in}	Inlet manifold Temperature
TDC	Top Dead Centre
TS	Toyota-Soken (Combustion Concept)
U	Internal Energy
u	Internal Energy per unit Mass
UNIBUS	Uniform Bulky Combustion System
V	Volume
V_c	Compression Volume
V_d	Displaced Volume
VOC	Volatile Organic Compound
VVT	Variable Valve Timing
VVA	Variable Valve Actuation
w	Characteristic Velocity
W_{ig}	Indicated Work calculated over the compression and expansion strokes only
γ	Ratio of Specific Heats
Φ	Fuel/Air Equivalence Ratio
λ	Relative Air/Fuel Ratio = 1/ Φ
η_{ig}	Gross Indicated Efficiency
$\eta_{i,net}$	Net Indicated Efficiency
η_T	Thermal Efficiency

1 Introduction....1
1.1 Background 1
1.2 Objective 2
1.3 Method....3
2 Internal Combustion Engine Concepts 4
2.1 The Working Principle 4
2.2 The Spark Ignition Engine....5
2.3 The Compression Ignition Engine....5
2.4 The HCCI Engine 6
2.4.1 HCCI History 7
2.4.2 HCCI Concepts 7
2.4.3 Boosting.... 10
2.4.4 Geometry Effects on HCCI Combustion Rate 12
3 Experimental Apparatus 16
3.1 Test Engines....16
3.1.1 The Volvo TD100 HCCI Engine.... 16
3.1.2 The Scania D12 HCCI Engine 17
3.1.3 Optical Access.... 19
3.1.4 Intake Air Preheating.... 20
3.1.5 Exhaust Gas Recirculation 21
3.1.6 Fuel Injection 21
3.1.7 Variable Valve Actuation.... 21
3.1.8 Laser Ignition.... 23
3.2 Test cell....23
3.2.1 Dynamometer.... 23
3.2.2 Data Acquisition 24

3.2.3 Emissions Measurements 24
3.2.4 In-Cylinder Pressure Measurements 24
4 Diagnostic Methods 26
4.1 Pressure Diagnostics.....26
4.1.1 Heat Release 26
4.1.2 Other Definitions based on Pressure Measurements 33
4.1.3 Knock in SI Engines 34
4.1.4 Acoustic Vibration Theory 35
4.2 Ion Current Diagnostics.....38
4.2.1 Why use Ion Current? 38
4.2.2 Ion Current Theory 38
4.2.3 Ion Current with HCCI Combustion 40
4.2.4 Measurement Technique 41
4.3 Chemiluminescence Imaging.....41
4.4 Planar Laser Induced Fluorescence (PLIF) Imaging.....42
5 Results.....43
5.1 HCCI Knock.....43
5.1.1 Frequency domain..... 46
5.1.2 The effect of Combustion Chamber Geometry 47
5.2 Ion Current in HCCI Combustion.....49
5.2.1 Effect of Sensor Location on Ion Current 49
5.2.2 Fuel Effects on Ion Current..... 53
5.3 Visualization of Spark Assisted HCCI combustion.....56
5.4. Visualization of Laser Assisted HCCI Combustion 57
5.4.1 Laser Assisted HCCI Combustion with PRF80 as Fuel..... 57
5.4.2 Laser Assisted HCCI Combustion with Natural Gas as Fuel..... 59

5.5 Combustion Chamber Geometry Effects on HCCI Operation..... 63

5.5.1. Chemiluminescence Imaging 64

5.5.2. Laser Induced Fluorescence 69

5.5.3. Large Eddy Simulations..... 71

5.5.4. Metal Engine Experiments..... 75

5.5.5 Discussion on Combustion Chamber Geometry Effects on HCCI Operation 83

6 Summary and Conclusions 85

7 Future Work 87

8 References 88

9 Summary of Papers.....95

1 Introduction

Internal combustion engines have been developed extensively over the last decades. The power density has increased, the fuel mileage has increased slightly while the emissions from spark ignition (SI) engines have decreased almost two orders of magnitude since the three-way catalyst was introduced. In the last decade alternative non-fossil fuels have reached the market, to eventually replace the fossil fuels such as diesel and gasoline which will be limited in supply in the future [1]. Another goal has been to reduce the emissions, especially of carbon dioxide mainly through increased efficiency and thus decreased fuel consumption of engines, to minimize the pollution of the environment.

The Homogeneous Charge Compression Ignition (HCCI) engine is a promising concept for achieving high efficiency in combination with low emissions. Another good feature of the HCCI engine is the possibility to run the engine with a range of fuels, fossil as well as non-fossil.

1.1 Background

In a perfect combustion process fuel and air is consumed by chemical reactions to form carbon dioxide (CO_2) and water (H_2O). The combustion processes in internal combustion engines are however far from perfect which results in the production of other hazardous emissions. These are mainly carbon monoxide (CO), nitrogen oxides (NO_x), particulate matter (PM) and unburned hydrocarbons (UHC) which are all regulated by emissions legislations. CO_2 is not yet subject to legislation but will be in the future since it is a greenhouse gas and contributes to global warming [2, 3]. Other substances that are not legislated might occur in the exhaust from engines. Examples are volatile organic compounds (VOCs), sulphur dioxide (SO_2) and ozone (O_3).

Carbon monoxide (CO) is toxic to humans since it prevents absorption of oxygen (O_2) in the blood. CO is emitted from internal combustion engines as a result of fuel rich combustion when there is a lack of oxygen to completely oxidize CO to CO_2. This is also the case when the combustion temperature is too low which reduces the oxidation reaction rates.

Nitrogen oxides (NO_x) is a term used for the emissions of NO and NO_2. NO_x emissions are toxic to humans and affect the nature in the form of acid rain and photochemical smog [4]. There are three sources of NO_x from internal combustion engines:

- Thermal NO_x
  The NO from this source is formed due to oxidation of nitrogen (N_2) at elevated temperatures. The process can be described by the extended *Zeldovich* mechanism [5] and the formation rate depends exponentially on temperature. The key factors that play a role in the amounts of thermal NO_x produced is the combustion temperature, residence time at high temperature and the concentrations of O_2 and N_2. Thermal NO_x is usually the major contributor to NO_x emissions from internal combustion engines.
- Prompt NO_x
  This source of NO_x is produced during fast reactions in fuel rich flames and through intermediate N_2O reactions. At low combustion temperatures like in HCCI engines at low load this path for NOx production has been found to be significant [6].

- Fuel NO_x
  NO_x can also be produced from the chemically bonded nitrogen in the fuel. Usually very small concentrations of nitrogen are present in the fuel and therefore this type of NO_x production path is of minor importance.

Particulate Matter (PM) is formed in internal combustion engines at locally fuel rich conditions with high enough temperature and is common in Diesel engines and direct injected (DI) gasoline engines. PM contains unburned fuel and polycyclic aromatic hydrocarbons (PAHs) which are harmful to humans since they are carcinogenic. They are easily inhaled into the lungs due to their small size and cause damage to the lung tissues and respiratory tract. [4]

Unburned Hydrocarbons (UHC) are emitted from internal combustion engines due to incomplete combustion at low temperature. The reasons for the incomplete combustion can be fuel trapped in crevices, hydrocarbons absorbed by the lubrication oil, bulk quenching and wall quenching. UHC is also a form of VOC together with halocarbons and oxygenates. Most VOCs are carcinogenic, irritating to eyes and respiratory tract. Oxygenates contribute to the formation of photochemical smog. [4]

Sulphur Dioxide (SO_2) emissions are the main source for acid rain but are also irritating to the respiratory tract of humans [4]. SO_2 is formed during combustion from the sulphur present in the fuel. The sulphur concentration in fuels has decreased substantially the last decades but is still present in the heavy fuel oil used in ship engines.

Ozone is formed in photochemical reactions of VOCs and NO_x in the atmosphere during exposure to sunlight and is hazardous to the lung tissue and respiratory tract [4]. By decreasing the VOCs and NO_x emissions from combustion engines Ozone is also reduced.

The extent to which these hazardous emissions are formed in combustion engines depends highly on the technology and fuel used and will be described in the section on internal combustion engines. After treatment systems have been developed the last decades starting with the 2-way catalyst for gasoline vehicles introduced in California, USA, in 1975 [7]. Oxidation catalysts, selective catalytic reduction (SCR) and diesel particulate filters are nowadays widely used in Diesel vehicles to reduce NO_x and PM.

1.2 Objective

This thesis is based on a research project that started in 1997 within the competence centre for combustion processes at Lund University. The objective of the project is to study the nature of HCCI combustion which was and still is a promising concept for achieving high efficiency and low emissions in internal combustion engines. In the first years of the project the goal was to investigate the combustion process in terms of efficiency, load range and emissions for different running conditions, fuels and hardware modifications. Later, deeper understanding of HCCI combustion was needed since it was discovered that the combustion process was not as homogeneous as it first seemed to be. Therefore experiments were performed in optical engines to increase the knowledge about local combustion phenomena.

As the knowledge about HCCI combustion has increased over recent years new ideas and findings have extended the research area. The engines are modified and operated differently to solve the problems associated with HCCI such as the limited load range and the control issues. Two different paths for running HCCI engines have been developed, a hybrid close to

the Diesel engine and a hybrid close to the (SI) engine. In this research mainly “pure” HCCI combustion has been studied, but a detour into the world of the hybrid SI – HCCI engine has also been covered. The objective of this work has been to compare local and global combustion phenomena throughout the engine load range using different diagnostic tools as such as in-cylinder pressure measurement, ion current sensing and optical diagnostics.

1.3 Method

The work presented in this thesis is mainly of experimental nature. Different diagnostic techniques have been used to study the combustion process in two single cylinder HCCI engines. The diagnostic techniques are both of a global nature, such as in-cylinder pressure measurements, and local nature, such as two-dimensional chemiluminescence imaging and ion current sensing.

2 Internal Combustion Engine Concepts

In this section different four-stroke internal combustion engine concepts are described, the spark ignition, the Diesel and the HCCI engine. The Diesel and the SI engines are just described briefly while the main focus is on the HCCI engine.

2.1 The Working Principle

SI, Diesel and HCCI engines can be both of two- and four-stroke types. The engines discussed in this thesis work according to the four-stroke principle. Therefore the focus in this section will be on four-stroke engines. There are differences between the three engine types regarding fuel preparation and ignition but the working principle is the same. The four-stroke cycle in an SI engine can be seen in Figure 1, where the piston and valve movement during the intake (a), compression (b), expansion (c), and exhaust (d) strokes are shown.

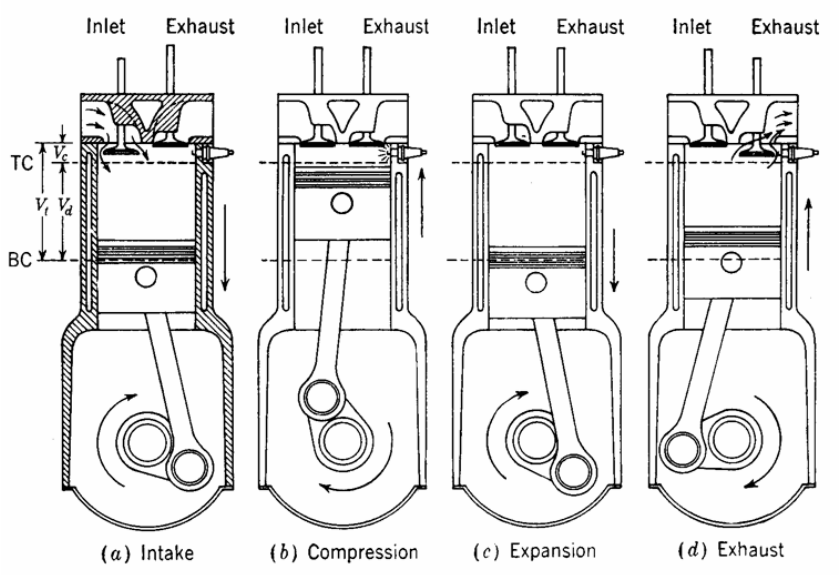

Figure 1: The four-stroke cycle in an SI engine [5].

During the intake stroke, the air and fuel is induced into the engine through the open intake valves as the piston moves towards its lower position, bottom dead centre (BDC).

In the compression stroke both intake and exhaust valves are closed and the charge is compressed as the piston moves towards its upper position, top dead centre (TDC).

Close to TDC the air/fuel mixture is ignited, differently depending on combustion principle. The combustion process usually occurs in the last part of the compression stroke and continues some time into the expansion stroke.

During the expansion stroke the gases, burned or unburned are expanded and work is produced.

In the exhaust stroke, the exhaust valves are open and the piston pushes the burned gases out from the cylinder. The four strokes described are repeated continuously as long as the engine is running.

2.2 The Spark Ignition Engine

In port fuel injected (PFI) SI engines, fuel and air are mixed in the intake manifold. The air/fuel mixture is then induced into the cylinder during the intake stroke. As the fuel is mixed with air, the fuel is atomized, vaporized and mixed with the air creating a fairly homogeneous charge. The charge is compressed during the compression stroke. Close to TDC the charge is ignited by a spark discharge, creating a turbulent flame which propagates through the combustion chamber, until it reaches the walls where it is quenched.

The load of the engine is controlled by throttling of the intake air, changing the flow rate of air into the engine. The mixture is kept close to stoichiometric proportions at all loads, which results in high output power. At stoichiometric mixture proportions, just enough air is supplied to combust all the fuel, neither more nor less. At part load, throttling of the air is necessary and leads to increased pumping losses since the engine has to produce work in order to induct the air/fuel mixture into the cylinder. This results in decreased part-load efficiency for the SI engine. The efficiency directly affects the fuel consumption, which results in higher carbon dioxide (CO_2) emissions. The positive side of SI engines is the use of 3-way catalysts, which decrease the emissions of carbon monoxide (CO), nitrogen oxides (NO_x) and unburned hydrocarbons substantially.

An alternative to PFI SI engines is direct injection (DI) SI engines where pure air is inducted into the cylinder and the fuel is introduced directly into the cylinder. The closer the injection timing is to TDC the more heterogeneous the charge will be. The charge is ignited by a spark plug. The advantage with this type of fuel injection is the temperature decrease of the charge in the cylinder due to vaporization of the fuel. A charge with a lower temperature is less prone to knock, which makes it possible to use a higher compression ratio (CR) which in turn increases the efficiency. At low loads the engine runs unthrottled and the power output is controlled by the amount of fuel injected into the cylinder. This leads to less pumping losses and thus higher efficiency. The down sides are emissions of particulate matter when injecting the fuel close to TDC resulting in diffusive combustion with locally rich zones and wall wetting with fuel which results in unburned hydrocarbons.

SI engines are mostly used in passenger cars due to high power density and low emissions, but with the penalty of high fuel consumption.

2.3 The Compression Ignition Engine

Compression ignition (CI) engines, or more commonly called Diesel engines, are direct injected. Air is induced into the cylinder during the intake stroke and then compressed during the compression stroke. The fuel is injected close to TDC and due to the high compression ratio of the engine and thereby high air temperature the fuel is atomized, ignited and combusted in a diffusive flame as long as fuel is injected.

Since the engine runs un-throttled the load is controlled by the amount of injected fuel. The engine is run globally lean and therefore the power density is limited, but with the use of turbo charging the power output can be increased. The downside with the CI engine is that the diffusive combustion causes increased emissions of NO_x and particulate matter. Lately, after treatment systems with filters have been introduced to reduce the particulate emissions from the CI engines. Also NO_x traps and selective catalytic reduction (SCR) catalysts have been used to decrease the emissions of NO_x. The unthrottled operation results in less pumping

losses and in combination with high compression ratio the CI engine has high efficiency and therefore low fuel consumption and lower emissions of CO_2.

CI engine equipped passenger cars are increasing in numbers due to low fuel consumption, improved power output and increasing fuel prizes. In trucks the CI engine has been the only alternative for a long time due to low fuel consumption and long maintenance intervals, but SI engines running lean on gaseous fuels are getting more and more popular in buses and distribution vehicles.

2.4 The HCCI Engine

As seen in the previous sections the trade off is between emissions and efficiency in the choice of internal combustion engines. A third alternative is Homogeneous Charge Compression Ignition (HCCI), which is rather a combustion process than an engine type, since it is known to combine the features of the SI and CI engines. The HCCI engine runs premixed by the use of PFI or very early DI so that the fuel and air has time to mix. During the compression the pressure and thus temperature is increased until auto ignition occurs. The charge is ignited at several locations simultaneously in the combustion chamber where the temperature is the highest or the mixture the richest and therefore more favourable for chemical reactions to occur [8]. The heat release is locally slow but globally fast compared to the SI and CI engines, which means that the fuel is gradually oxidized, almost simultaneously throughout the charge, making the chemical kinetics the limiting factor of the combustion process [9].

As the combustion rate is high, diluted mixtures are needed in order to keep the pressure rise rates at acceptable levels. This means that the power density is low. Diluents can be air, exhaust gas recirculation (EGR) or trapped residuals, i.e. burned gases. The diluted mixture also keeps the combustion temperature down suppressing NO_x formation. The downside with low temperature combustion is that sometimes the fuel is not entirely oxidized causing increased emissions of CO and UHC [10]. Since the charge is fairly homogeneous, less particulate matter is formed. The HCCI engine runs unthrottled like the CI engine and therefore the pumping losses are reduced compared to the SI engine. In combination with high CR to reach auto ignition and fast combustion close to TDC this results in decent efficiency, similar to the CI engine [10].

The HCCI engine beats the SI engine in terms of efficiency and the CI engine in terms of emissions. The higher emissions of CO and HC could be fixed with an oxidation catalyst but the low power density is still a problem. This limits HCCI to a combustion concept instead of being an engine type. Furthermore, controlling the ignition timing is an issue since it is only governed by the temperature, pressure history and composition of the charge during compression. Pressure measurement can be used to globally follow the combustion progress but the method is expensive and to date limited to lab use. Other methods such as ion current sensing are investigated in this thesis and seem promising.

When information on the ongoing HCCI combustion is at hand, different methods for controlling the ignition timing can be used. One is controlling the temperature of the intake air [10-12, Paper 1-10], another is variable compression ratio [13]. A third is injecting different mixture fractions of two fuels with different ignition properties [14]. A fourth is variable valve timing (VVT) where negative valve overlap (NVO), i.e. early exhaust valve closing

(EVC) in combination with late inlet valve opening (IVO), is used to trap hot residuals that work both as diluents and heat sources [15].

2.4.1 HCCI History

The first HCCI study reported in literature was presented by *Onishi* et al. [16] in 1979. He achieved auto ignition at part load in a 2-stroke SI engine by throttling of the exhaust, resulting in increased amounts of trapped residuals. The engine out emissions of unburned hydrocarbons were thereby decreased. The authors called the concept ATAC which is an abbreviation for Active Thermo-Atmosphere Combustion. In the same year *Noguchi* et al. [17] presented similar results with decreased fuel consumption and decreased emissions of unburned hydrocarbons. The engine was of a 2-stroke opposed piston type and the concept was called Toyota-Soken (TS) combustion.

The first 4-stroke HCCI experiments were presented by *Najt* and *Foster* in 1983 [18]. They used inlet air preheating and EGR to control auto ignition of the charge and called it Compression-Ignited Homogeneous Charge (CIHC) combustion. It was not until 1989 that the combustion process was called HCCI by *R.H. Thring* [19].

2.4.2 HCCI Concepts

There are several ways of controlling the combustion phasing in an HCCI engine. In most of the work presented here inlet air preheating has been used, but other methods such as Controlled Auto Ignition (CAI) combustion with different amounts of trapped hot residuals can also be used. In the case of inlet air preheating it is possible to run the HCCI engine close to idle since the inlet temperature can be adjusted between room temperature and maybe 200 °C. Due to the compression of the charge the resulting temperature range at TDC is large. The downside with inlet air preheating using an electrical heater is that the method is slow which makes load transients difficult and therefore it is not feasible in a production engine. A faster way of heating the intake air is to use the exhaust heat in a heat exchanger. The method is called fast thermal management (FTM) [11, 12]. An even faster and more reliable way is the NVO strategy, where valve timings can be adjusted from cycle to cycle with resulting change in trapped residuals and charge temperature at TDC. The drawback with this method is that the minimum load is limited due to the low temperature achieved. Since the method is based on hot residuals, lower load will result in lower temperature of the burned gases which means that the amount of residuals has to be increased. Since the combustion rate decreases with increment of burned gases due to higher ratio of specific heats, eventually this will lead to misfire.

The basic HCCI concept, where a homogeneous premixed charge is inducted into the engine and compression ignited close to TDC, has a limited load range compared to an SI or CI engine. At high load the pressure rise rate is high, limiting further load increase due to excessive noise and knock. This not only decreases efficiency but can also cause damage to engine hardware. Therefore HCCI combustion is nowadays more known as a combustion mode in a CI or SI engine. In the SI case, HCCI combustion is used at low load and when higher power is needed, the engine runs as a normal SI engine. The same thing is adapted to CI engines; HCCI is run at low load to achieve a more premixed charge which suppresses NO_x and particulate formation and diffusive CI is run at higher load.

2.4.2.1 Partially Premixed Combustion (PPC)

In the CI engine the intermediate HCCI concept is known as partially premixed combustion (PPC). When running the engine in PPC mode the ignition delay depends on the injection timing and if the ignition delay is long enough, thus creating a more premixed charge, the emissions are closer to HCCI than to the CI engine [20]. Many different strategies can be adopted to reach some sort of PPC combustion and a few examples of how this is achieved will now be mentioned:

- Exhaust Gas Recirculation (EGR) can be used to decrease the temperature of the charge. When the fuel is injected close to TDC the lower temperature and the higher specific heat of the gases cause an increase in the ignition delay so that the fuel, air and burned gases have time to mix. This results in decreased NOx emissions and less PM. The downside is the low temperature decreasing the combustion efficiency due to increasing emissions of UHC and CO. Compared to HCCI, PPC offers better control since the combustion phasing is controlled by the injection timing of the fuel [20, 21]. Nissan MK is a concept using EGR where MK is an abbreviation for Modulated Kinetics [22]. In this DI Diesel engine all the fuel is injected close to TDC and with high amounts of swirl the fuel and air mix during the ignition delay time.

- Combined PFI and DI can be used to induce a premixed lean charge of air and gasoline or natural gas from the intake system and ignite it with a DI diesel spray close to TDC. The concept is called Homogeneous Charge Diesel Combustion (HCDC) [23, 24]. The NO_x emissions from this type of engine are directly related to the amount of diesel fuel injected. This strategy is also called fumigation.

- Split injection has been adopted by Toyota in the part-load regime of a production Diesel engine. The concept is called UNIBUS which is an abbreviation for Uniform Bulky Combustion System [25, 26]. One early injection is used to start the low temperature reactions (LTR) and an injection close to TDC is used to control the ignition of the remaining combustion.

- Another type is when all the fuel is injected early in the compression stroke creating a stratified charge which is ignited by compression at TDC and is called PREmixed lean DIesel Combustion (PREDIC) [27] or Premixed Compression Ignited (PCI) combustion [28].

In the next subsections ways of extending the load range for HCCI and CAI operation are described.

2.4.2.2 Spark Assisted HCCI Combustion

A way of increasing the temperature of the charge during running conditions that normally would result in partial or total misfire is spark assistance. The discharge of a spark fired such as in an SI engine creates a flame front which propagates throughout the combustion chamber. Due to the dilution by residuals the flame propagation is slower than in a conventional SI engine. But the effect of the flame propagation on the unburned gases is that temperature and pressure are increased. This results in improved conditions for auto ignition, with resulting advancement of the HCCI combustion phasing. Thus applying spark ignition to CAI combustion at low loads the combustion phasing can be advanced with resulting increase in

efficiency, or even prevention of misfire. This concept is called SACI, an abbreviation for Spark Assisted Compression Ignition. An example of how the load range can be increased using SACI compared to CAI is seen in Figure 2 [15].

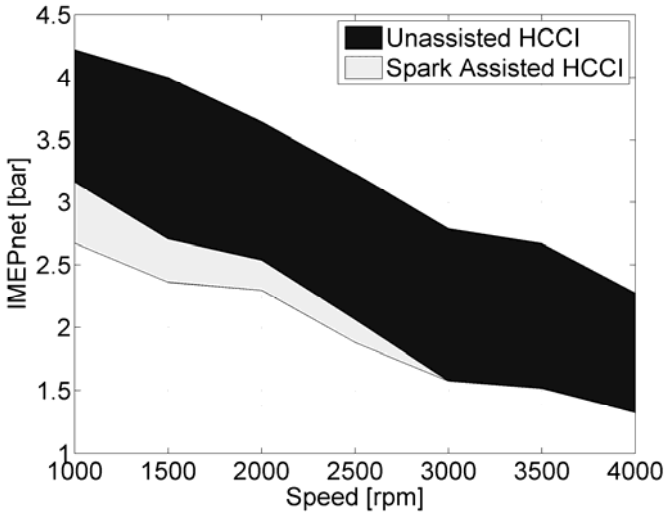

Figure 2: Load regime for a CAI engine with and without spark assistance [15].

SACI can also be necessary when performing mode switches, going from HCCI/CAI combustion to SI combustion and back. Throttling of the intake air can be used to perform the mode switch, where a richer mixture is obtained if the amount of fuel is kept fairly constant. Meanwhile the charge temperature has to be decreased to avoid excessive pressure rise rate, and eventually the charge is within the flammability limit. Now the engine runs in SACI mode and if the throttling is increased even further and the heat source for achieving HCCI combustion is gradually removed, normal SI operation is achieved. The opposite method is used to switch back to HCCI operation. In the case of CAI operation, decreased NVO will result in a less residual diluted charge, with a lower temperature and if the intake air is throttled stoichiometric SI operation can finally be achieved. When switching back, increased NVO and decreased throttling is used to replace the air by trapped residuals resulting in a diluted hot charge which promotes auto ignition.

Since the rate of heat release (ROHR) is slow during the initial flame propagation and fast during auto ignition in SACI combustion, it is possible to estimate how much of the heat release is due to flame propagation. *Hyvönen* [29] defined the initial slow heat release (ISHR) fraction as;

$$ISHR = \frac{Q_{\text{threshold}}}{Q_{\max}} \cdot 100[\%],$$

where $Q_{threshold}$ is the breakpoint where the combustion changes from flame propagation to auto ignition and Q_{max} is the maximum accumulated heat release in the cycle. An accumulated heat release trace for a spark assisted HCCI cycle can be seen in Figure 3, where the difference between slow and fast heat release is clearly visualized. The ISHR definition is thereby a quantitative measure of SI combustion fraction.

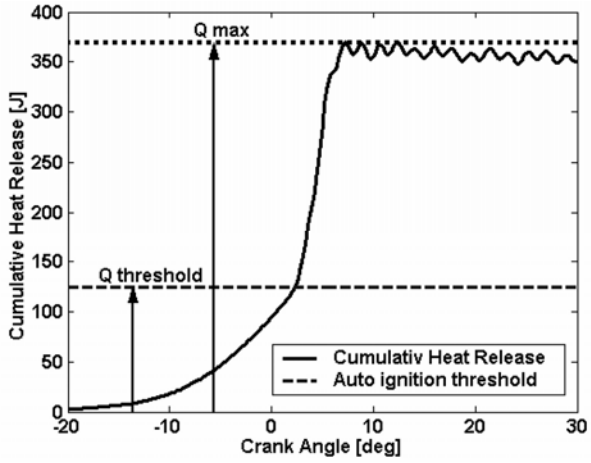

Figure 3: Heat release trace for a spark assisted HCCI cycle with slow flame propagation and faster auto ignition [29].

2.4.2.3 Laser Assisted HCCI Combustion

An alternative to spark ignition is laser ignition, where a laser is used to ignite the charge and initiate flame propagation instead of the spark plug [30-34]. A short laser pulse is focused in a small volume of an air/fuel mixture which results in a non-resonant electrical breakdown of the gas, similar to the one resulting from an electrical spark discharge, in the focal region followed by the formation of hot dense plasma. After a short ignition delay a flame propagates through the combustion chamber like in an SI engine. Laser ignition is believed to have advantages compared to spark ignition. For example in SI engines cycle to cycle variations occur due to heat losses to the spark plug electrodes which makes the ignitability of the charge in the electrode gap sensitive to the local air/fuel ratio. This is not the case for laser ignition where the plasma is located well inside the charge, since no heat losses occur to the surrounding hardware of the engine. As a result the ignition process is more effective resulting in shorter ignition delays. Furthermore, multiple ignition points can be used and focused in an arbitrary location inside the combustion chamber since it is just an issue of optical arrangement. Laser ignition is also known to be appropriate when ignition at high pressure is needed, since the plasma will ignite more of the charge enclosed in a reference volume due to the increased density. Under these circumstances the spark from a spark plug can be quenched due to high pressure. The downside with laser ignition is first and foremost the cost. The spark plug is cheap and reliable while the laser components are costly and optical access is also needed into the engine.

2.4.3 Boosting

A way of increasing the load range of an SI, CI and HCCI engine is to boost the intake air. This means that the intake air pressure and thus the density are increased by either a mechanical supercharger and/or an exhaust driven turbocharger. With more air flow into the engine more fuel is also added to maintain appropriate mixture composition. This results in higher heat release from combustion and thus higher load and higher output power. Both ways of boosting has advantages and drawbacks. The mechanically driven supercharger consumes power from the crankshaft in order to compress the intake air which means that the friction mean effective pressure (FMEP) is increased [35]. Usually the gain in indicated mean

effective pressure (IMEP) is higher resulting in higher load but there is usually a penalty in efficiency especially at low load if the supercharger cannot, for technical reasons be disengaged. With a turbocharger, the enthalpy of the exhaust gas is used to run a turbine which is connected with a shaft to a compressor for the intake air, thus the heat loss to the exhaust is partially recovered. However, in large parts of the load and speed range the pumping losses increase due to increased exhaust back pressure. Another drawback is that enough gas flow with high enough temperature is needed to drive the turbine. In HCCI engines, this is a problem since the exhaust temperature is low due to low temperature combustion, high efficiency and short combustion duration which means that the pressure and thus temperature are lower at Exhaust Valve Opening (EVO). This has to be taken into account when designing the turbocharger which usually is smaller than the ones used with SI and CI engines [36]. A smaller turbocharger has lower moment of inertia and thus lower flow and temperature is needed to accelerate the turbine. Another way is to use a variable geometry turbine (VGT) to extend the operating range of the turbocharger [37, 38] and to control the EGR rate [38].

When the intake air is compressed in the boosting system the air temperature is increased which necessitates intercooling to increase the density and decrease the thermal stress of the engine. In HCCI engines intercooling in combination with heating can be used for intake air temperature control.

In SI and CI engines using low temperature combustion (LTC) concepts like HCCI, CAI or PPC at low load a small turbocharger will limit the maximum power when the engine is run in SI or CI since it is designed for lower exhaust flows with lower temperature. A solution to this can be 2-stage boosting which means that the intake air is compressed in two stages, with cooling in between. One small and one large turbocharger are fitted to the engine where the smaller turbocharger is used to increase the intake air pressure at relatively low loads when the engine is run with LTC and the larger or both turbochargers are used at high loads in SI and CI combustion to get enough mass flow of compressed air. By the possibility to use boosting during LTC operation in SI and CI engines the high efficiency in combination with low emissions can be utilized further up in the engine load range before switching to traditional SI or CI combustion.

In addition to boosting, a VVA system can be used to improve the efficiency and load range. With the VVA system it is possible to adjust the valve timings in such manner that the exhaust gas conditions entering the turbine can be optimised for the selected turbocharger characteristics. One such strategy can be to control EVO which directly affects the exhaust temperature and the amplitude of the pressure pulses entering the turbine from blow down when the exhaust gases leave the cylinder. This strategy enables improved operation with the turbocharger at certain loads and engine speeds where the exhaust temperature would normally not be high enough for running the turbine properly. However, there also exists a trade off between increasing exhaust temperature and loosing usable work if EVO is too early. Another advantage of combining boosting with VVA is the possibility to improve transient response, that is the time to build up intake pressure and thus increase the load.
IVC timing can also be used to control HCCI combustion phasing and optimize towards minimum NOx emissions [39].

In the work presented in this thesis the engines have been run naturally aspirated, i.e. without turbocharging or supercharging. Instead, the strategy of using different combustion chamber geometries has been evaluated to extend the load range in HCCI combustion mode.

2.4.4 Geometry Effects on HCCI Combustion Rate

In the work by *Christensen* et al. [40, 41] geometry generated turbulence was studied in a Volvo TD100 HCCI engine. Two different combustion chamber geometries were compared, one disc shaped combustion chamber and one square bowl in piston. The later one was designed with a narrow squish region creating a strong squish motion into the bowl which results in a turbulent environment. The disc shaped combustion chamber was used as a reference case. Also one high and one low swirling cylinder head were investigated. In Figure 4 (a) the measured turbulence by Laser Doppler Velocimetry (LDV) as function of crank angle degree (CAD) for both piston geometries can be found. The turbulence was measured above one of the upper corners in the bowl and the same position was measured in the disc case. The turbulence level in the disc case is fairly undisturbed during the compression and expansion stroke. In the bowl case the turbulence increases rapidly around 15 CAD before top dead centre (BTDC) and decreases again after TDC due to the strong squish motion into the bowl. The rate of heat release (ROHR) as function of CAD for both geometries can be seen in Figure 4 (b). Start of combustion was in both cases 2 CAD BTDC. In the disc case the ROHR peak is twice as high and occurs much earlier than the ROHR for the bowl case. This means that the combustion rate was much lower and the combustion duration much longer when using the square bowl in piston geometry. Since the ROHR is much lower the pressure rise rate is also decreased in the bowl case. This means that the load can be increased using the bowl geometry. The bowl case is suspected to suffer from increased heat losses due to larger wall area and the overall efficiency should be suffering. As seen from Figure 5 (a) the indicated efficiency in the bowl case is surprisingly better than the disc case for early combustion phasing. The combustion phasing is shown as the crank angle for peak ROHR. The gross indicated efficiency is defined as the work on the piston during the compression and expansion stroke in relation to the input fuel energy per cycle [41]:

$$\eta_{ig} = \frac{W_{ig}}{m_f Q_{lhv}}$$

However, for later combustion phasing the efficiency is better for the disc case. The reason why is found in Figure 5 (b) where the thermal efficiency is plotted for the same combustion phasing sweep. As seen, the thermal efficiency is better for the disc case at late combustion phasing. The thermal efficiency can be defined as the work on the piston during the compression and expansion stroke in relation to the heat released [41]:

$$\eta_T = \frac{W_{ig}}{Q_{hr}}$$

The same trend as for the indicated efficiency is also seen in the thermal efficiency. An explanation could be increased heat losses from increased wall area. This is counteracted by lower inlet air temperature in the bowl case in order to keep constant combustion phasing. The result is lower overall cycle temperatures and in turn reduced heat losses. The combustion efficiency was also found to be higher for early combustion phasing in the bowl case.

The effect of different swirl is not so pronounced as the effect of combustion chamber geometry on the ROHR; therefore the focus was on the turbulence effects.

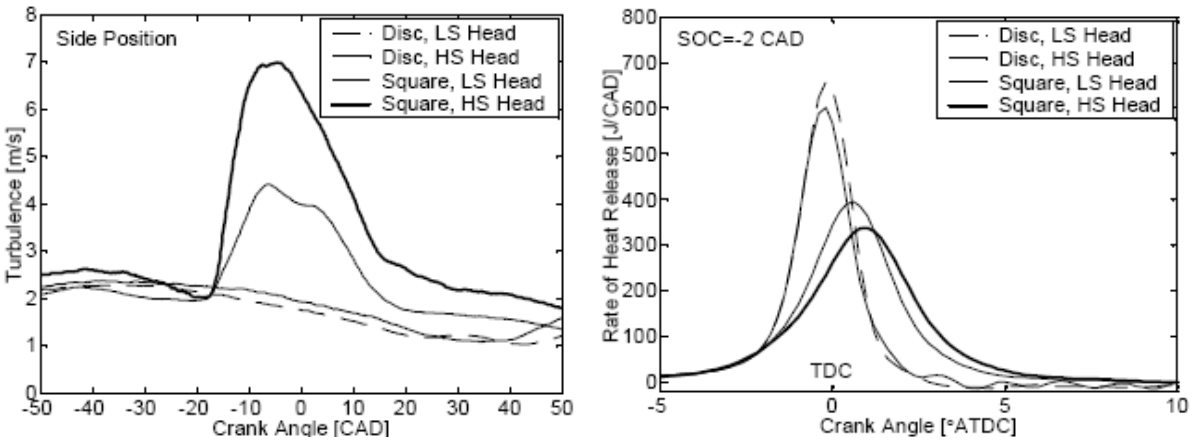

(a) (b)

Figure 4: (a) Turbulence as function of CAD for square bowl in piston and disc shaped combustion chamber. (b) ROHR as function of CAD for square bowl in piston and disc shaped combustion chamber. [41]

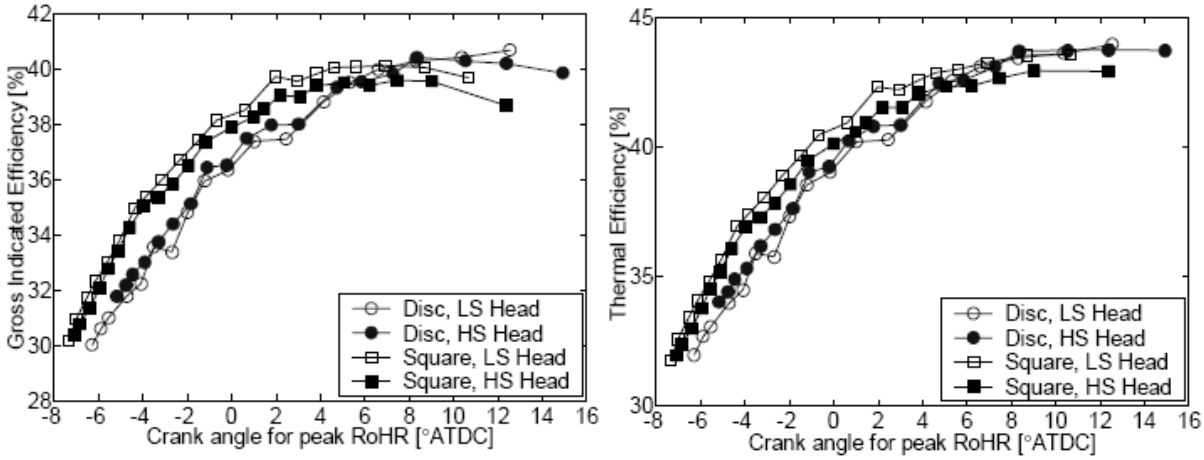

Figure 5: (a) Gross indicated efficiency as function of crank angle for peak ROHR. (b) Thermal efficiency as function of crank angle for peak ROHR. Both combustion chamber geometries are represented [41].

At first it was believed that the decreased combustion rate was due to the increased turbulence level in the cylinder, but other effects of the geometry were also considered.
These can be divided into direct and indirect effects:

- Direct effects could be the turbulence effects on chemical kinetics.
- Indirect effects could be:
  - Increased heat losses due to larger wall area, counteracted by the overall lower cycle temperatures
  - Stratification in temperature, locations with higher temperature ignite first which results in longer combustion duration
  - Stratification in air/fuel ratio, locations with richer mixtures ignite first which results in longer combustion duration
  - Boundary layer behaviour; turbulence is known to break up the boundary layers which will increase wall heat transfer
  - Dissipation phenomenon; turbulence mixing will decrease temperature in hot zones making the overall temperature more uniform.
  - Time scales. The question if the turbulence will have time to mix the different zones.

Each of the phenomena listed above are of interest, and more extensively described in the work by *Christensen* et al. [42]. As the explanation for the decreased ROHR when running the engine with a square bowl in piston combustion chamber is not quite clear, more studies are necessary to distinguish the different contributions of direct and indirect effects caused by the geometry and the turbulence itself. Modeling is one way of doing this and some summarized results can be found in the following text. For readers with deeper interests into the world of modeling, please refer to the papers of the authors mentioned below.

Kong et al [43] modelled the direct effect of turbulent flow on chemical kinetics by the eddy break-up concept using Computational Fluid Dynamics (CFD) with detailed chemical kinetics code. The model predicted the longer combustion duration in the bowl case due to increased wall heat transfer caused by the turbulence, but more comprehensive CFD models are needed to predict turbulence and heat transfer accurately.

Aceves et al. investigated the topic using CFD and multi-zone chemical kinetics modeling in two studies [44, 45]. In the first study [44] CFD was used to model temperature histories for 40 zones in the two combustion chambers respectively. The chemical kinetics code was used to model the time of ignition and propagation for each of these zones based on the CFD modelled temperature histories. An assumption was made that the turbulence has no direct effect on the chemical kinetics. The longer combustion duration and lower heat release rate were well predicted by the model. It was explained by an increase in boundary layer thickness due to the large wall area in the bowl case. En estimate revealed that 70% of the difference in wall heat transfer between the geometries was due to the difference in wall area and the rest was due to the turbulence. The maximum and minimum temperatures were found to be about the same for the geometries but the mean temperature was lower in the bowl case. This can explain the longer burn duration since the charge ignites in the hottest location and propagates into the colder ones. If the difference between the maximum and mean temperatures is higher the combustion will be longer, since the heat and pressure from the burned zones must heat up the unburned zones for auto ignition to occur.

In the second study by *Aceves* et al. [45] the temperature distribution in the cylinder from inlet valve closure (IVC) to start of combustion (SOC) was investigated using CFD modelling. No combustion was studied instead the focus was on the temperature distribution in the combustion chamber prior to auto ignition. In this study some simplifications of the model were done to study the effects of differences in wall area and the ability of the turbulence to dissipate cold gas from the boundary layer into the bulk. Therefore it was assumed that the inlet temperatures, wall temperatures, residual temperatures were the same at IVC for both geometries. Furthermore, no residual mixing with the fresh charge was accounted for. Since there are differences between the two geometries regarding the parameters mentioned above the study should be seen as fundamental. The main conclusions were that the square bowl has 24% higher heat transfer rates compared to the disc and approximately 70% of this difference is due to the larger wall area while the rest is due to turbulent transport of cold gases from the boundary layers to the bulk. In the intake stroke it was found that the square bowl piston heated the gas in the bowl even though the overall heat transfer was from the gas to the walls. This induces higher temperatures inside the bowl compared to the rest of cylinder. The largest mass of boundary layer was found in the squish and the bowl corners.

To summarize, the modeling found that during the intake stroke the heat transfer is from the hot walls to the gas. During the compression the heat losses are higher in the bowl case

compared to the disc due to increased turbulence. Since the temperature difference between gas and the walls is higher during the compression stroke than the intake stroke the heat losses has a larger impact on the higher square bowl heat transfer rates. The corners in the bowl were found to be large contributors of cold zones due to large local area to volume ratios and low levels of turbulence decreasing the possibility of raising the local temperature through mixing.

The model by *Kong* assumes that turbulence has a direct effect on chemical kinetics while the first model by *Aceves* does not. What can be concluded is that both models explain the longer burn duration due to increased wall heat transfer. But the difference is that the model by *Kong* explains the increased wall heat transfer with turbulence while the model by *Aceves* explains it mostly with difference in wall area and only partly with turbulence. It can be concluded that more studies are needed to find the explanation for the longer burn duration in the bowl but the models indicate that it is related to the heat transfer and a wider temperature distribution in the cylinder. The work presented in this thesis is an attempt to further explain the complexity of the effect of turbulence and combustion chamber geometry on ROHR. Experiments that can be conducted are for example fuel tracer Laser Induced Fluorescence (LIF) to see if the fuel distribution is homogeneous in the cylinder, an assumption which the models are based on. Further, chemiluminescence imaging can be used to find how stratified the combustion is. The combination of these two optical diagnostic methods may help to explain if the charge is stratified in temperature and/or air/fuel ratio.

As far as modelling is concerned, different strategies and model types evolve with time and so does computing power. Large eddy simulations (LES) can be used to study the temperature field in the cylinder more extensively and more in detail than the Reynolds Averaged Navier Stokes (RANS) equation based modeling. However since the flow field and temperature field is to be coupled with detailed chemical kinetics modelling for each grid or zone, a finer mesh consumes tremendously larger amounts of computing power and to reduce calculation time's simpler chemical kinetic models are used in LES. The benefit with LES is the possibility to quantify the temperature distribution during intake and compression which will affect where and when the combustion starts and ends.

3 Experimental Apparatus

In this chapter the two HCCI engines used for the experiments, the Volvo TD100 and the Scania D12 are presented along with necessary modifications and the equipment used in the laboratory.

3.1 Test Engines

3.1.1 The Volvo TD100 HCCI Engine

The engine used in Papers 1-3 was an in-line six cylinder Volvo TD100 Diesel engine. Only one of the cylinders was in operation in order to simplify the measurements and the rest of the cylinders were motored. The turbocharger was removed. Holes were drilled in the motored pistons which results in lack of compression. Furthermore, the push rods were removed since the valve trains for these cylinders were not in use. Thus the mechanical work required to motor the five additional cylinders was minimized and the engine was still balanced unlike a true single cylinder engine. This arrangement results in less reliable brake specific values since the total friction is high compared to the output power from the single operational cylinder. Therefore only indicated results have been used. The same limitations holds for the Scania D12 engine, see below. In order to run the engine in HCCI mode it was modified for PFI instead of DI and used preheating of the intake air in order to achieve auto ignition and to control the combustion phasing. The compression ratio was adjustable by changing the piston crown which was mounted directly on top of the piston. This modification also made it possible to run with different combustion chamber geometries. A drawback is that the piston rings are located below the piston crown which results in larger topland volume with increasing compression ratio. The topland volume is defined as the narrow crevice between the piston and cylinder wall from the piston rings to the top of the piston. Larger crevice volume results in higher emissions of unburned hydrocarbons [42]. In Table 1 some vital engine data can be found and in Figure 6 a picture of the engine can be seen.

Table 1: Geometric properties of the Volvo TD100 HCCI engine.

Displaced Volume	1600 cm^3
Bore	120.65 mm
Stroke	140 mm
Connecting Rod Length	260 mm
Number of Valves	2
Inlet Valve Diameter	50 mm
Exhaust Valve Diameter	46 mm
EVO	39 (BBDC @ 1mm lift)
EVC	10 (BTDC @ 1mm lift)
IVO	5 (ATDC @ 1mm lift)
IVC	13 (ABDC @ 1mm lift)
Valve Lift Intake	13.4 mm
Valve Lift Exhaust	11.9 mm
Combustion Chamber Type	Disc, Hill or Bowl
Swirl Ratio	2
Compression Ratio	Adjustable
Fuel Injection	PFI

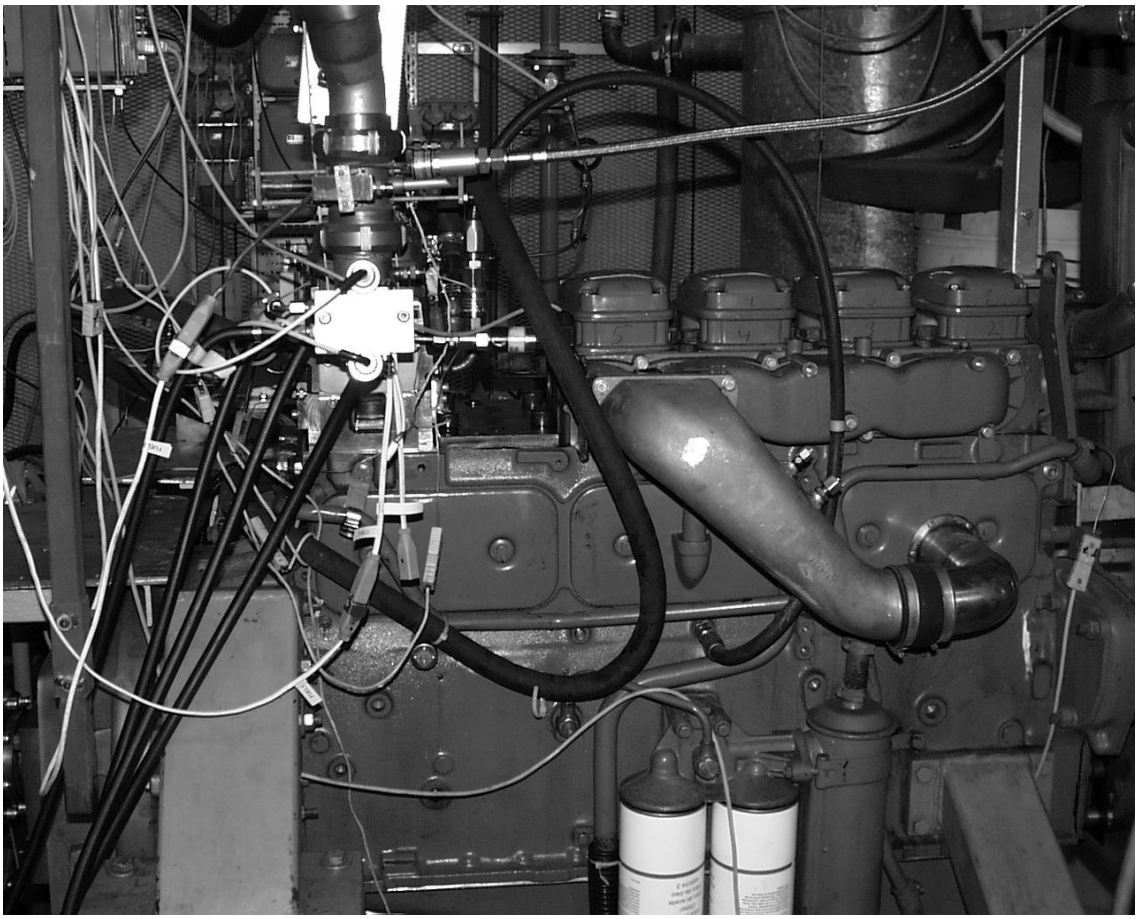

Figure 6: The modified Volvo TD100 HCCI engine. The operating cylinder is to the left in the picture.

The camshaft was designed for lean-burn natural gas SI operation [81, 42] which can be seen by the valve timings in Table 1. These camshafts typically have short cam duration and some negative valve overlap (NVO) to get acceptable idle running conditions, which results in increased residual gas fraction. With HCCI operation this is advantageous since the residual gas acts as a heat source which means that less inlet air preheating is needed to initiate combustion. However the valve timing of the natural gas camshaft also results in lower volumetric efficiency, especially at high engine speed where the time is limited to fill the cylinder with fresh air. Another issue that affects this problem is the 2-valve per cylinder design limiting the gas exchange efficiency in this old-style Diesel engine.

3.1.2 The Scania D12 HCCI Engine

For the experiments in Paper 4 - 10 a more modern engine with better breathing capabilities was used, the Scania D12 HCCI engine. The engine has 4 valves per cylinder and a camshaft with standard Diesel valve timings. A picture of the engine can be seen in Figure 7 and some engine specifications can be found in Table 2. This 6 cylinder engine was also in single cylinder operation and the cylinder heads of the five motored cylinders were removed and replaced by steel covers. Holes were drilled in the motored pistons to reduce the compression work and counter weights were mounted on top of the motored pistons to achieve a balanced engine. The engine has also been modified with optical access in order to conduct optical diagnostics of the HCCI combustion process. These modifications will be described in Section 3.1.3.

Table 2: Geometric properties of the optical Scania D12 HCCI engine.

Displaced Volume	1966 cm^3
Bore	127.5 mm
Stroke	154 mm
Connecting Rod Length	255 mm
Number of Valves	4
Inlet Valve Diameter	44 mm
Exhaust Valve Diameter	41 mm
EVO	34 (BBDC @ 0.15mm lift)
EVC	6 (BTDC @ 0.15mm lift)
IVO	2 (BTDC @ 0.15mm lift)
IVC	29 (ABDC @ 0.15mm lift)
Valve Lift Intake	14.1 mm
Valve Lift Exhaust	14.1 mm
Combustion Chamber Type	Disc or Bowl
Swirl Ratio	2.1
Compression Ratio	Adjustable
Fuel Injection	PFI
Optical Access	*Bowditch* piston extension with a quartz window and quartz liner beneath the cylinder head

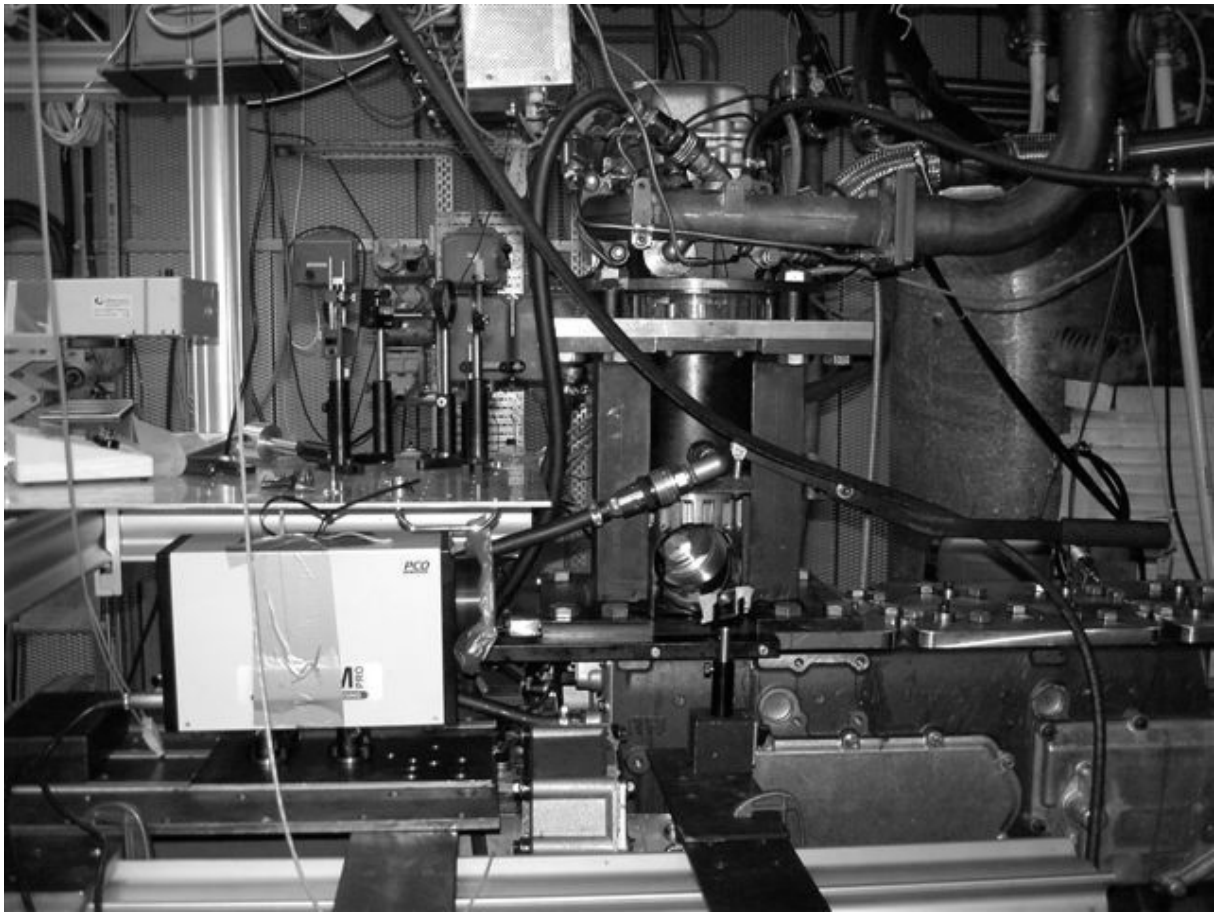

Figure 7: The Scania D12 HCCI engine with optical access.

3.1.3 Optical Access

Optical access in combustion engines can be achieved in numerous ways but there are three main paths that can be used: through the piston, the cylinder liner or the cylinder head. Depending on the diagnostic technique one, two or all three are needed. The optical access through the cylinder head is limited by the space left by the valves, the fuel injector and/or the spark plug. However when using pent-roof style combustion chambers in SI engines, access can be enabled through the side of the cylinder head where the combustion chamber normally is located. In Diesel engines with bowl in piston geometries optical access is usually achieved from the cylinder head. Optical access through the cylinder liner is achieved using whole or parts of the liner in quartz glass which can restrain high gas pressures and temperatures.

In Paper 5 - 8 the Scania D12 HCCI engine was modified with a *Bowditch* [49] piston extension with a quartz piston window and a mirror. The engine is also equipped with a 30 mm high cylinder liner made of quartz glass placed between the steel liner and the cylinder head, granting optical access to the upper part of the combustion chamber and close to walls. When using piston windows the field of view is often limited due to mounting necessities which in this work means that the outer part of the radius is not accessible and thus only 51% of the projected combustion chamber area is visible from beneath. The Scania D12 HCCI engine modified with the optical access described above can be seen in Figure 9 where the main parts are described.

The use of optical access makes it possible to perform optical diagnostics such as laser induced fluorescence (LIF) [8, 46, Paper 5 and 8], laser induced phosphorescence (LIP) [47, 48], schlieren photography [Paper 5] and chemiluminescence imaging [8, Paper 5, 6 and 7]. Laser sheets can enter through the quartz liner both in a horizontal and a vertical plane. The mirror and the piston window are used to retrieve signals from the field of view of the horizontal laser sheet or signals in the form of emitted light. The steel cylinder liner is vertically adjustable in order to facilitate cleaning of the piston glass and the quartz liner. Since the cylinder head is elevated compared to normal mounting position the push rods had to be elongated. Unfortunately they have a tendency to elastically compress due to the high valve spring stiffness. This affects the valve timings and the maximum lift height and also depends on engine speed. In order to compensate for the extra weight that the piston extension constitutes, tungsten counter weights were mounted on top of the motored pistons resulting in a balanced engine.

Optical access into engines is not a new technique. Even as early as 1872 *Nicolaus Otto*, the establisher of the four stroke cycle, built a hand operated optical engine [50]. The optical access was enabled through a hand-blown glass cylinder liner and the engine was used to study charge stratification and mixing of cigarette smoke and fresh air. However, optical engines operated with combustion of fuel and air appeared far later in engine history. Two pictures of Otto's optical engine can be found in Figure 8. Note the four intake mounted cigarettes used to generate smoke into the cylinder.

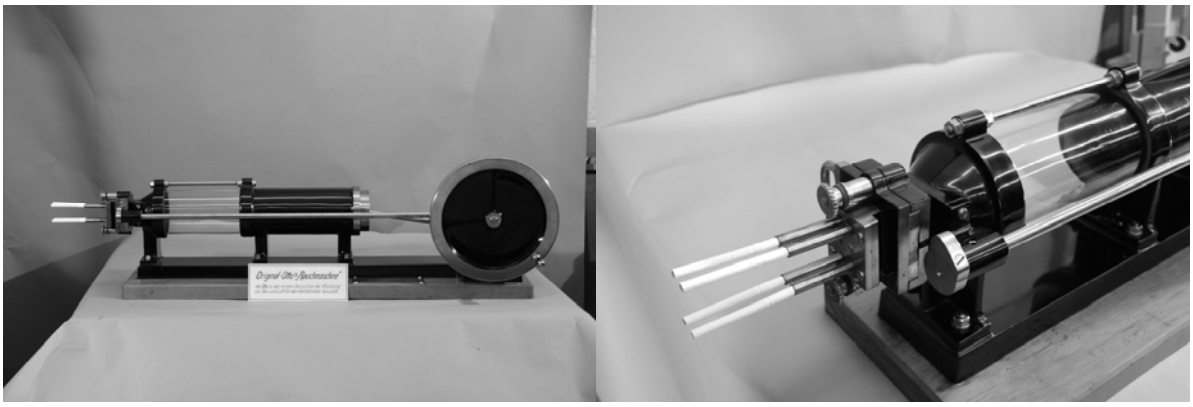

Figure 8: ***Nicolaus Otto's*** **experimental cigarette smoke gas engine from approximately 1872 is believed to be one of the first optical engines [50]. The engine was donated by Deutz AG in 1934 to the Henry Ford museum in Dearborn, MI, USA, where these pictures were taken.**

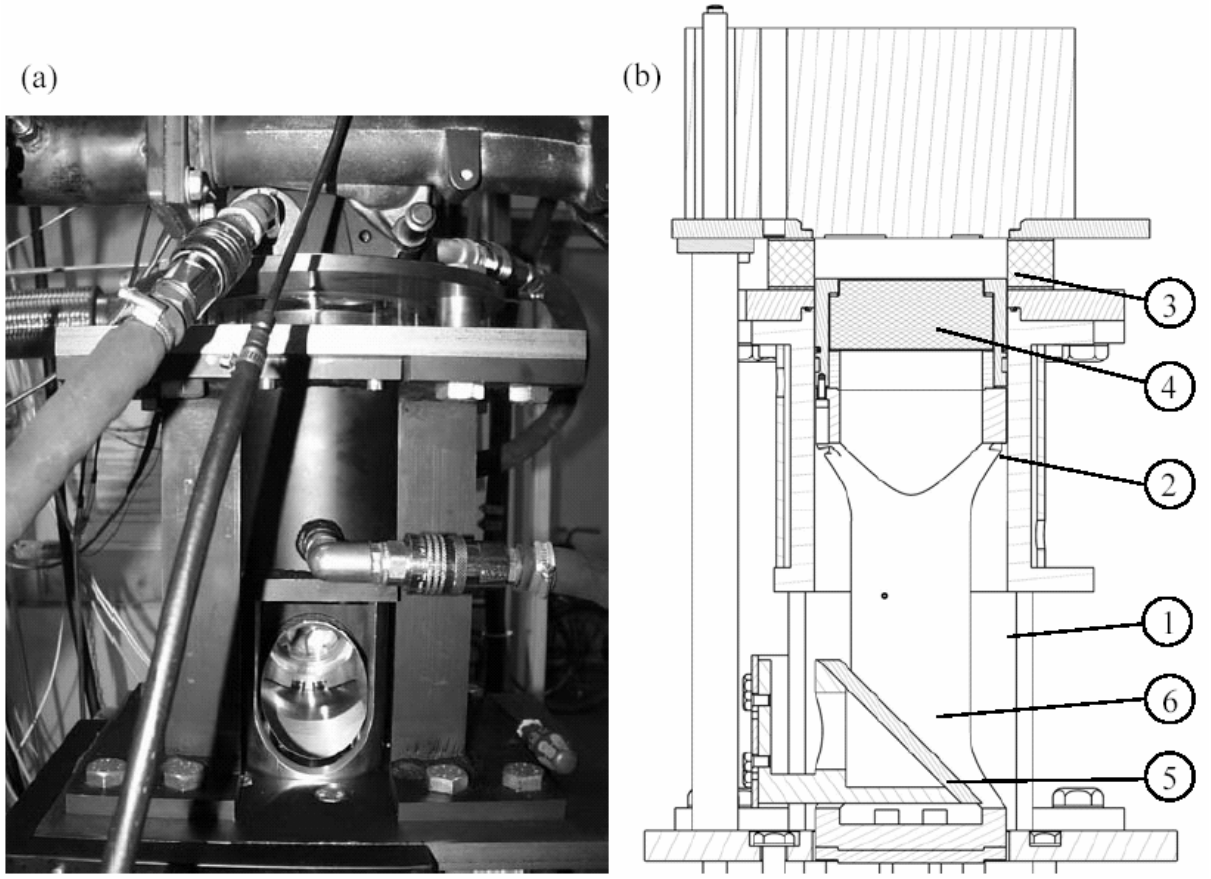

Figure 9: The ***Bowditch*** **piston extension. Picture of the setup in (a) and a blueprint of a sectioned view in (b); U-shaped beams (1), steel cylinder liner (2), quartz glass ring (3), quartz glass piston (4), 45 degree mirror (5) and piston extension (6).**

3.1.4 Intake Air Preheating

In order to initiate HCCI combustion in engines, charge heating is necessary. One purpose is to avoid using excessive compression ratios, where the heat losses increase due to high combustion chamber area to volume ratios. Another purpose is to control the combustion phasing as mentioned in the HCCI introduction. In this project intake air heating has been used where an electrical heater has been mounted before the intake plenum and the fuel

injectors. The heater has a maximum power of 7.5 kW resulting in air temperatures of up to 230° C.

3.1.5 Exhaust Gas Recirculation

One way to dilute the air/fuel mixture is to use exhaust gas recirculation (EGR) which decreases the cycle temperature [42] due to high specific heat (C_p). Low cycle temperature results in lower combustion rate and peak pressure. Moreover lower peak pressure leads to less heat transfer which improves the efficiency. On the other hand λ decreases. In the presented experiments an EGR loop has been used circulating the burnt gas from the exhaust back into the intake piping. When running the engine with high amounts of EGR it is necessary to use a back pressure valve in the exhaust pipe to force the exhaust gases into the intake pipe. The downside is that the pumping losses will increase. A heat exchanger is attached to the EGR valve in order to cool the burnt gases. The amount of EGR is calculated from the CO_2 concentrations in the intake compared to the exhaust.

3.1.6 Fuel Injection

Two different fuel injection systems have been used. For liquid fuels, as for example isooctane and gasoline, a standard SI engine fuel injection system from Bosch has been used. It consists of fuel tank, fuel pump, fuel pressure regulator and fuel injectors. The working principle is that constant fuel pressure is maintained relative to the intake air pressure meaning that there is a constant pressure difference over the injector. The amount of fuel then depends on the time that the injector is open per cycle. Fuel is injected each cycle and the injection timing is just after inlet valve closure to evaporate the fuel properly making use of the relatively high temperature of the inlet valve. Fuel balances are used to measure the mass of fuel injected over time and thus the fuel flow can be calculated. When running on gaseous fuels e.g. natural gas, the fuel is delivered in a pipe line to the laboratory. The gas pressure is then regulated to a suitable level for the natural gas injectors. The natural gas injectors have the same working principle as the liquid fuel injectors. A gas flow meter is used to measure the flow of fuel over time. For controlling the amount of fuel injected an in-house control program has been developed. In the program it is possible to set the amount of fuel, EGR levels, intake air temperature and triggers for external laser and camera systems. The in-cylinder pressure and, from a simple calculation, the heat release can be monitored.

3.1.7 Variable Valve Actuation

In the experiments where the effect of laser ignition on natural gas HCCI combustion was investigated, a Variable Valve Actuation (VVA) system from Cargine Engineering AB® was used. It is a pneumatic system that for each valve consists of an actuator, two solenoids, a piston and logical channels inside the system housing [51]. The actuators are mounted on a steel plate that is placed directly on top of the cylinder head. With this setup the actuators act directly on the valve caps and thus the valves themselves. A picture of the steel plate with the four actuators, one for each valve, can be seen in Figure 10. Air is supplied to the system at a pressure of about 3 bar which enables a maximum valve lift of 14 mm. The solenoids are used as air regulators which enables/disables the air to affect the pneumatic piston which in turn acts on the valve. 3 mm before the valve hits the valve seat a hydraulic brake is activated in order to decelerate the valve before closure to minimize noise and wear. Since the solenoids are controlled by electric pulses, the valve timing can be set arbitrary. This means that it is possible for the user to freely set valve opening, closing, lift height and valve overlap events.

It is then possible to run different NVO strategies with resulting residual gas trapping. Another strategy is to activate the valves twice during the same engine cycle, which for example can be used for rebreathing. Rebreathing is when the exhaust valve is opened and closed a second time shortly after the normal closing. By doing this hot exhaust gases will flow back into the cylinder. This is similar to residual gas trapping but the gases have cooled down a bit during the time spent in the exhaust system compared to the burnt gases that stay in the cylinder. This is a very handy tool for closed loop combustion control since this is a way of controlling the charge temperature and dilution. Another possibility is to use variable timing of IVC which is a way to change the effective compression ratio. This is also an interesting means of control since the compression ratio has a strong influence on the combustion phasing and the rate of heat release [42]. Further, controlling IVC is usable for cold start conditions where a higher charge temperature is needed in order to obtain auto ignition when the cylinder walls are cold.

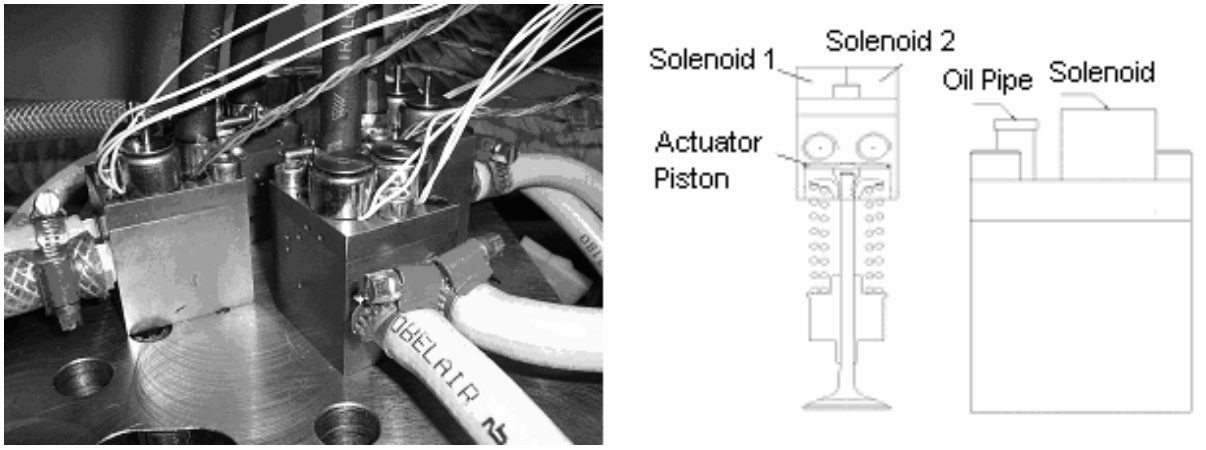

Figure 10: The actuators to the left and a sectioned view of one of the actuators to the right [51].

In Figure 11 valve lift as function of time can be seen for different maximum lift heights and lift durations. The shape of the lift curve is much sharper compared to the normal lift curve obtained by a mechanical camshaft. This means that by using the VVA system the lift movement of opening and closing is much faster and the time that the valve is at maximum lift is longer.

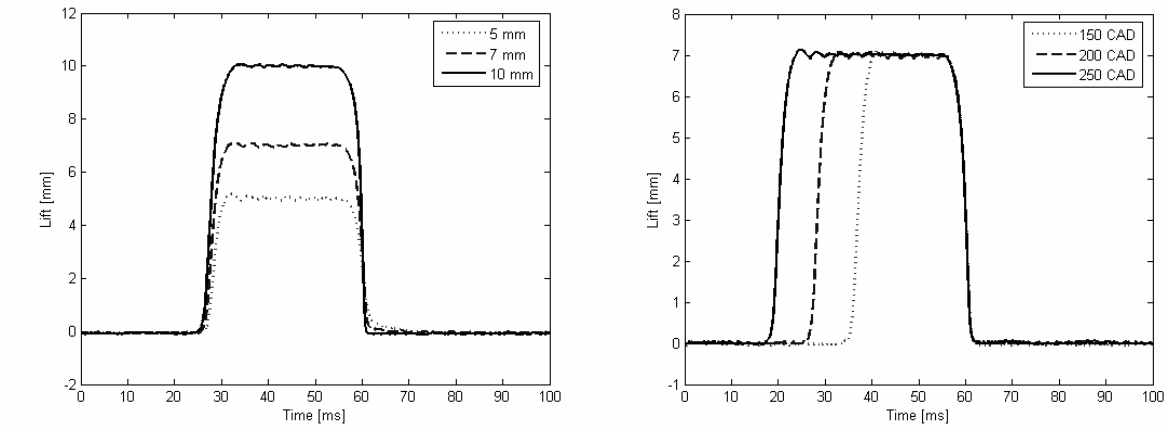

Figure 11: Valve lift curves as function of time at 1000 rpm. To the left 3 different lift heights can be seen at 200 CAD lift duration. To the right is 3 different durations displayed for the maximum lift of 7mm [51].

However during the studies presented in this text the system was under development. Therefore standard valve timing settings were used and the VVA system was validated

regarding reliability. The cold start feature of early IVC was found to be a convenient tool. In the future the purpose is to use the full features of variability and study the different effects it has on engine operation.

3.1.8 Laser Ignition

As described in the section on laser assisted HCCI combustion lasers can be used to ignite an air/fuel mixture as an alternative to spark ignition. In paper 5 and 6 a Q switched, flashlamp pumped Nd:YAG solid-state laser has been used. The laser light wavelength was 1064 nm and the pulse duration was approximately 5 ns. The maximum laser energy was 35 mJ, but due to losses the ignition energy is less. The laser beam is focused inside the combustion chamber using optical lenses. The focused laser light in a small volume of air/fuel mixture results in a non-resonant breakdown (electrical breakdown of the gas similar to the one resulting from an electrical spark discharge) in the focal region followed by the formation of hot dense plasma. If the temperature and energy of the plasma is high enough, it will ignite the charge. A picture of the emitted light from a non-resonant breakdown in air at room temperature and pressure is seen in Figure 12.

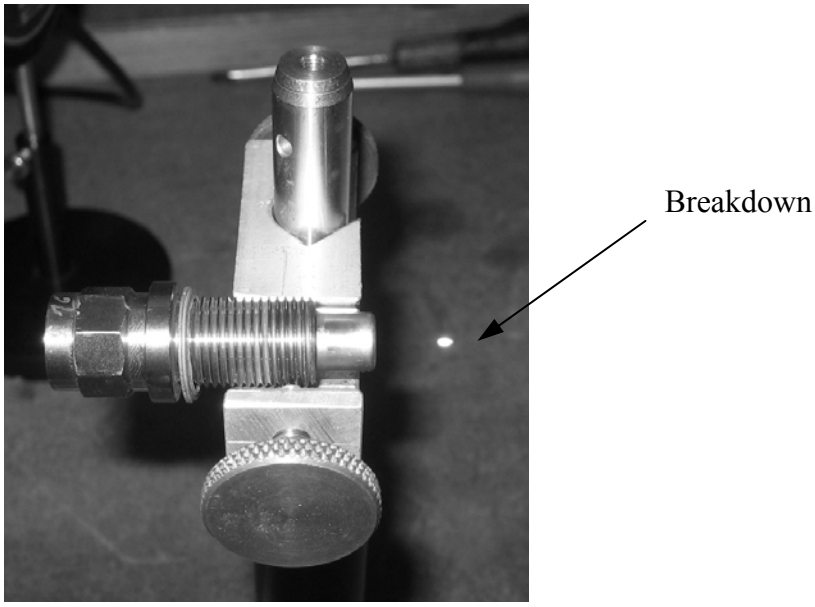

Figure 12: The light emitted from breakdown in air created by a focused laser beam.

3.2 Test cell

3.2.1 Dynamometer

The dynamometer used for this work was an *ABB*® AC motor. It has a rated power of 55 kW and the maximum speed of 2000 rpm. A control system is used to achieve constant engine speed. An engine speed set point is defined by the user and accordingly the dynamometer either motors or brakes the engine depending on the engine's output power and desired engine speed.

3.2.2 Data Acquisition

For the slow measurements of pressure, temperature and flow, for example in intake and exhaust pipes, an *HP® 3825A* data logger was used. The logger works as an accurate voltage meter for many channels. The voltage is then converted to different units before stored in data files in a PC. Generally temperatures are measured by type K thermocouples and pressures by piezo-resistive transducers. The fuel consumption is calculated from the change of mass measured by the fuel balance over time. When using natural gas the fuel flow is measured by a *Bronkhurst® Hi-Tech* flow meter inserted in the gas rail. NO_x, HC, CO, CO_2 and O_2 in the exhaust are sampled by the HP logger and the relative air/fuel ratio (λ) is calculated from these concentrations by the PC. As reference an *ETAS® LA3* Lambda meter was used. The relative air/fuel ratio is defined as the ratio between the actual air/fuel ratio and the stoichiometric air/fuel ratio:

$$\lambda = \frac{\left(\frac{A}{F}\right)_{Actual}}{\left(\frac{A}{F}\right)_{Stoichiometric}}$$

If λ is higher than one, the air/fuel mixture is fuel lean, i.e. with excess of air.

For high speed measurements of pressure and ion current a *DAP 5400a* A/D converter from *Microstar Laboratories* has been used. With this system it is possible to simultaneously collect data in 8 channels at 1.25 MHz each.

3.2.3 Emissions Measurements

For the emissions measurements an analyzing system from *BOO Instruments AB®* was used with the capability of measuring NO, NO_x, HC, CO, CO_2 and O_2. The system has dual CO_2 instruments in order to measure the CO_2 concentrations in both intake and exhaust when running the engine with EGR. All gases are measured dry except for HC, NO and NO_x which are measured wet. The NO/NO_x is measured with an *Eco Physics® CLD 700 EL ht* which uses a Chemiluminescence Detector (CLD) in the concentration range of 0 – 10000 ppm. The unburned HC is measured by Hydrocarbon Analyzer Model 109A from *J.U.M Engineering®* which uses a Flame Ionization Detector (FID) in the range of 0-100000 ppm. A mixture of 40% Hydrogen and 60% Helium is used as fuel for the flame. The concentrations of CO and CO_2 are measured by an instrument called *UNOR 611* from *Maihak®* which uses a Non Dispersive Infrared analyzer (NDIR) in the ranges of 0-10% for CO and 0-16% for CO_2. For the O_2 measurements a paramagnetic detector has been used in the concentration range 0-25%. All the analyzers have the possibility to auto range the measurements into smaller steps at lower emissions concentrations.

3.2.4 In-Cylinder Pressure Measurements

3.2.4.1 Pressure Transducer

The pressure transducers used for the experiments were the *Kistler® 7061B* with M14 thread and the *6067C1* with 10 mm thread. The *7061B* is normally used as a standard pressure transducer while the *6067C1* is used when there is lack of space in the combustion chamber. This is the case when the pressure transducer has to be mounted in the centre of the

combustion chamber between the valves. The environment inside the combustion chamber is tough both regarding pressure and temperature. Therefore both types of pressure transducers are water-cooled in order to resist thermal shock which would otherwise cause distorted signals. The pressure transducer generates an electrical charge which is proportional to the pressure change inside the combustion chamber. This means that the transducer does not measure absolute pressure, only changes in pressures. Therefore the signal has to be compared to a reference pressure before it can be used.

3.2.4.2 Charge Amplifier

The electrical charge from the pressure transducer is converted in the charge amplifier to an analogue voltage signal. In the charge amplifier it is also possible to change the amplification of the signal depending on the pressure range that is used. The charge amplifier used for this work was a *Kistler® 5011*.

3.2.4.3 A/D Converter

Before the computer can sample the pressure data the pressure signal has to be digitized in an A/D converter. This was done by a fast sampling 16-bit *National Instrument 6052E A/D* board. Two parameters have to be determined before accurate pressure measurements can be done, the reference pressure and the calibration constant. The reference pressure can be determined by measuring the exhaust back pressure while motoring the engine. The calibration constant is simply the whole gain of the measurement system from the pressure transducer to the computer.

3.2.4.4 Calibration Constant

There are several ways of determining the calibration constant. In this work the following expression for the calibration constant was used.

$$Constant\left[\frac{Pa}{count}\right] = \frac{Range}{2^{Bits}}\left[\frac{V}{count}\right] * S_{ca}\left[\frac{MU}{V}\right] * T_{ca}\left[\frac{pC}{MU}\right] * \frac{1}{C_{pt}}\left[\frac{Bar}{pC}\right]$$

,where

Range: The voltage measurement range in the A/D converter, normally from -10 to +10 volts, resulting in a range of 20 volts.

Bits: Number of bits of resolution in the A/D converter, in these studies a 16 bit A/D converter was used resulting in 2^{16} discrete levels.

S_{ca}: Charge amplifier scale, 10 bar/volt.

MU: Mechanical Units, usually bar.

T_{ca}: Charge amplifier sensitivity, normally set to the pressure transducer sensitivity.

C_{pt}: Pressure transducer sensitivity which is given by the transducer manufacturer. When using the Kistler 7061B model the sensitivity was for that particular transducer 87.8 pC/bar

4 Diagnostic Methods

In this section different diagnostics methods used in the work will be presented.

4.1 Pressure Diagnostics

In-cylinder pressure sensing is maybe the easiest and most reliable method of retrieving information about the ongoing combustion process and is applicable for SI, CI and HCCI engines. The downside is the high cost of the equipment used which makes the method limited to experimental lab use only and is not feasible for on-board engine diagnostics. The information that can be extracted from the pressure history is substantial. It is possible to derive the start, progress and rate of combustion and if misfires or knock occurs. In HCCI engines the pressure history is vital information to derive the combustion phasing from heat release analysis. This is essential since the HCCI combustion phasing depends on the pressure and temperature history during compression. In SI engines the combustion phasing is fairly well known from the timing of the spark and in DI CI engines from the timing of the fuel injection. In HCCI engines the calculated combustion phasing from the pressure history is used for closed loop combustion control by changing operating parameters as for example inlet air temperature, injected amount of fuel or valve timing settings.

4.1.1 Heat Release

If the in-cylinder pressure is measured over the engine cycle, the heat release (HR) from the combustion can be calculated. In this work a single zone model [5] has been used, which means that it is assumed that the temperature and pressure are uniform throughout the cylinder. This is not the case in real life since stratification in air/fuel ratio, temperature and differences in wall temperature will affect the local heat release and heat transfer. As long as knock does not occur the pressure is assumed to be uniform throughout the cylinder. The single zone model uses the pressure to calculate the global gas temperature and global heat release. The model uses the equation of state in combination with constant mass from IVC to EVO to calculate the in-cylinder temperature. The instantaneous cylinder volume can easily be calculated. From the measured pressure, calculated volume and temperature the heat release can be estimated. To calculate heat losses the *Woschni* model [52] has been used. For the heat release model to be fairly accurate the initial charge conditions have to be estimated correctly. The intake pressure is measured and a small pressure loss over the intake valves is estimated to set the charge pressure at IVC. The initial charge temperature is estimated in the same manner from the measured intake temperature. Since the heat release analysis is a rough estimation, the most reliable parameters, which are not so sensitive to errors in the initial charge conditions, are indicated mean effective pressure (IMEP) and crank angle of 50% heat release (CA50). IMEP is a measure of the engine load and CA50 is an estimation of the combustion phasing. A software program developed by Professor *Bengt Johansson* and others include the heat release model with heat transfer calculation and numerous parameters are calculated as for instance CA50, IMEP and efficiencies.

4.1.1.1 Heat Release Derivation

The heat release is calculated as follows. The energy balance in the engine is estimated using the first law of thermodynamics for an open system:

$$\partial Q = \partial U + \partial W + \partial Q_{HT} + \partial Q_{Crevice} \quad (1)$$

where

∂Q = Rate of Heat Release (ROHR) from chemical reactions
∂U = Change in internal energy
∂W = Work on the piston
∂Q_{HT} = Heat transfer to the cylinder walls
$\partial Q_{Crevice}$ = Energy loss from mass flow across the system boundary, i.e. from and to the crevices. This term is usually neglected and therefore set to zero.

The internal energy, U, can be expressed by the mass, m, the specific heat, C_v and the temperature, T:

$$U = m\,u = m\,C_v\,T \quad (2)$$

where

m = Mass in cylinder
u = Internal energy per mass unit
C_V = Specific heat at constant volume
T = Temperature

By differentiating (2) the change in internal energy can be derived:

$$\partial U = mC_v dT + udm \quad (3)$$

Since the mass between IVC and EVO is assumed to be constant, i.e. no blow by over the piston rings, the derivative of mass is assumed to be zero and dT has to be determined. If the gas in the cylinder is assumed to be ideal, the equation of state yields:

$$pV = mRT \quad (4)$$

where

p = In-cylinder pressure
V = Cylinder volume
R = Universal gas constant

From (4) the derivative of the temperature can be determined:

$$\partial T = \frac{1}{mR}\left(pdV + dpV\right) \quad (5)$$

where mR is assumed to be constant.
By inserting (5) into (3) the internal energy is expressed:

$$\partial U = \frac{C_v}{R}\left(pdV + dpV\right) \quad (6)$$

The work on the piston can be expressed using the pressure and the volume change:

$$\partial W = pdV \tag{7}$$

Inserting (6) and (7) into (1) yields:

$$\partial Q = \left(1 + \frac{C_v}{R}\right) pdV + \frac{C_v}{R} dpV + \partial Q_{HT} + \partial Q_{Crevice} \tag{8}$$

Since the content in the cylinder is assumed to be an ideal gas the gas constant is expressed as:

$$R = C_p - C_v \tag{9}$$

and the ratio of specific heats:

$$\gamma = \frac{C_p}{C_v} \tag{10}$$

By inserting (10) into (9):

$$1 + \frac{C_v}{R} = \frac{\gamma}{\gamma - 1} \tag{11}$$

And rewriting:

$$\frac{C_v}{R} = \frac{1}{\gamma - 1} \tag{12}$$

By inserting the expressions (11) and (12) into (8) the heat release can be expressed:

$$\partial Q = \frac{\gamma}{\gamma - 1} pdV + \frac{1}{\gamma - 1} dpV + Q_{HT} + Q_{Crevice} \tag{13}$$

If the rate of heat release is to be expressed in terms of CAD (θ) the final expression yields:

$$\frac{\partial Q}{\partial \theta} = \frac{\gamma}{\gamma - 1} p \frac{\partial V}{\partial \theta} + \frac{1}{\gamma - 1} V \frac{\partial p}{\partial \theta} + \frac{\partial Q_{HT}}{\partial \theta} + \frac{\partial Q_{Crevice}}{\partial \theta} \tag{14}$$

For calculating the rate of heat release in terms of CAD the pressure, temperature and volume has to be known. The pressure is usually measured with a resolution of 0.2 CAD and the temperature can be determined using the equation of state (4). The instant in-cylinder volume is determined as follows:

$$V = V_c + \frac{\pi B^2}{4}\left(l + \frac{S}{2} - d\right) \tag{15}$$

where

V = Cylinder volume
V_c = Clearance volume or Compression volume
B = Bore of cylinder
S = Stroke
l = Connecting rod length
d = Distance between the crank shaft axis and the piston pin axis

The compression ratio, CR, is expressed as the largest cylinder volume divided by the smallest cylinder volume, i.e. the compression volume:

$$CR = \frac{V_c + V_d}{V_c} \tag{16}$$

where V_d is the displaced or swept volume. Rewriting (16):

$$V_c = \frac{V_d}{CR - 1} \tag{17}$$

The distance d can be expressed in terms of CAD (θ) where θ is equal to zero at TDC:

$$d = \frac{S}{2}\cos\theta + \left(l^2 - \frac{S^2}{4}\sin^2\theta \right)^{\frac{1}{2}} \tag{18}$$

The ratio of specific heats can be approximated by the following expression under the assumption that γ decreases linearly while the temperature increases:

$$\gamma = \gamma_0 - \frac{k}{100}\frac{T}{1000} \tag{19}$$

γ_0 is a reference ratio of specific heats at an temperature around 300 Kelvin and depends on gas composition, i.e. fraction of air, fuel and burnt gases. γ_0 is approximately 1.4 for air and decreases when air is mixed with fuel. A typical value for gasoline at a relative air fuel ratio of λ = 1 is 1.34 estimated over the compression stroke and expansion stroke. For lean mixtures using isooctane γ_0 is around 1.38. The constant k is in this work set to about 8.

4.1.1.1 Heat Transfer Model

In this work a heat transfer model has been applied to the heat release calculations. The model was developed by *Woschni* [52] with the aim to estimate heat transfer for turbulent flows over flat plates and in pipes. The model can be used for internal combustion engines with quite good accuracy for overall cycle heat transfer estimations. A downside with the model is that it does not take into account that combustion occurs at different locations at different time steps in the cycle even though HCCI is considered to be a fairly homogeneous combustion process in comparison to SI or Diesel combustion. The heat transfer from unburnt zones is quite

different from zones reacting or with burnt gases. The heat transfer from unburnt zones is quite different compared to reacting or burned gas zones. It is however almost impossible to predict where combustion starts and ends and therefore the model assumes a fully homogeneous combustion process which means that the temperature is uniform throughout the cylinder and the wall temperature is constant throughout the whole combustion chamber.
The energy loss to the walls can be expressed:

$$\frac{dQ_{HT}}{dt} = hArea_{wall}\left(T_{gas} - T_{wall}\right) \tag{20}$$

where

h = Heat transfer coefficient
$Area_{wall}$ = Instantaneous wall area
T_{gas} = In-cylinder gas temperature
T_{wall} = Wall temperature

Woschni's work mainly consisted of determining the heat transfer coefficient, h, by experiments and the following expression was derived:

$$h\left[W/m^2K\right] = CB[m]^{-0.2}\, p[kPa]^{0.8}\, T[K]^{-0.55}\, w[m/s]^{0.8} \tag{21}$$

where

C = Correlation coefficient for specific engine
B = Bore
p = In-cylinder pressure
T = In-cylinder temperature
w = Characteristic velocity

The characteristic velocity, w, can be expressed as:

$$w = C_1 S_p + 3.24 \cdot 10^{-3} C_2 \left(\frac{V_d}{V_{ivc}}\right)\left(\frac{p_f - p_m}{p_{ivc}}\right) T_{ivc} \tag{22}$$

where

S_p =Mean piston speed=2 Stroke x Engine Speed
V_d = Displaced volume
p_f = In-cylinder pressure with combustion
p_m = In-cylinder pressure without combustion
p_{ivc} = In-cylinder pressure at inlet valve closure (IVC)
T_{ivc} = In-cylinder temperature at inlet valve closure (IVC)
V_{ivc} = In-cylinder volume at inlet valve closure (IVC)
C_1 = Correlation coefficient for specific engine
C_2 = Correlation coefficient for specific engine

The in-cylinder gas temperature can be estimated from the measured pressure. Assuming that the gas composition is constant between IVC and EVO, the following expression can be derived from (4):

$$\frac{T_1}{\mathrm{p}_1 V_1} = \frac{T_2}{\mathrm{p}_2 V_2} = \ldots = m \cdot R = \text{constant} \tag{23}$$

When using the model there are several parameters that have to be estimated. The volume at IVC can be accurately calculated. The temperature and pressure at IVC have to be estimated from the measured inlet temperature and inlet pressure as mentioned earlier in the introduction to this chapter. Small losses are accounted for when the gas flows next to the inlet valves. From the in-cylinder pressure the in-cylinder temperature can be calculated using (4). The three major tuning parameters are C, C_1 and C_2. Since the original values for these parameters were correlated for a diesel engine by *Woschni* they are expected to be different depending on the combustion process and engine since heat transfer characteristics will differ. The parameters to tune except the coefficients for the *Woschni* heat transfer model are:

- CR
- TDC offset
- Temperature and pressure at IVC.

The compression ratio is calculated from the geometry of the combustion chamber and is quite accurate. The temperature and pressure is estimated from the measured inlet conditions with a small pressure drop over the inlet valves and heat transfer compensation. The crank angle encoder used to find TDC is very difficult to mount 100% correctly. Therefore the TDC offset is used to compensate this error. However if the TDC offset is wrong the impact on IMEP and engine efficiency is large. A motored pressure trace is used to tune the model to zero heat release since no fuel is injected into the engine. The intake conditions should be as close to the fired conditions as possible for high accuracy. For the fired cycles the heat release including the heat transfer model is tuned in such way that the heat release trace after finished combustion is horizontal. If the heat release trace is still increasing at this stage, this will introduce an error in the calculation of crank angle of 10%, 50% and 90% burned, i.e. CA10, CA50 and CA90. To validate the maximum accumulated heat release calculated with the model the values are compared with the amount of fuel injected per engine cycle measured by a balance times the lower heating value of the fuel times the combustion efficiency which can be calculated from the emissions.

Figure 13 shows the in-cylinder pressure, in-cylinder temperature, rate of heat release and accumulated heat release as function of CAD calculated using the model described in this section. The markers seen in the accumulated heat release trace correspond to 10%, 50% and 90% heat release. The crank angle of 50% heat release, CA50, is used as a measure of combustion phasing. In a similar way CA10 and CA90 mean the crank angle of 10% and 90% heat release respectively. The combustion duration is defined as:

$$CombustionDuration = CA90 - CA10 \tag{24}$$

In the example shown in Figure 13, CA10 was 6.4 CAD ATDC, CA50 was 8.8 CAD ATDC and CA90 was 12.4 CAD ADTC. The combustion duration was 6 CAD. The combustion

event is distinctively seen in the pressure trace, temperature trace and in both the rate of heat release and accumulated heat release.

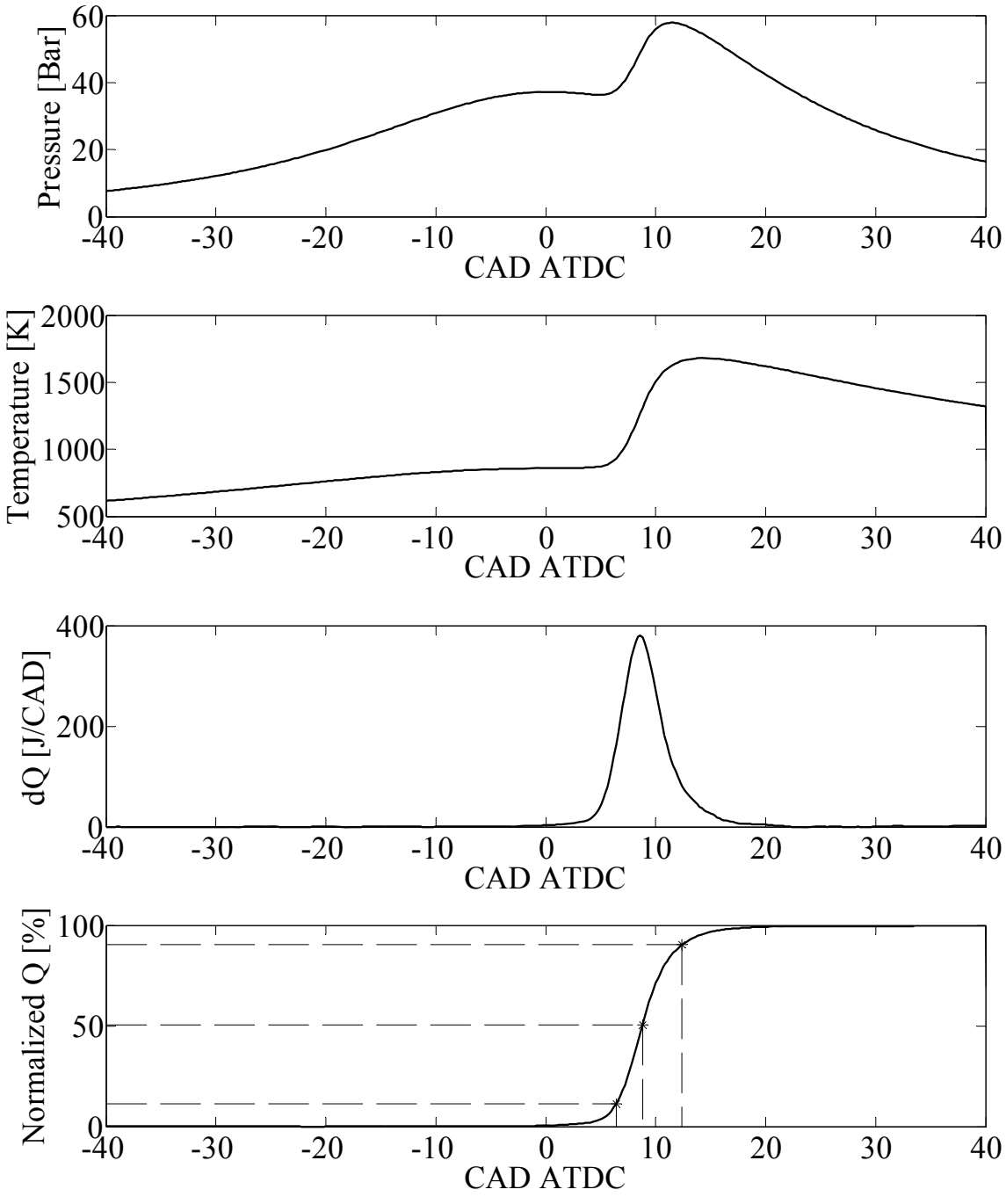

Figure 13: In-cylinder pressure, in-cylinder temperature, rate of heat release dQ and normalized accumulated heat release Q with markers showing 10%, 50% and 90% heat release, all as function of CAD. The engine used in the experiments was the Scania D12 HCCI engine with 18:1 in CR using ethanol as fuel. The engine speed was 1200 rpm, λ was 2.3, inlet air temperature was 125ºC and the load was 4.5 bar $IMEP_{net}$.

4.1.2 Other Definitions based on Pressure Measurements

Substantial information can be derived from the pressure measurements along with emissions and fuel consumption measurements. The heat release has been mentioned earlier but there are other parameters that are useful to calculate. Since the engines used in this work are 6-cylinder engines converted to single cylinder operation while the rest of the cylinders are motored the brake power is not a representative value of engine performance since there is only power produced by one cylinder alone but the friction losses are related to all the cylinders. Therefore indicated values are used in this work which can be calculated from the measured in-cylinder pressure. The engine load is calculated as the indicated mean effective pressure, *IMEP*:

$$IMEP = \frac{\int pdV}{V_d} \approx \frac{\sum p_k \Delta V_k}{V_d} \tag{25}$$

Two different *IMEP* definitions are seperated, $IMEP_{net}$ and $IMEP_{gross}$. $IMEP_{net}$ is calculated over the entire engine cycle while $IMEP_{gross}$ is calculated only over the compression and expansion strokes. The difference between $IMEP_{net}$ and $IMEP_{gross}$ is the pumping mean effective pressure, i.e. the work used to exhaust the burned gases from the previous cycle and induce the fresh air/fuel mixture:

$$PMEP = IMEP_{gross} - IMEP_{net} \tag{26}$$

The amount of fuel energy put in to the engine can be expressed as a mean effective pressure, FuelMEP:

$$FuelMEP = \frac{m_f Q_{LHV}}{V_d} \tag{27}$$

where

m_f = Mass of fuel
Q_{LHV} = Lower heating value of fuel
V_d = Displaced volume

By the knowledge of how much fuel energy that has been put into the engine and the measured unburned products in the exhaust the combustion efficiency can be calculated as:

$$\eta_{comb} = 1 - \frac{\sum m_i Q_{LHV,i}}{m_f Q_{LHV}} \tag{28}$$

where m_i is the mass of each unburned product in the exhaust and $Q_{LHV,i}$ is the lower heating value for each of the unburned products. The measured unburned products used to calculate the combustion efficiency are unburned hydrocarbons (UHC) and carbon monoxide (CO).

The combustion efficiency and FuelMEP can be used to calculate the heat release mean effective pressure:

$$QMEP = FuelMEP \times \eta_{comb} \tag{29}$$

If the model used for the heat release calculation described previously is well tuned the accumulated heat release normalized with the displaced volume should be equal to *QMEP*. This is a model tuning criterion.

By the use of FuelMEP and QMEP the efficiencies of the engine can be calculated. The net indicated efficiency is defined as:

$$\eta_{i,net} = \frac{IMEP_{net}}{FuelMEP} \tag{30}$$

The indicated efficiency describes how much work the engine delivers related to the energy of fuel put in. The thermal efficiency describes how effectively the heat released from combustion is converted to indicated work. The thermal efficiency is calculated from $IMEP_{gross}$:

$$\eta_T = \frac{IMEP_{gross}}{QMEP} \tag{31}$$

Lastly, the heat losses to the walls calculated from the *Woschni* model can be expressed as a mean effective pressure:

$$QHTMEP = \frac{Q_{HT}}{V_d} \tag{32}$$

4.1.3 Knock in SI Engines

In the SI engine there are basically two ways to ignite the premixed charge. The common and desired way of ignition is by a spark. The spark is generated by a spark plug and will cause a turbulent flame to consume the unburned gas. Another way of igniting the charge is the highly unwanted spontaneous combustion. Spontaneous combustion occurs when the unburned gas is exposed to high pressures and temperatures during a considerable amount of time. The auto ignition most often takes place after the spark from the spark plug has started the reactions in the unburned gas surrounding the plug. By igniting a part of the charge and letting the flame start to propagate the regions which have not yet been reached by it will experience yet higher temperature and the unburned gas region is more likely to ignite spontaneously. So, it is possible to have two combustion processes occurring at the same time, one flame propagating in an orderly fashion and one rapid spontaneous combustion.

When the unburned gas ignites spontaneously the heat release is tremendously rapid, almost instantaneous. The rapid heat release will, in its turn, cause a rapid pressure and temperature rise locally and will cause an inhomogeneous pressure distribution in the cylinder. Due to the inhomogeneous pressure distribution an oscillation phenomenon on the pressure trace can be observed.

Now, the oscillating phenomenon described is commonly known as knocking and is in many ways of great interest to SI engine engineers. The compression ratio has a great influence on knock. Using a too high CR will expose the unburned charge to higher temperatures and

pressures, increasing the risk for unwanted rapid, spontaneous combustion. On the other hand, using a too low compression ratio the thermal efficiency of the engine will drop [5] so the challenge is to operate the engine as close to knocking conditions as possible, without crossing the limit into knock territory. The theoretical maximum thermal efficiency, as demonstrated by [54] among others is calculated:

$$\eta_T = 1 - \frac{1}{CR^{\gamma-1}} \tag{33}$$

So why is it so unwanted for an engine to knock? Well, there are basically two major reasons:

- When knocking, the engine will exhibit a dramatic increase in heat exchange to the combustion chamber walls. Running the engine over a substantial amount of time under these circumstances will eventually cause the engine hardware to reach temperatures far above the recommended level. Eventually the structural strength of the engine components will fail due to the high temperatures and result in an engine breakdown. In HCCI engines the indicated efficiency is known to decrease substantially during running conditions that provoke pressure oscillations in the combustion chamber due to increased wall heat transfer [42].

- When a pressure wave leaves a larger sized crevice and enters a smaller one, its amplitude will increase. Theory suggests that the amplification factor of the amplitude can reach as high as 10. In an SI-engine with squish surfaces and top-land crevices the oscillating waves will undergo two amplifications before eventually reaching the top piston ring. When the wave is reflected from the piston ring the amplitude will increase once again, this time an amplification factor of 2 is suggested. All this means that not a whole lot of pressure oscillation is required in the open combustion chamber to cause large damage to piston rings and piston rims. And, of course, destruction of a piston or a piston ring is very severe and an expensive affair to repair.

4.1.4 Acoustic Vibration Theory

The frequencies at which the engine knocks are determined by the acoustic vibration modes specific to the combustion chamber. When the charge ignites spontaneously a high rate of heat is released. The amount and high rate of energy released will in its turn excite specific vibration modes. These modes cause pressure waves to traverse the combustion chamber at the local speed of sound, i.e. the acoustic velocity [54 - 56]. The modes can be of both circumferential and of radial nature. For passenger sized engines the generated frequencies are in the range of 6 to 20 kHz [5]. Since the experimental part of this work is conducted on a large bore heavy duty Diesel truck engine these frequencies should be somewhat lower.

To calculate the vibration mode frequencies for complex combustion geometries is quite complicated. The calculations are suitable for numerical CFD or FEM computer software. But, for a simple cylindrical combustion chamber the vibration mode frequencies can be calculated analytically using *C.S. Draper's* acoustic pressure wave formula [56]:

$$f_{m,n} = \frac{C \cdot \rho_{m,n}}{\pi \cdot B} \tag{34}$$

where:

$f_{m,n}$ = specific vibration frequency for mode m, n [Hz]

C = local speed of sound [m/s]

$\rho_{m,n}$ = vibration mode factor

B = cylinder bore [m]

m = circumferential mode number

n = radial oscillation mode number

And further, the vibration mode number for a cylindrical chamber:

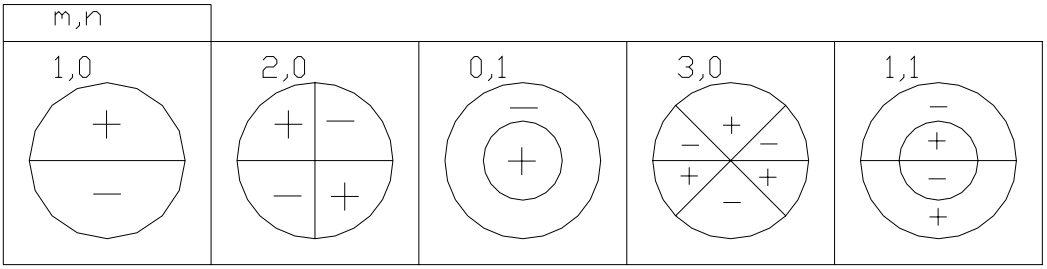

$\rho_{m,n}$	1.841	3.054	3.832	4.201	5.332

Figure 14: The different mode shapes with accompanying mode factors for a cylindrical chamber.

In the *Draper* equation, the axial vibration modes are neglected because of the small height of the combustion chamber compared to the bore.

While studying the Draper equation one can note that C, the speed of sound, is a key factor in determining the acoustic vibration frequencies. Assuming that the premixed charge behaves like an ideal gas, an assumption that is not that far fetched, it is well known that [57]:

$$C = \sqrt{\gamma \cdot R \cdot T} \tag{35}$$

where:

γ = ratio of specific heats = $\dfrac{C_p}{C_v}$ = temperature dependant

R = gas constant for air = $\left[\dfrac{R_{Universal}}{M_{Air}}\right] = 2.869 \cdot 10^2\ J/kgK$

T = temperature

As one can clearly see, the speed of sound is not constant in the combustion chamber during engine operation and therefore needs to be investigated further.

In the equation for the speed of sound the ratio of specific heats is mentioned. The ratio of specific heats, γ, is a temperature dependent variable, see equation 19. For a deeper understanding and further information on the approximation of the ratio of specific heats, the interested reader is referred to the work of *Heywood* [5].

The in-cylinder temperature is also needed for the calculation of γ and the speed of sound. The temperature affects the acoustic velocity C, as well as the ratio of specific heats, γ. Assuming that the gas composition is constant between IVC and EVO, Equation 23 can be used to calculate the temperature trace from any given pressure data. Shown in Figure 15 are two examples of how the temperature varies inside the combustion chamber between IVC and EVO. Now that all variables and constants are known, the speed of sound in the combustion chamber can be estimated. Please note that the calculations of the speed of sound are based on estimates and rough approximations. The result for a motored and fired cycle can be found in Figure 16.

The speed of sound varies in the combustion chamber during the pressure variations from compression, expansion and ignition. Therefore the frequencies associated with the acoustic vibration modes, as proposed in the *Draper* equation, will vary also. For any engine cycle some sort of median vibration frequency needs to be extracted in order to let any comparison between theoretical frequencies and experienced frequencies take place. So for any case studied, air/fuel ratio, inlet temperature et cetera, a corresponding acoustic vibration frequency needs to be calculated for that specific case. Examples on how the acoustic vibration frequencies vary for a fired engine cycle are shown in Figure 17.

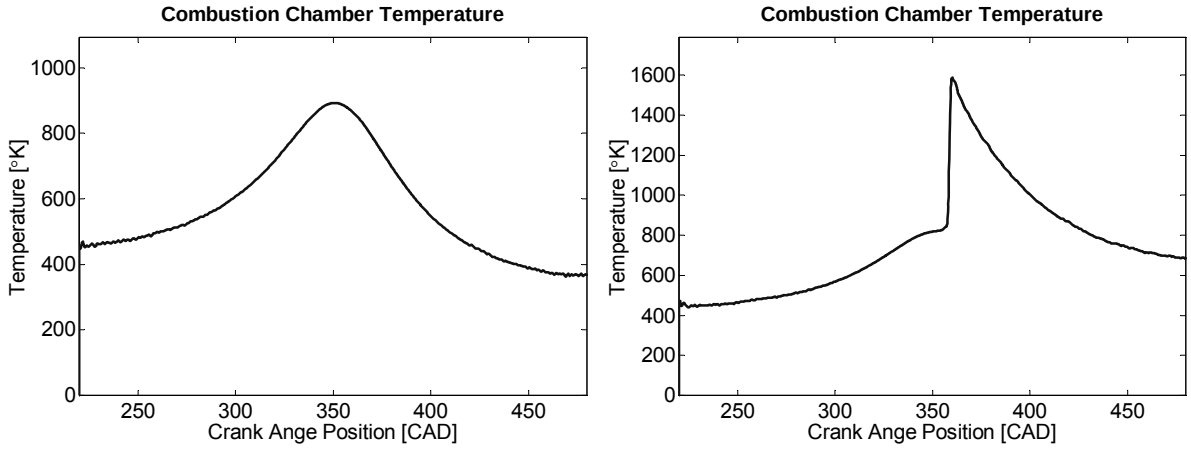

Figure 15: The combustion chamber temperature as it varies between IVC and EVO for a motored (left) and a fired (right) engine cycle.

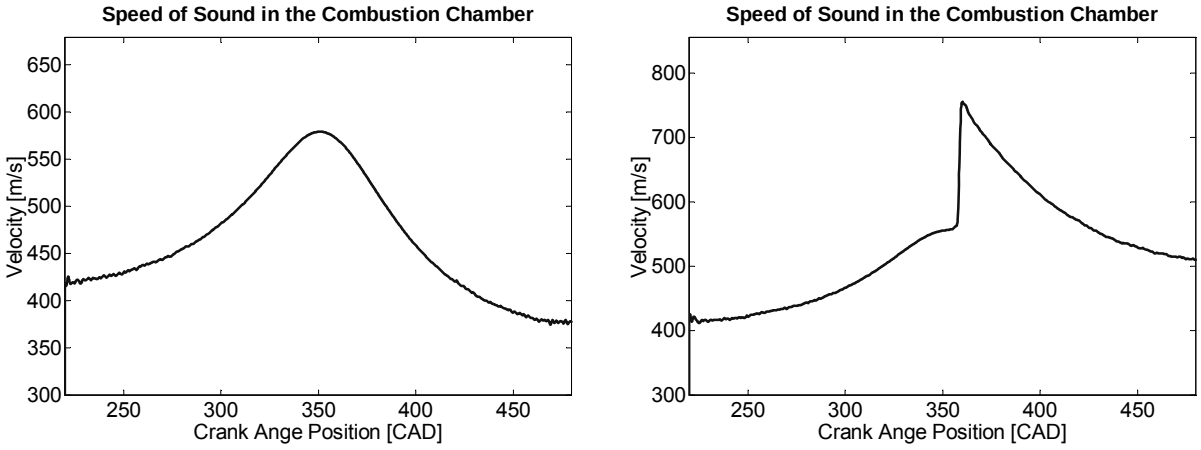

Figure 16: The speed of sound as it varies during a motored (left) and a fired (right) engine cycle.

Over the CAD window where the pressure oscillations appear, mean theoretical frequencies for each vibration mode are calculated in order to compare with the measured frequencies from the pressure trace. Despite being derived from an arbitrary engine cycle Figure 17

suggests that the theoretical frequencies experienced in the Volvo TD100 engine with a 120.65 mm bore are in the range of 3-11 kHz. As mentioned earlier the frequency range in passenger car sized SI engines are in the range of 6-20 kHz, which as suspected is higher than the theoretically calculated frequencies for the Volvo TD100 engine, mainly due to the large bore of the heavy duty truck engine.

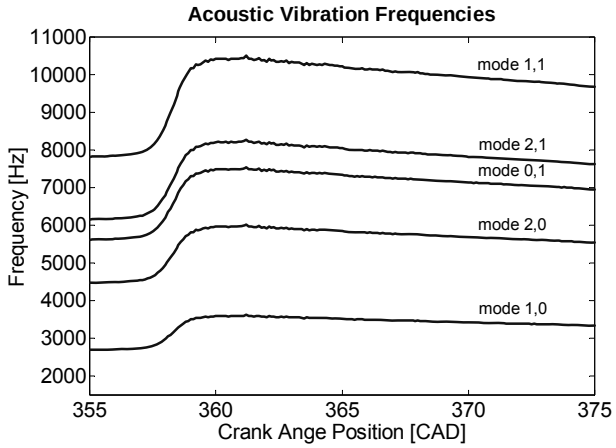

Figure 17: Figure showing the theoretical acoustic mode frequencies as function of CAD for a fired engine cycle.

4.2 Ion Current Diagnostics

4.2.1 Why use Ion Current?

Ion current has been used as a tool to monitor the combustion process in SI engines for a long time [58 - 62]. Information that can be found from the ion current is for example misfire or knock conditions. The technique is cheap since the probe used for measurements is the spark plug which already is used for the spark discharge to initiate combustion. In addition to misfire and knock, information regarding the combustion phasing is needed in HCCI engines. In SI engines the onset of the combustion process is controlled by the spark and in DI Diesel engines by the injection of fuel. Since the only thing controlling the combustion in HCCI engines is the pressure and temperature history during compression, some sort of feedback sensor is needed as guidance for changing the operational parameters to either advance or retard the combustion phasing. Commonly used is the piezoelectric pressure transducer but it is expensive and demands modifications to the cylinder in order to be mounted which makes it less viable for a production HCCI engine. By the use of ion current measurements through the spark plug a cheap probe for combustion feedback can be obtained.

4.2.2 Ion Current Theory

During combustion of fuel and air, chemical reactions occur that will result in dissociation and ionization. The energy that is released during the process can be high enough to ionize one of the reaction products which will produce free electrons. This is called the chemi-ionization mechanism [63 - 65]. The first reaction producing ions (CHO^+) in hydrocarbon/air flames, is

$$CH + O \rightarrow CHO^+ + e \quad (1),$$

followed by the proton transfer reaction producing the most common ion H_3O^+:

$$CHO^+ + H_2O \rightarrow H_3O^+ + CO \quad (2)$$

The reason for H_3O^+ occurring in larger concentrations than the CHO^+ ion is that Reaction 2 is very fast and thus as soon as CHO^+ is formed in Reaction 1 it is also consumed in Reaction 2 [65]. Lastly the slower recombination Reaction (3) consumes the H_3O^+ ion. Since this reaction is slow the H_3O^+ ion can be found far into the post flame region.

$$H_3O^+ + e^- \rightarrow H_2O + H \quad (3)$$

Another process of producing ions in flames is thermal ionization. This happens when the combustion temperature has increased further as the combustion proceeds. During this combustion phase, collisions between particles lead to the formation of pairs of ions and electrons [66]. The thermal ionization is heavily temperature dependant while the chemical ionization is affected more by air/fuel ratio [63, 64]. It should be mentioned that this theory is based on the chemical reactions in a sharp flame front. With HCCI combustion the combustion is characterized by gradual oxidation of the fuel with a weaker border between burned and unburned zones. Therefore it is hard to state that the chemical ionization theory is entirely valid for HCCI combustion.

If applying a DC voltage over a certain gas volume in the combustion process an electric field is generated which promotes the movement of ions. The movement is seen as a current which can be measured. An example of an ion current trace in an SI engine is seen in Figure 18 [67]. The first two distinct peaks are related to the spark ignition system for coil charge and spark discharge. Closely after the spark discharge the actual interesting part of the ion current measurement is seen. Two peaks are found with a time separation. The first peak reflects the conditions in the flame front as it passes the spark plug electrode gap and is due to the chemi-ionization process. The second peak appears when the flame has passed the electrode gap and therefore burned gases are present. The post-flame region with burned gases reflects the thermodynamical state of the combustion volume and therefore the second ion peak is mostly related to thermal ionization. The shape and signal level of the two peaks are related to the air/fuel ratio of the charge and the combustion temperature in the flame as well as in the post-flame region. Since most SI engines run at stoichiometric mixture proportions at all loads, a change in load results in a change in density of the charge. More fuel reatcs in the flame front which in turn results in higher temperatures for higher loads. Due to the running conditions in SI engines, the ion current signal strength is usually very good.

Applying ion current in HCCI engines might be challenging since the mixture is lean and/or diluted with low combustion temperature which may not be favourable for the chemical nor the thermal ionization process.

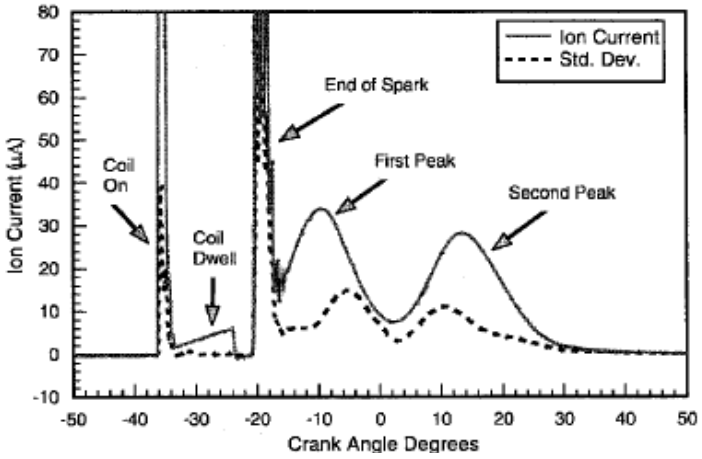

Figure 18: An example of ion current trace in an SI engine [67].

4.2.3 Ion Current with HCCI Combustion

In Paper 2 it was found that ion current sensing can be used for HCCI combustion feedback with a relative air/fuel ratio (λ) of 1.2 or richer. The limitation in relative air/fuel ratio was mainly due to low in-cylinder temperatures in combination with low amounts of fuel at low loads, decreasing the ionization process. Further it was found that only one ion current peak exists. Since the combustion in an HCCI engine is a gradual oxidation process at many locations simultaneously the heat release is locally slow, but globally fast. Thus, both types of ionization might be present since the reaction zone is gradually formed in one location and coexists with the burned gases. The ion current appearance was correlated with the in-cylinder pressure and heat release. Different parameters describing the combustion process and ion current trace shape were compared, as maximum ROHR, maximum pressure and CA50 with maximum ion current amplitude and so on. The best correlation was found between CA50 and ion50 which is the crank angle position for 50% of the maximum ion current amplitude. The correlation coefficient was around 0.87. Later, *Strandh* et al. [69] successfully used the ion current signals obtained in the TD100 engine for cycle to cycle control of the HCCI combustion phasing.

In the work by *Aulin* et al [70] the ion current appearance was investigated for spark assisted HCCI combustion. When running the engine in spark assisted mode, two peaks were found, as in SI engines. This is not so strange since flame propagation is present in the first stages of combustion and as the global pressure and temperature is increased the rest of the charge auto ignites. As described before, the ionization in the flame front is quite fast and appears in the vicinity of the spark plug while it is suspected that the auto ignition is present further away form the spark plug; therefore the second peak appears later.

A solution to the low load problem of using ion current feedback control of HCCI combustion may be throttling of the intake air. By using throttling with constant fuel rate lambda will decrease meaning that the mixture will be richer. When running the engine under these conditions the combustion efficiency will improve due to the richer mixtures. To sustain auto ignition the inlet air temperature has to be increased. However the pumping losses will increase due to higher exhaust pressure compared to intake pressure. These two effects counteract each other and the indicated efficiency is not changed compared to unthrottled operation with leaner mixtures. This has been shown by *Hyvönen* et al. [35]. An advantage with this type of operation is that the mixture is richer, producing more ions and thus higher

ion current signal, at about the same in-cylinder temperature without any loss in engine efficiency. However, this method has not been tested by the author and is left to be investigated in the future work at the division.

4.2.4 Measurement Technique

In Figure 19 a schematic of the ion current sensing system can be found. The principle of ion current measurement is that a voltage (U), in these studies 85 volts, is applied over the spark plug gap. The ion current is measured by measuring the voltage over a resistance (R) inserted in the electrical circuit. During this work a resistance of 100 kΩ was used. The obtained signal is usually weak, in the range of a few microamperes and has to be amplified (A). An amplification factor of 20 was selected. The signal is then sampled by an A/D sampling board in a computer. For each spark plug used for ion current measurements a separate ion current sensing system is used, in addition to the computer where all the data is stored.

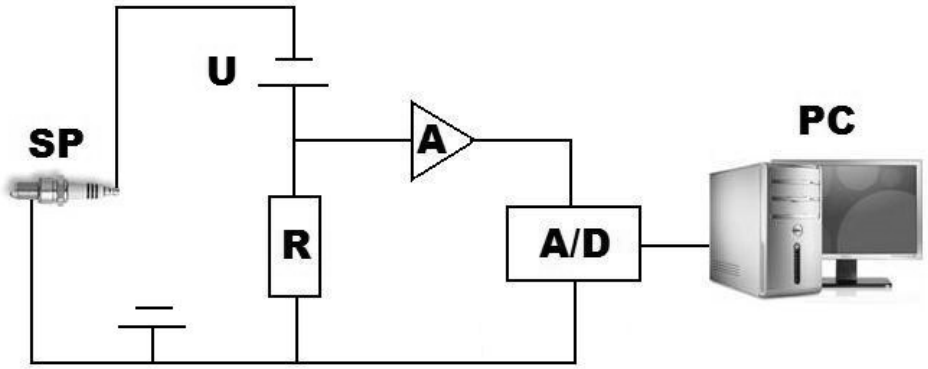

Figure 19: Schematic of a simple ion current measurement system including spark plug (SP), power source (U), resistance (R), amplifier (A), analogue to digital sampling board (A/D) and the personal computer (PC).

4.3 Chemiluminescence Imaging

Chemiluminescence imaging or in other words flame photography is an optical diagnostic technique used to study combustion processes in internal combustion engines as well as in other research areas were combustion studies are of interest. Chemical reactions during combustion of air/fuel mixtures emit light that can be captured by a high speed camera. The chemiluminescence intensity is known to be strongly coupled with the local heat release in the reaction zone [74]. It is possible to retrieve information about the global and local combustion process as flame front propagation, shape and thickness. Chemiluminescence imaging has also been used to successfully study the gradual oxidation process during HCCI combustion [8, Paper 5-7].

The camera used in the studies presented in this text is a *Phantom v7.1* from *Vision Research.* The maximum resolution of the camera is 800 x 600 pixels and the temporal resolution is increasing with decreasing spatial resolution. When the camera was used in this work the spatial resolution was around 300 x 300 pixels and the temporal resolution was in the range of 24 kHz. This corresponds to four images per CAD with a pixel size of 0.4 x 0.4 mm at an engine speed of 1000 rpm. This temporal resolution is close to the one used for the pressure measurement which was five samples per CAD. The temporal resolution of the camera should

be enough to cover the fast process of HCCI combustion. A *Hamamatsu* image intensifier has also been used to intensify the rather weak light from the combustion. What has to be taken into account is that chemiluminescence imaging is a line of sight method, meaning that the signal level is the integrated sum of the emitted light in the line of sight.

4.4 Planar Laser Induced Fluorescence (PLIF) Imaging

Planar laser-induced fluorescence (PLIF) imaging is a laser-based optical diagnostic technique, commonly used for measuring species distributions with high spatial resolution in combustion processes. The basic principle is that a laser beam is converted to a narrow laser sheet by means of cylindrical- and spherical lenses. The laser sheet is directed into the gas in a combustion process. When the laser radiation enters the gas, molecules of certain species are excited to higher energy states through absorption of laser photons. The wavelength of the laser radiation is adapted to the specific wavelength at which the species of interest is excited. When the species is excited to a higher state the molecule is unstable and therefore returns to its ground state. During this transition, the excess energy is released as radiation, i.e. fluorescence. In general, the fluorescence wavelength is shifted towards longer wavelengths as compared to the incident light. An image-intensified CCD (Charge Coupled Device) camera can then be used for detection of the LIF signals. By recording images perpendicular to the laser sheet the species distribution over the sheet is captured. By employing a high-repetition-rate laser system, the species distribution can be followed in time. In Paper 5 PLIF imaging has been used to study the formaldehyde distribution during HCCI combustion. The formaldehyde is formed during low temperature reactions around 20 CAD BTDC and consumed in the main heat release closer to TDC [46]. By synchronizing the PLIF measurement with the formaldehyde consumption in the main heat release the locations where the combustion starts can be studied. In Paper 8 PLIF imaging was used to follow the acetone consumption during the main heat release within a single-cycle event. Here acetone was used as a tracer of the main fuel, which was ethanol. The technique allows the fuel consumption to be spatially studied throughout the combustion chamber at different time steps in the combustion cycle.
For further insight into PLIF imaging the interested reader is referred to the work of *Olofsson* [75] and *Seyfried* [76].

5 Results

In this section the most important results from the enclosed papers in thesis are presented along with some new results from a recent study concerning combustion chamber geometry effects in HCCI combustion. Figure 20 shows the load ranges for each of the experiments performed with HCCI combustion. Paper 1 was a study on pressure oscillations during rapid HCCI combustion and was performed at fairly high HCCI loads. The combustion phasing was highly advanced to provoke knock-like combustion. Paper 2 – 4 was an investigation of the feasibility of using ion current sensing for feedback control. The load range for these experiments was limited by insufficient ion current signal levels at low loads and knock at high loads. The laser ignition studies in Paper 5 and Paper 6 were performed on the lean limit for flame propagation which means that the limitation in these experiments was towards minimum load. Optical diagnostics (Papers 5 – 8) in combustion engines is mainly limited in load due to mechanical stress on the optical parts and therefore this type of experiment has not been performed above 3.5 bar $IMEP_{net}$. The unpublished results on combustion chamber geometry effects were performed in the full load range of the Scania D12 HCCI engine with limiting factors as knock, noise and NOx emissions.

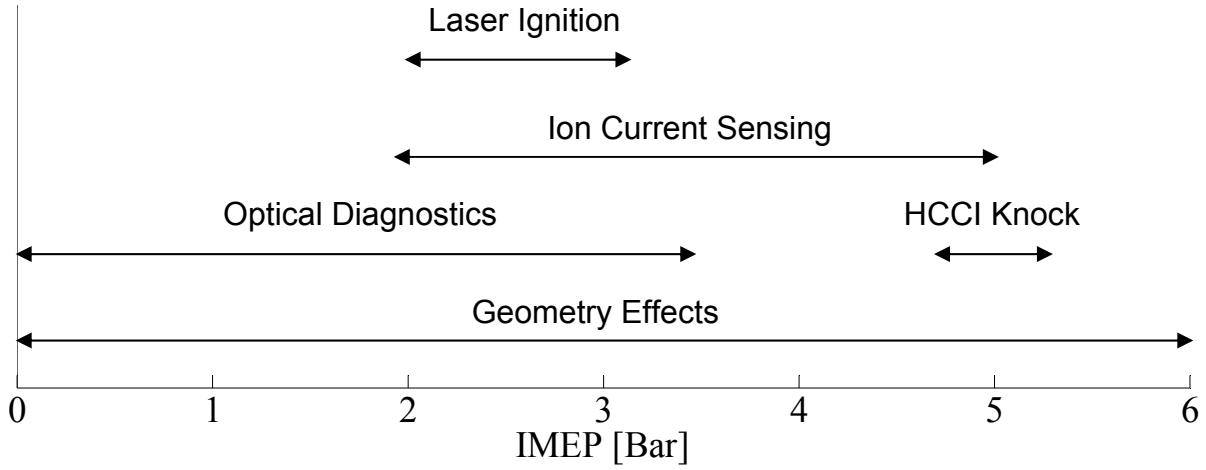

Figure 20: Graph showing the different HCCI loads tested during the experiments presented in this chapter.

5.1 HCCI Knock

The aim of the study presented in Paper 1 was to investigate the pressure oscillations seen in the pressure trace after a fast burning HCCI combustion process. It was believed that these pressure oscillations would have the same origin as those seen after knocking combustion in an SI engine i.e. excitation of the natural frequency of the cylinder by pressure waves. On the other hand should the combustion process in the HCCI engine should be close to homogeneous. Thus the pressure increase due to combustion should be uniform and hence no pressure wave should exist. Could it be that the very rapid pressure increase generates an impulse high enough to make the connecting rod vibrate? In this case the pressure should oscillate in phase in the entire cylinder.

In order to investigate the nature of the pressure oscillations during HCCI combustion with rapid heat release, a spacer design was manufactured allowing several pressure transducers to

be mounted in the same combustion chamber. This spacer was placed between the cylinder head and the engine block. Six pressure transducers were mounted in the spacer resulting in sensor locations in the topland volume. Two additional pressure transducers were mounted in the cylinder head, one along the bore axis and one with a slight offset, allowing pressure measurement in the bulk of the combustion chamber. A drawing of the spacer can be found in Figure 21. The engine used for the experiments was the Volvo TD100 engine with a disc shaped combustion chamber and the compression ratio was set to 17.5:1. The fuel used was isooctane.

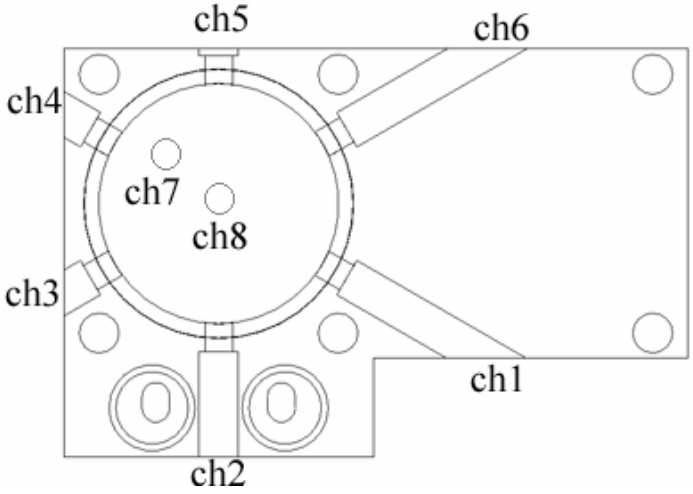

Figure 21: Drawing of the spacer with the locations of the six pressure transducers along with the corresponding locations of the pressure transducers mounted in the cylinder head.

During the experiments the engine was run with rich mixtures and high load in combination with early combustion phasing to provoke high peak in-cylinder pressure and temperature leading to knock-like combustion. The engine speed was 1000 rpm, $\lambda = 2.58$ and CA50 at 0.2 CAD ATDC. The engine load was around 5 bar $IMEP_{net}$ as seen in Figure 20.

Figure 22 shows eight pressure traces for a single cycle. As seen the pressure did not oscillate in phase and thus it was very likely that the traditional pressure wave theory would be applicable also for rich HCCI combustion. It is rather hard to extract information from Figure 22, as the eight traces tend to overlap. Three groups of pressure transducer locations could be defined, where the pressure traces oscillate in-phase in each group. Group one consists of Channel 1, 2 and 6. Group two consists of Channels 3, 4, 5 and 7. The third group is not really a group since it only has one member, Channel 8. Overall the pressure traces oscillate in counter-phase between Groups 1 and 2. Figure 23 shows pressure traces for one representative of each group, Channels 1, 4 and 8. Here it is seen that the pressure traces for Channel 1 and 4 oscillate in a counter phased fashion, suggesting that the pressure should oscillate between Channels 1 and 4. This direction of the oscillations was found to be very random from cycle to cycle but a slight preference for the direction in Figure 23 could be detected.

From Figure 23 it can be seen that the oscillations of Channel 8 have much lower amplitudes compared to Channels 1 and 4. The explanation can be found in the pressure wave theory suggesting an increase in amplitude when the pressure wave is leaving a large space entering a small space. According to energy conservation laws, the energy a pressure wave represents is constant and related to the volume in which it traverses. Pressure wave energy is in turn a

result of frequency and amplitude. Since the frequency is constant for a given space, governed by the acoustic velocity, the amplitude will vary.

Since Channel 8 is in the bulk of the combustion chamber and Channels 1 and 4 are in the topland volume which is smaller than the bulk, the amplitude of the pressure waves will therefore also be smaller in the bulk of the combustion chamber. Another explanation could be that Channel 8 is located in a nodal point of the oscillations.

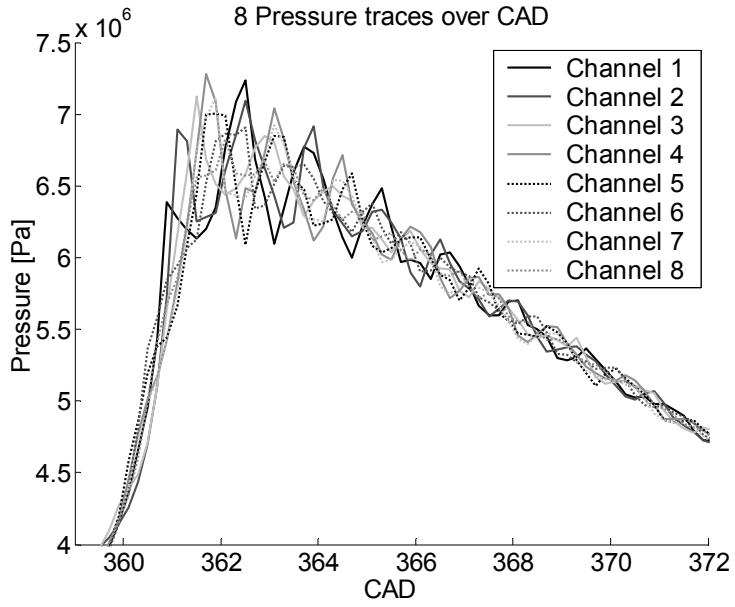

Figure 22: Eight pressure traces for different pressure transducer locations as function of CAD.

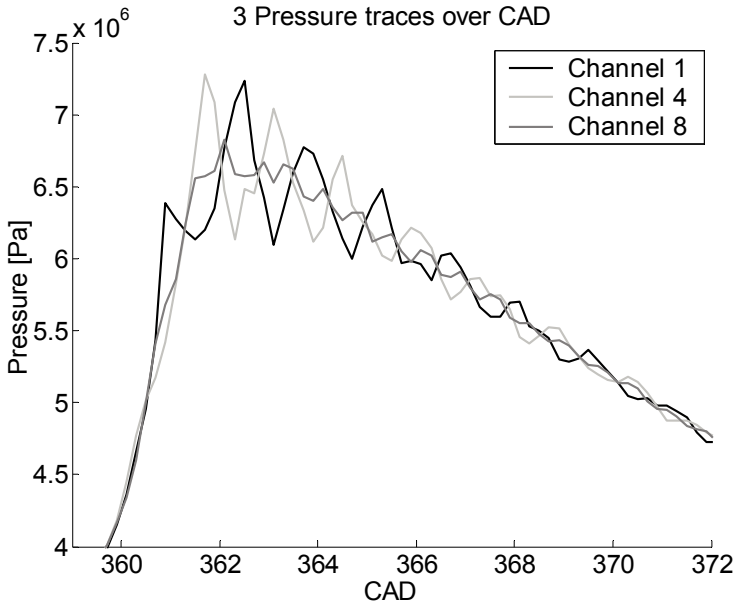

Figure 23: Three pressure traces showing counter phase wave oscillations.

5.1.1 Frequency domain

Now that it has been established that pressure oscillations and thus pressure waves exist during rapid HCCI combustion it is of interest to see what their nature is and if they can be compared to SI knock theory. Thus the frequency content of the pressure oscillations has to be calculated. The power spectral density (PSD) of the frequency content can be found in Figure 24. The engine speed was 1000 rpm, λ at 2.58 and CA50 at 0.2 CAD ATDC. Four acoustic frequency modes are present, 4.0 kHz, 6.9 kHz, 8.7 kHz and 12.2 kHz. None of these are multiples of each other suggesting that no overtone frequencies exist. The main HCCI oscillation frequency is at 4 kHz which has the largest amplitude. According to the theory the main frequency mode at 4 kHz should correspond to a pressure wave traversing the combustion chamber described by the acoustic vibration mode (1,0) in Figure 14. The explanation to several modes can be the presence of several pressure waves traversing and interfering through the cylinder as well as the knock frequencies changing with crank angle. The amplitudes depend on the strength of the signal, the duration and the frequency range it has. A very distinct first circumferential pressure oscillation mode during HCCI combustion as seen in Figure 24 has also been found by *Eng* [77] and *Andreae* et al. [78].

The filtered pressure traces for the CAD window where the oscillations occur can be found in Figure 25 and Figure 26. The pressure traces have been filtered using a *Butterworth* digital filter for each frequency domain of the four vibration modes as seen in Figure 24. By doing this the effect of decreased global pressure during the expansion of the gases which occurs with a low frequency is removed. As expected from the frequency domain plot the highest oscillation amplitudes are found in the first mode. The mean amplitude over the oscillation cycle in this case was 1.24 bar while the maximum amplitude was 3.94 bar. Decreased maximum and mean amplitudes are experienced with higher mode number. The frequency increases with the mode number and thus the period time decreases.

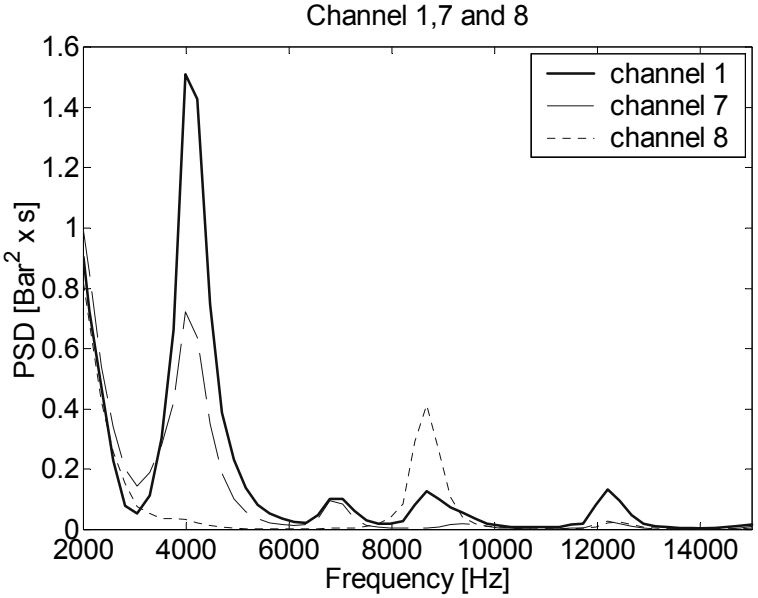

Figure 24: Frequency domain plot for three different sensor locations.

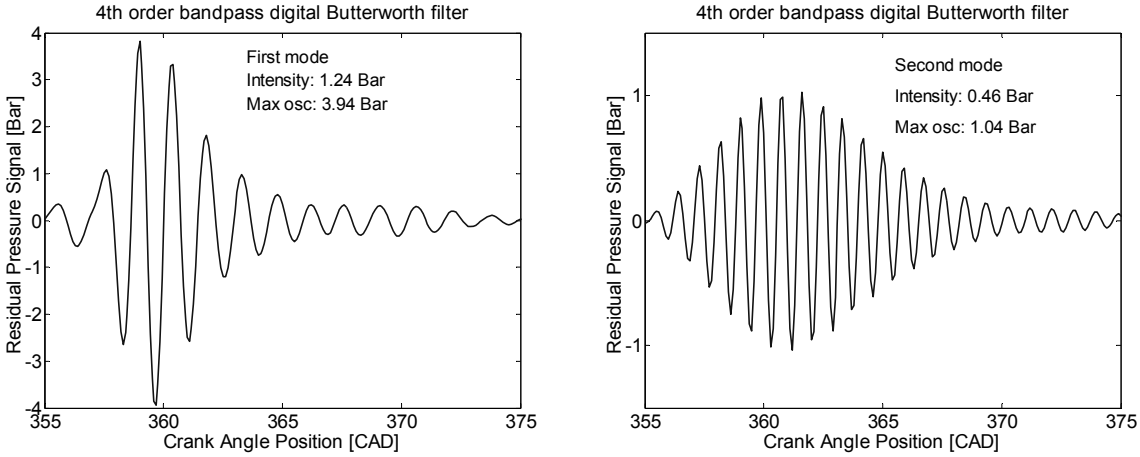

Figure 25. First and second Butterworth filtered frequency modes.

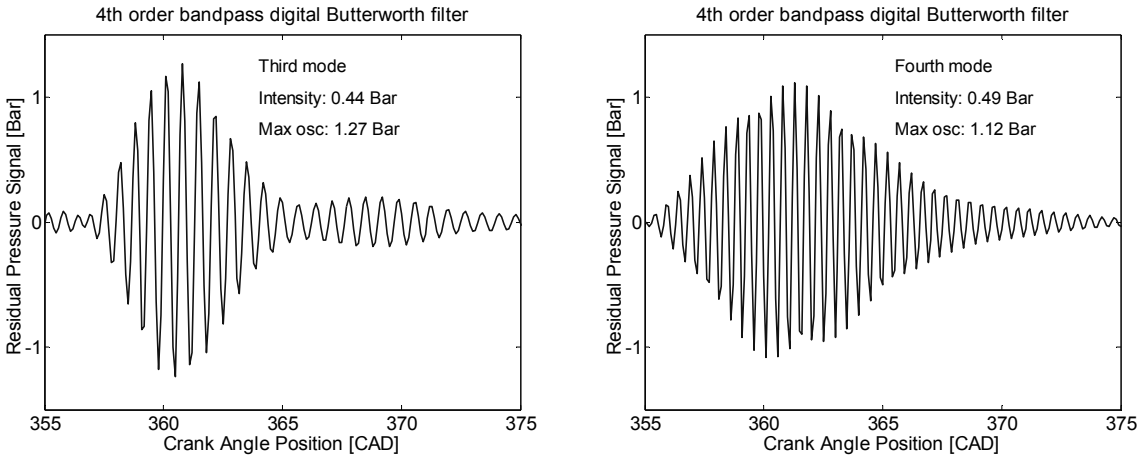

Figure 26: Third and fourth Butterworth filtered frequency modes.

5.1.2 The effect of Combustion Chamber Geometry

Two additional combustion chamber geometries were evaluated using the same technique as for the pancake geometry previously shown. The combustion chamber geometries can be seen in Figure 27, with a hill shaped piston to the left and a bowl shaped piston to the right. By using a bowl in piston geometry a small bore (87mm diameter) cylindrical combustion chamber is simulated. This geometry is expected to generate higher vibration frequencies than the disc case. The squish distance in both the hill and bowl cases was set to 1 mm in order to limit the combustion chambers to the volume around the hill and inside the bowl respectively.

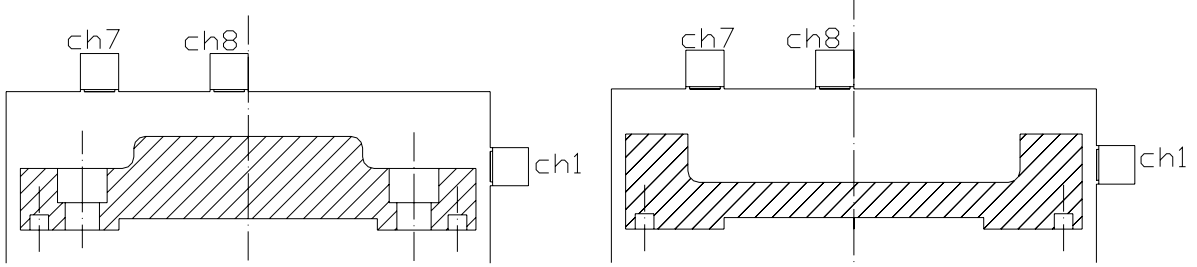

Figure 27: Drawings of the two additional combustion chambers tested. The hill shaped piston to the left and the bowl shaped piston to the right.

In Figure 28 the PSD plots for both the hill and bowl geometries can be found. As for the pancake case in Figure 24 Channels 1, 7 and 8 are presented. In the hill case the first vibration mode is found at 3.3 kHz which is slightly lower than for the pancake case, where the first mode was found at 4.0 kHz. As for the pancake case the first mode is found by Channels 1 and 7 but not by 8. The next two modes are found at 6.4 and 8.9 kHz. The 8.9 kHz mode is solely found by Channel 8. Regarding the bowl geometry two distinct modes are found at higher frequencies as expected, at 5.3 and 7.8 kHz. The first mode is seen by both Channels 1 and 7, while the second mode is seen only by Channel 1. Channel 8 shows virtually no intensities at any mode or frequency, probably due to the large damping volume it is exposed to.

Table 3: Operating conditions for the three combustion chamber studies.

Geometry	Engine Speed [rpm]	λ	T_{Inlet} [°C]	CA50 [CAD ATDC]
Pancake	1000	2.48	177	0.2
Hill	1000	2.50	178	0.4
Bowl	1000	2.50	181	0.0

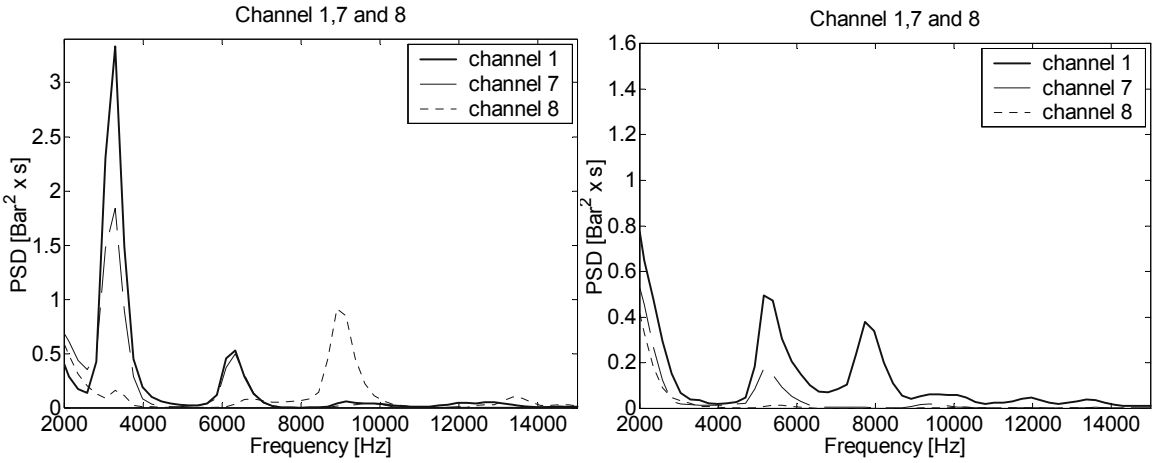

Figure 28: Frequency domain plots for the hill geometry to the left and the bowl geometry to the right.

From Figure 24 and Figure 28 it can be seen that there are large differences regarding the maximum amplitudes between the geometries. The hill shaped combustion chamber provokes the strongest oscillations with PSD values in the range of 3 bar^{2}s, followed by the pancake geometry with PSD values around 1.5 bar^{2}s, which is a decrease of 50%. For the bowl geometry the PSD value is only about 0.5 bar^{2}s. By comparing these values it is shown that the combustion rate is much lower for the bowl case compared to the pancake case. This means that the pressure derivative must be lower by using the bowl geometry for the same compression ratio. Since the pressure derivative limits the possible load range, it is suggested that by using the bowl the load range can be extended.

To summarize the study on the effect of combustion chamber geometry on pressure oscillations during rapid HCCI combustion, a comparison between theoretical and experienced frequencies is needed. For each geometry case the temperature has been estimated using the method described earlier with the ideal gas law. The estimated cylinder temperature is then used to find the local speed of sound and thus the theoretical frequencies for each vibration mode according to the *Draper* formula can be calculated. See Section 4.1.4 for details. In the bowl case a smaller diameter has been used for the calculations since the

bowl itself can be interpreted as a small bore combustion chamber. In the hill case no theoretical frequencies have been calculated. This is due to the complex shape of the combustion chamber demanding a numerical method to be applied in order to quantify the theoretical frequencies. The result of the comparison can be seen in Figure 29 for the three combustion chamber geometries. The correlation between the theoretical and experienced frequencies is very good for the pancake case. Slightly lower theoretical frequencies compared to the experienced frequencies are seen. The vibration mode 3.0 has not been found in the experienced frequency domain, which makes it an outliner in the figure. If this vibration mode is neglected the correlation coefficient is close to 100% in the pancake case. In the bowl case the theoretical frequencies are slightly higher than the experienced frequencies, with a correlation close to 97%, still a very good result.

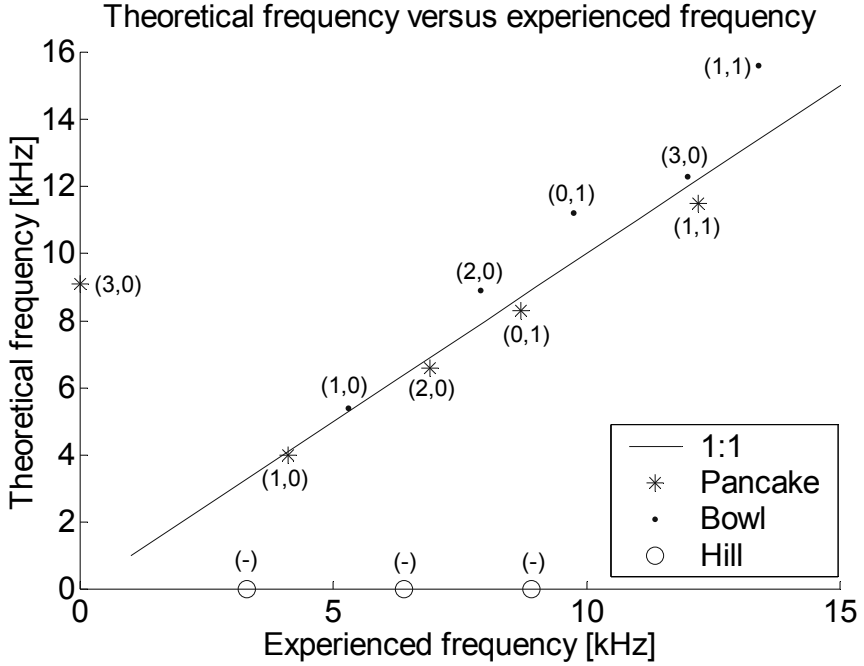

Figure 29: Plot showing the correlation between the theoretical and experienced frequencies for the three combustion chambers studied.

As seen the pressure oscillations during rapid HCCI combustion show good agreement with vibration mode shapes and frequencies suggested by acoustic vibration theory normally applied to SI engine knock. The effect of in-cylinder pressure sensor location is also of importance since the knock amplitude detected will be higher in the topland volume compared to the open combustion chamber, see Section 4.1.4. Knocking combustion in excess of the recommended limits could thus be achieved without being noticed if the pressure transducer is located in the centre of the combustion chamber.

5.2 Ion Current in HCCI Combustion

5.2.1 Effect of Sensor Location on Ion Current

In Paper 2 it was found that ion current can be used for HCCI combustion feedback with a relative air/fuel ratio of 1.2 or richer in the Volvo TD100 Engine. The load range tested during these experiments was limited in upper load due to knock and excessive noise and limited in lower load due to lack of ion current signal. The behaviour of the ion current signal for different HCCI operating conditions had to be further investigated. Also the suspicion that the ion current would be different depending on measuring location inside the combustion chamber arises since it could be influenced by stratifications in air/fuel ratio and temperature.

Therefore experiments were performed with a modified spark plug where the side electrode had been removed in order to measure the ion current in a larger gas volume. This measure was found to decrease the error in the combustion phasing calculated from the ion current (ION50) compared to the combustion phasing calculated from the pressure (CA50), see Figure 31. The signal level was also found to increase. Therefore it was decided to use modified spark plugs without side electrodes in the experiments of Papers 3 and 4. Even though these spark plugs measure over a larger gas volume it is believed that there still are large differences in thermodynamic conditions throughout the cylinder where the measurements have taken place. The definition of ION50 can be found in Figure 30. The ION50 is defined as the crank angle on the rising flank of 50% of the maximum ion current amplitude.

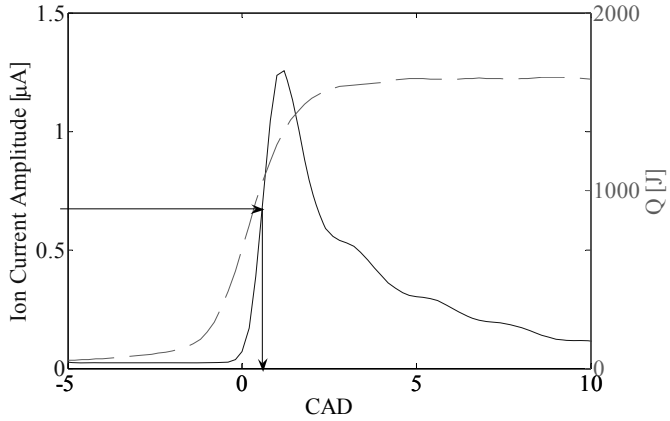

Figure 30: Ion current amplitude and heat release (Q) as function of CA50. The combustion phasing calculated from the ion current signal is marked with an arrow in the figure.

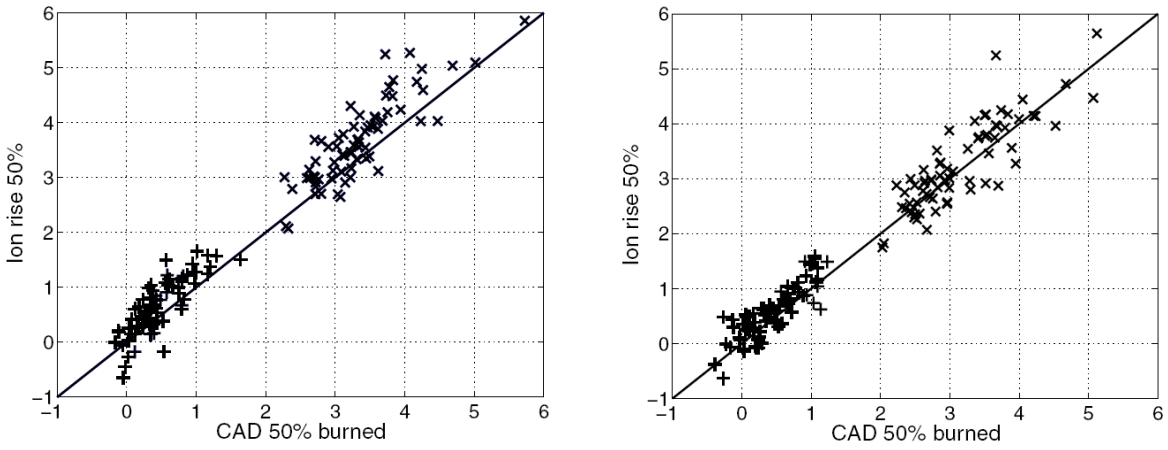

Figure 31. Correlation between ION50 and CA50 for the standard spark plug (left) and modified spark plug without side electrode (right). The overall correlation coefficient was 0.75 for the standard spark plug and 0.87 for the modified spark plug without side electrode.

In order to investigate the ion current at different locations throughout the combustion chamber the spacer geometry was used from the study on pressure oscillations. The spacer enabled seven spark plugs to be mounted in the same combustion chamber of the Volvo TD100 engine, see Figure 32. The seven ion currents were simultaneously measured with the in-cylinder pressure, see Figure 33. The measurements were crank angle based. The fuel used was isooctane and the compression ratio was 15:1. A disc shaped combustion chamber was used.

It was found that there were differences both in ion current timing and amplitude depending on the measuring location. The pressure oscillations during rapid HCCI combustion could be seen in both the pressure trace and the ion current traces.

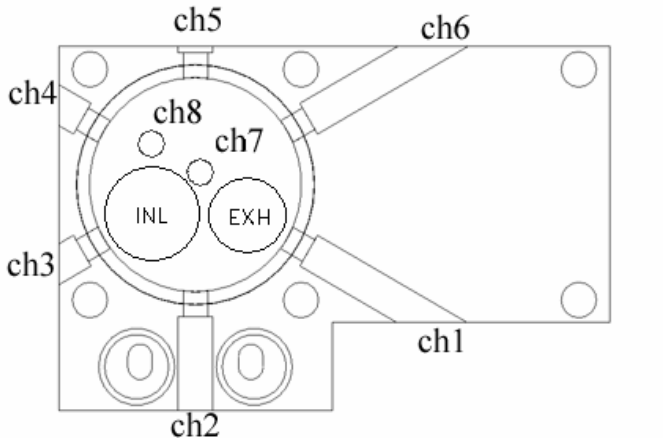

Figure 32: Sketch of the spacer with seven ion current measuring positions, ch1 to ch7, and one pressure measuring position, ch8.

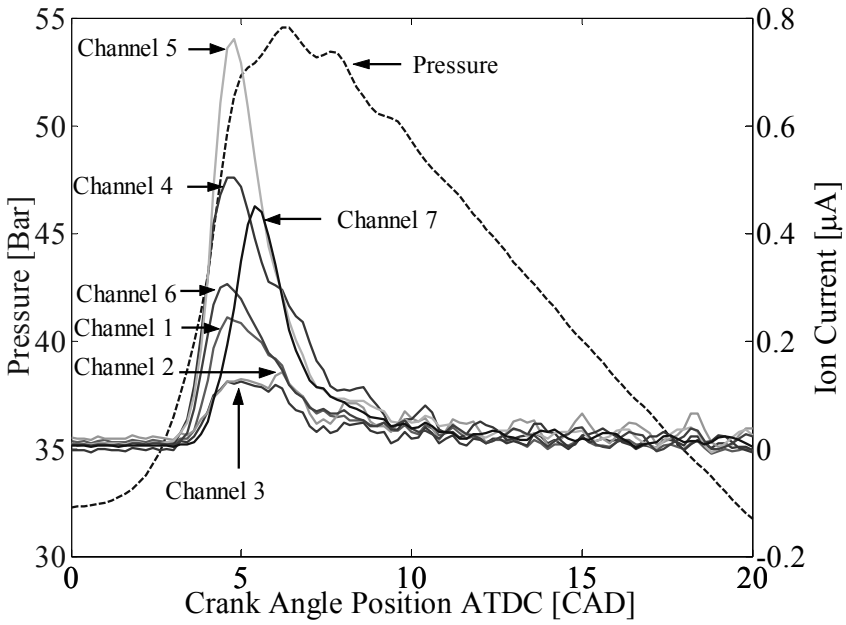

Figure 33: Seven simultaneously measured ion current traces along with the in-cylinder pressure trace in a single engine cycle. The engine speed was 1000 rpm, λ of 2.6 and the fuel was isooctane.

In Figure 34 averaged ion current amplitudes and timings based on 500 cycles can be found for different air/fuel ratios and measuring locations. For the case of an relative air/fuel ratio (λ) of 2.6 locations number 4 and 5 would be the most appropriate to use in comparison to locations 1 and 2 which have very weak signals and are probably not usable as feedback signals for closed loop control. It can also be noted that the ion current timing is about 1 CAD advanced compared to CA50 depending on location. However if the combustion phasing is changed there seems to be a constant offset between CA50 and the ion current timing for a given ion current measuring location. It can also be noted that Channels 4 and 5 which have the highest amplitudes also have the most advanced ion current timing. The reason for this is probably that the gas igniting first in the combustion chamber is closer to these ion sensors.

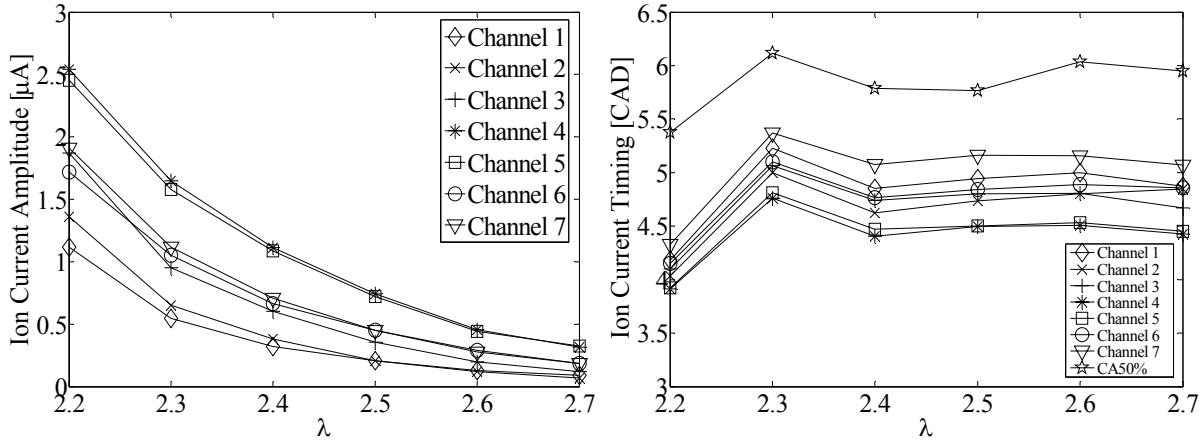

Figure 34: Ion current amplitude and timing information and CA50 for different relative air/fuel ratios and measuring locations. The engine speed was 1000 rpm and the fuel used was isooctane.

It is vital that the ion current timing is not deviating too much from the actual combustion phasing. This can be seen in Figure 35 where there is a constant offset between the ion current and CA50 independent of ion current amplitude. The ion current amplitude increases with advanced combustion phasing due to increased in-cylinder temperature promoting ionization. The reason for different ion current amplitudes in different measurement locations may be differences in the ionization process due to stratification in temperature and/or air/fuel equivalence ratio throughout the charge. To ensure that there were no manufacturing defects or variations between the spark plugs themselves, the spark plugs were switched to different locations.

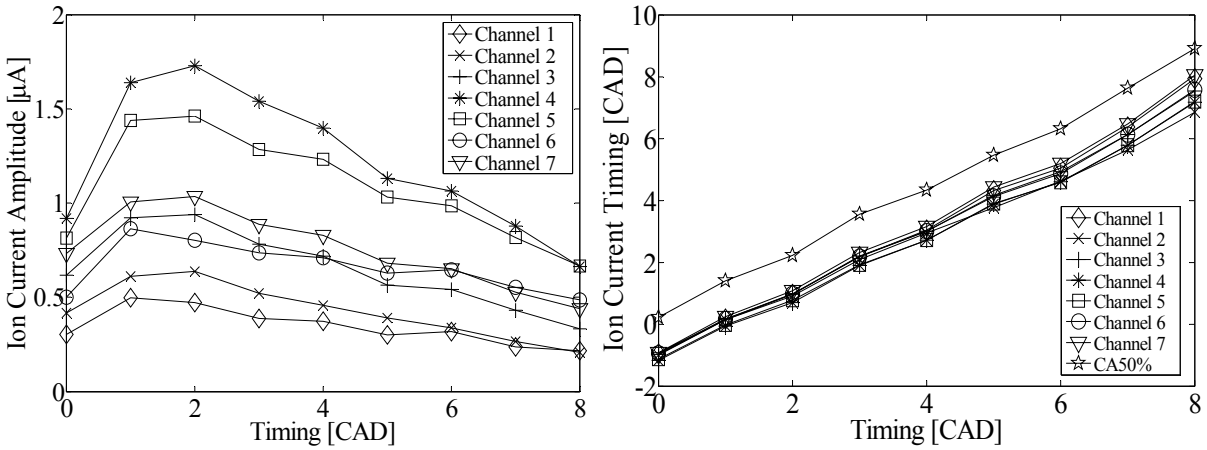

Figure 35: Ion current amplitude and timing as function of desired combustion timing. The engine speed was 1000 rpm and the fuel used was isooctane.

5.2.2 Fuel Effects on Ion Current

Since it was found that the presence of ion current is load dependent the question arises if there is a more appropriate fuel for achieving a signal at lower loads. Therefore the load range was tested for seven different fuels in the Scania D12 engine. The fuels were iso-octane, PRF80 (80% iso-octane mixed with 20% n-heptane), ethanol, methanol, gasoline, n-heptane and diesel. Octane and cetane ratings can be found for the different fuels in Table 4 together with the selected compression ratios used during the experiments.

Table 4: Fuels, octane and cetane numbers with corresponding compression ratios.

Fuel	Octane / Cetane Number	Compression Ratio
N-heptane	RON 0	11.5:1
Diesel (Swedish MK1, low Sulphur)	Cetane 54	11.5:1
Gasoline	RON 98	16.5:1
PRF80	RON 80	16.5:1
Iso-octane	RON 100	18:1
Ethanol	RON 107	18:1
Methanol	RON 106	18:1

The upper limit in load was due to high combustion rates and the lower limit due to lack of ion current signal. N-heptane, Diesel and PRF80 are fuels provoking low temperature reactions (LTR). LTR is chemistry occurring earlier in the compression stroke, usually around 15-25 CAD BTDC, at lower temperatures than the main combustion. Some heat is released with LTR for a short period raising the pressure and temperature in the combustion chamber. Closer to TDC the main combustion starts with high temperature reactions.

Figure 36 shows the result of this experiment for the ion current probe location which provoked the best signal levels in this particular engine. As can be seen the high octane fuels render about the same amplitude of ion current for a given lambda. Thus, the fuel should be selected solely based on desirable maximum load range which in turn is depends on pressure rise and excessive noise. It can also be seen that the low octane number fuels as n-heptane and diesel do not provoke ion current easily. The difference between ion current timing (ION50) and CA50 can be seen in Figure 37. Here it is shown that as long as the ion current amplitude is sufficient the estimation of the combustion phasing from the ion current signal is adequate. The difference between ION50 and CA50 is close to zero for gasoline, isooctane, ethanol and methanol when the engine is run richer than λ 3.2. The reason for poor estimations of the combustion phasing from the ion current signal for diesel, n-heptane and PRF80 is insufficient signal to noise ratios. The low signal levels achieved while using these fuels with LTR is due to the lean mixtures and thus low combustion temperatures, see Figure 38. It is not until 1700K that the ion current amplitudes for the different fuels start to increase.

Please note that the ION50 and CA50 values presented here are mean values of 500 engine cycles. Cycle to cycle variations in local air/fuel ratio and temperature will cause variations in the ion current amplitude and timing from cycle to cycle. This fact has to be taken into account when performing closed loop combustion control based on ion current diagnostics.

It is not until close to stoichiometric conditions that the combustion of the low octane fuels produces any ion current, which can be seen in Figure 39. In this case the dilution is based on EGR instead of pure air with EGR rates up to 55%. The amount of fuel has been kept constant. The reason for this behaviour is partly believed to be lower in-cylinder temperatures. Another reason could be that the fraction of CH radicals during combustion is lower for these

fuels resulting in lower amounts of positive ions. When using EGR there are large differences in ion current amplitude depending on the fuel used. Isooctane, gasoline, methanol and ethanol provoke ion current signals through the entire λ range tested. The estimation of the combustion phasing from the ion current is therefore good, as can be seen in Figure 40. When running the engine with N-heptane and Diesel fuels close to stoichiometric mixture proportions, the difference between ION50 and CA50 approaches zero.

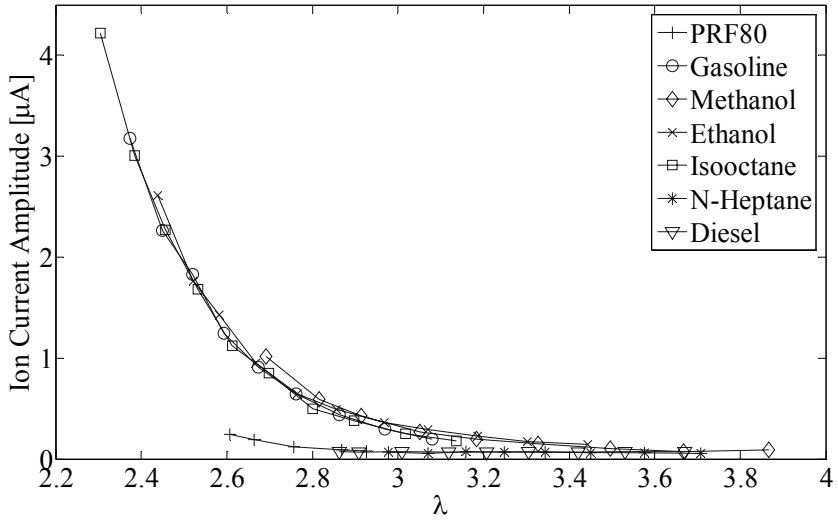

Figure 36: Ion current amplitude as function of relative air/fuel ratio (λ) for seven different fuels. Scania D12 engine at 1000 rpm.

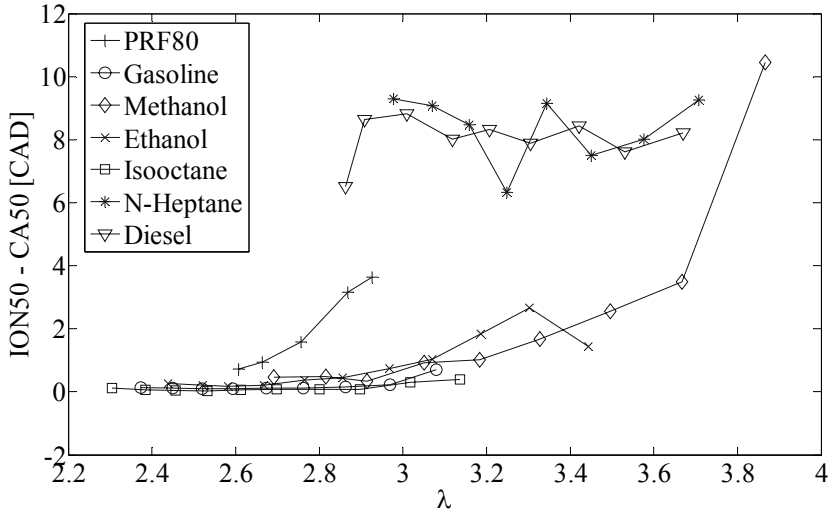

Figure 37: Difference between ion current timing (ION50) and CA50 as function of relative air/fuel ratio (λ) when running the engine without EGR and for a range of fuels. Scania D12 engine at 1000 rpm.

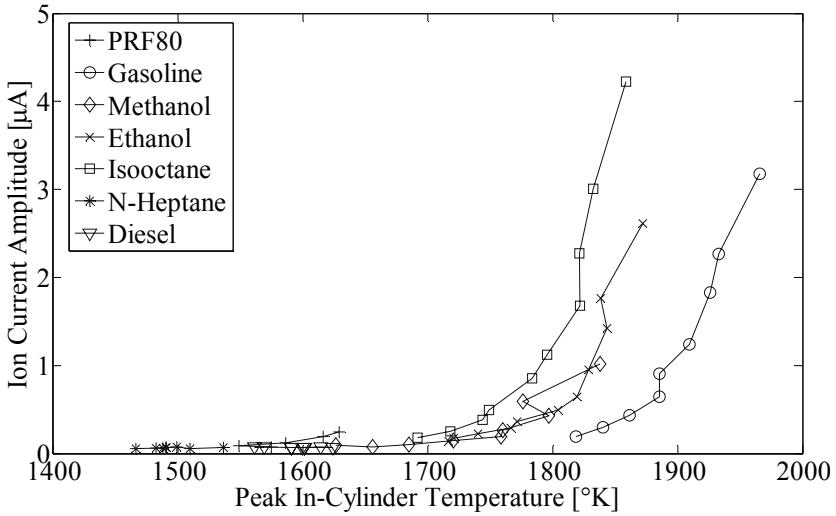

Figure 38: Ion current amplitude as function of peak in-cylinder temperature when running the engine without EGR and for a range of fuels. Scania D12 engine at 1000 rpm.

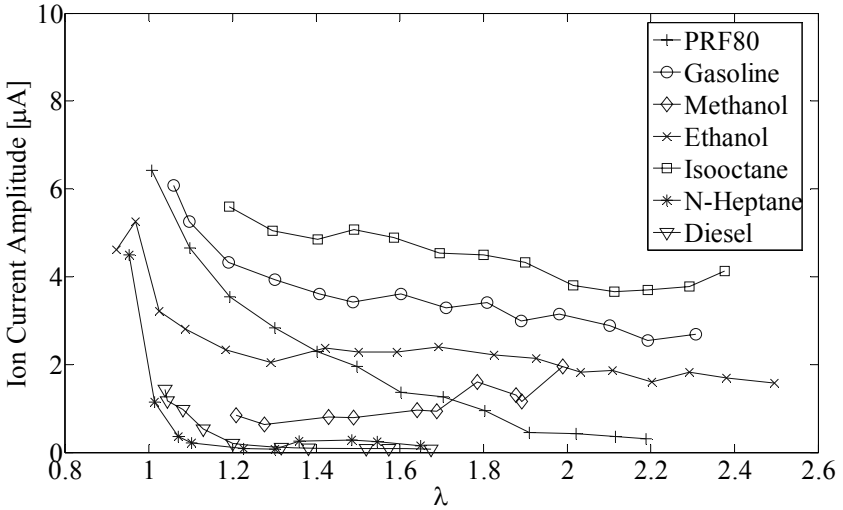

Figure 39: Ion current amplitudes as function of relative air/fuel ratio (λ) when running the engine with different levels of EGR and different fuels. Scania D12 engine at 1000 rpm.

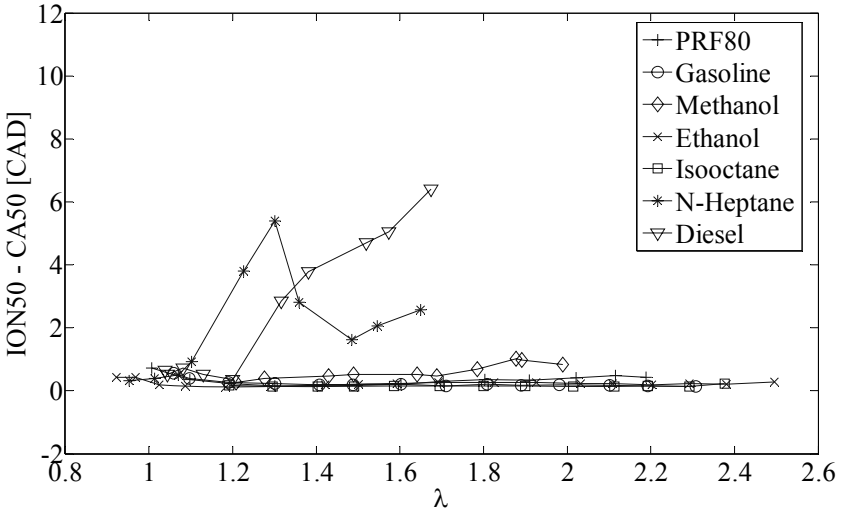

Figure 40: Difference between ion current timing (ION50) and CA50 as function of relative air/fuel ratio (λ) when running the engine with different levels of EGR and for a range of fuels. Scania D12 engine at 1000 rpm.

What can be concluded from the ion current studies is that an air/fuel equivalence ratio of 3.2 is needed in order to obtain any decent ion current signals to be used for closed loop control. This mixture proportion corresponds to an engine load of about 2.5 bar $IMEP_{net.}$ In HCCI combustion experiments performed in a multicylinder Scania D12 engine [37] the $IMEP_{net}$ was approximately 1.5 bar at zero load (0 bar BMEP) conditions for the same engine speed. This means that there is a gap of 1 bar $IMEP_{net}$ between zero load and the load needed to be able to use ion current for feedback control purposes. The ultra lean mixtures used in HCCI engines at low loads have the disadvantage of poor combustion efficiency resulting from insufficient combustion temperature and low heat release. The low heat release and low combustion temperature are disadvantageous for ion current sensing since less ions will be present in the mixture. A solution to this problem could be throttling of the intake air. As shown by *Hyvönen* et al [35] this strategy improves the combustion efficiency without loosing indicated efficiency of the engine despite the increased pumping losses. For the engine tested in the ion current experiments the relative air/fuel ratio should not be higher than 3 for loads lower than 2.5 bar $IMEP_{net}$ to provoke sufficient ion current signal levels while using high octane fuels. Another strategy to improve ion current sensing at lower engine loads is variable detection voltage as shown by [79] where improved signal to noise ratios were achieved with higher voltages applied over the ion current sensor. As long as the ion current signal quality is good enough the estimation of the combustion phasing is quite accurate and cheap ion current sensing could be utilized in the full load range of the HCCI engine. However, this theory has not been experimentally investigated and is therefore left to be proposed as future work at the combustion engines division at Lund University.

5.3 Visualization of Spark Assisted HCCI combustion

In Paper 5 spark assisted HCCI was investigated in the optical Scania engine running on a mixture of n-heptane and isooctane as fuel, i.e. PRF80. Chemiluminescence imaging and planar laser induced fluorescence (PLIF) imaging were used to distinguish flame propagation from auto ignition. The main objective of the study was to compare spark assisted HCCI combustion with laser assisted HCCI combustion, the latter one being described in the next subsection. For PLIF imaging the formaldehyde distribution from the n-heptane fuel was visualized by the use of a multi-YAG laser system allowing 8 laser pulses to be fired in a rapid sequence. By the use of a high speed framing camera with individual CCD modules, eight consecutive PLIF images were obtained in the same cycle. For more information on the optical setup, see Paper 5. A PLIF sequence for a spark assisted HCCI combustion cycle with six images can be found in Figure 41. The images are white where fuel is present and the greyscale towards black shows how much of the fuel that has been consumed. In the upper left part of the images slow flame propagation is seen. In the third image the gradual oxidation process of auto ignition is starting in the lower right corner. In the last three images the oxidation rate of the fuel is increasing and the fuel is consumed at several locations simultaneously which is a sign of auto ignition.

Chemiluminescence imaging was applied to study the flame propagation and HCCI combustion during similar running conditions. Figure 42 shows the single shot chemiluminescence images for the same operating conditions as in the PLIF sequence. Black means no chemical reactions and the greyscale towards white is where detectable reactions are seen. Since the camera was only able to take one image per cycle, the differences in the combustion progress caused by cycle to cycle variations can be seen in the images. However the images indicated that a flame propagates from the location of the spark plug. At 6 CAD

ATDC an auto ignition point can be found just beside the flame and in the next images the fast oxidation process of HCCI combustion is seen.

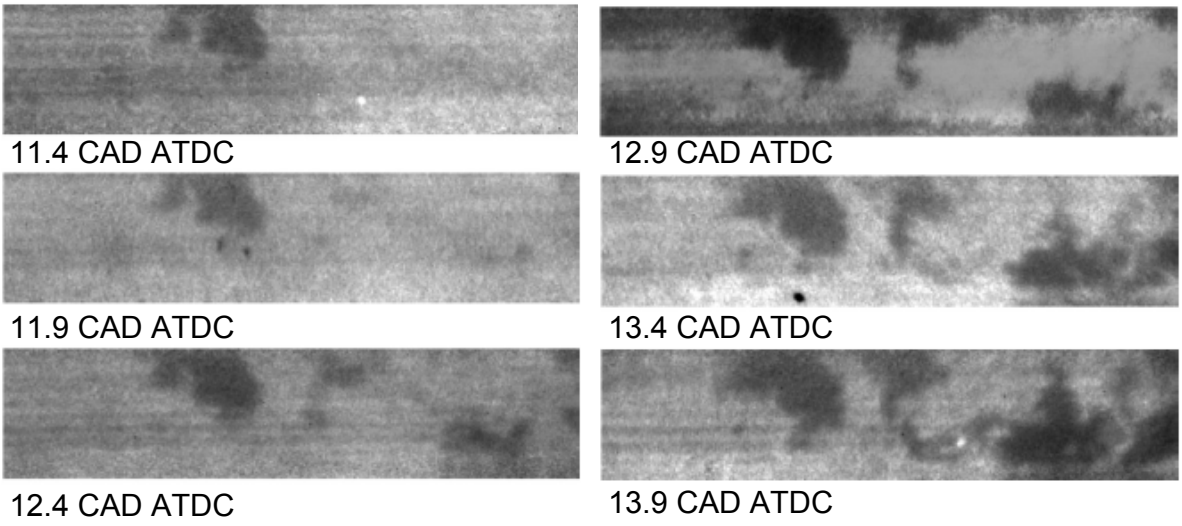

Figure 41: Cycle resolved PLIF image series for a case of spark plug assisted HCCI with a vertical laser sheet. The ignition timing was set to 25 CAD BTDC. λ was 2.8 and the engine speed was set to 1200 rpm.

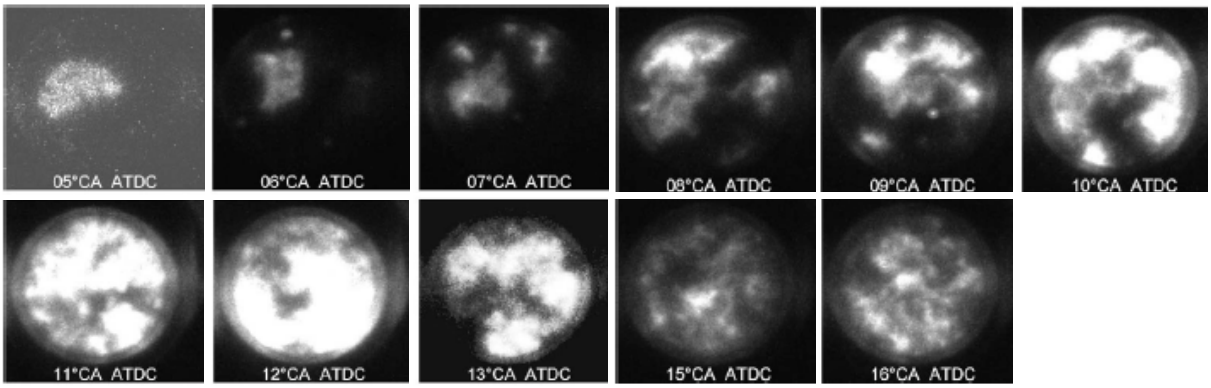

Figure 42: Chemiluminescence image series for a case of spark plug assisted HCCI combustion. Ignition timing was set to 25 CAD BTDC. λ was 2.8 and the engine speed was set to 1200 rpm.

5.4. Visualization of Laser Assisted HCCI Combustion

Two studies have been performed on laser assisted HCCI combustion in the Scania D12 optical engine, Paper 5 and 6. In the first study of Paper 5 the concept was investigated using PRF80 as fuel, i.e. a mixture of 20% n-heptane and 80% isooctane. The optical diagnostics methods used in that paper were chemiluminescence imaging and PLIF imaging. The details of the optical techniques used can be found in Paper 5. In Paper 6 the study on laser assisted HCCI combustion continued but this time natural gas was used as fuel instead. Here chemiluminescence imaging was used to distinguish flame propagation from auto ignition.

5.4.1 Laser Assisted HCCI Combustion with PRF80 as Fuel

In Figure 43, to the left, chemiluminescence images of laser assisted HCCI combustion can be seen. The images are taken by a single shot camera which means that one image per cycle can be taken for a specific crank angle position. By changing the crank angle at which the images are taken the whole combustion event is covered, but with the influence of cycle to cycle

variations. In the first image, 10 CAD BTDC, flame propagation from the location of the laser plasma can be seen. The flame grows slowly until 6 CAD ATDC where the fast oxidation process of HCCI combustion starts. Multiple ignition kernels appear in the combustion chamber at the same time consuming the mixture at a high rate. In the next few crank angles the HCCI combustion process is completed. An air/fuel equivalence ratio of 2.8 was used and the laser ignition timing was set to 25 CAD BTDC. The compression ratio was 11.2:1 and the engine speed was 1200 rpm.

A PLIF image series for the same running conditions as mentioned previously can be seen in Figure 43, to the right. For PLIF imaging the formaldehyde distribution from the LTR was visualized by the same multi-YAG laser system described above. For the PLIF images the white areas are where fuel is present and the locations where the images are darker are where the fuel is being consumed. Flame propagation is seen in the right part of the images, growing at a slow rate. As the temperature and pressure is increased in the surrounding charge, auto ignition occurs in the left side of the images. The rate at which the fuel is consumed is much faster in this area compared to the area the flame has covered. It can also be noticed that the auto ignition characteristic of HCCI combustion is a gradual oxidation process, since the fuel is consumed at several neighbouring locations simultaneously. The area which the flame front has covered is completely black. The conclusion from this is that the flame consumes the fuel entirely but at one location at the time. The HCCI combustion gradually consumes the fuel at several locations simultaneously but the overall combustion rate is higher than for flame propagation.

The combustion phasing was advanced just a few CAD for these running conditions. The slow and early flame propagation seen in the PLIF and chemiluminescence images suggests that heat is released during this period. However this was not found from the heat release analysis. The conclusion was that the effect of laser assistance on HCCI combustion while using PRF80 as fuel is only minor. A theory explaining this fact is that the early flame propagation was too slow and did not increase the temperature of the surrounding charge enough. It could also be that the heat released from the flame is consumed in the low temperature reactions associated with the n-heptane fuel. Richer and less diluted mixtures would certainly improve the conditions for flame propagation, but the objective of the study was to run retarded HCCI combustion close to misfire. Another reason for not using richer mixtures is the high heat release rates achieved which would definitely cause hardware damage to the fragile optical engine. Therefore diluted lean mixtures were used.

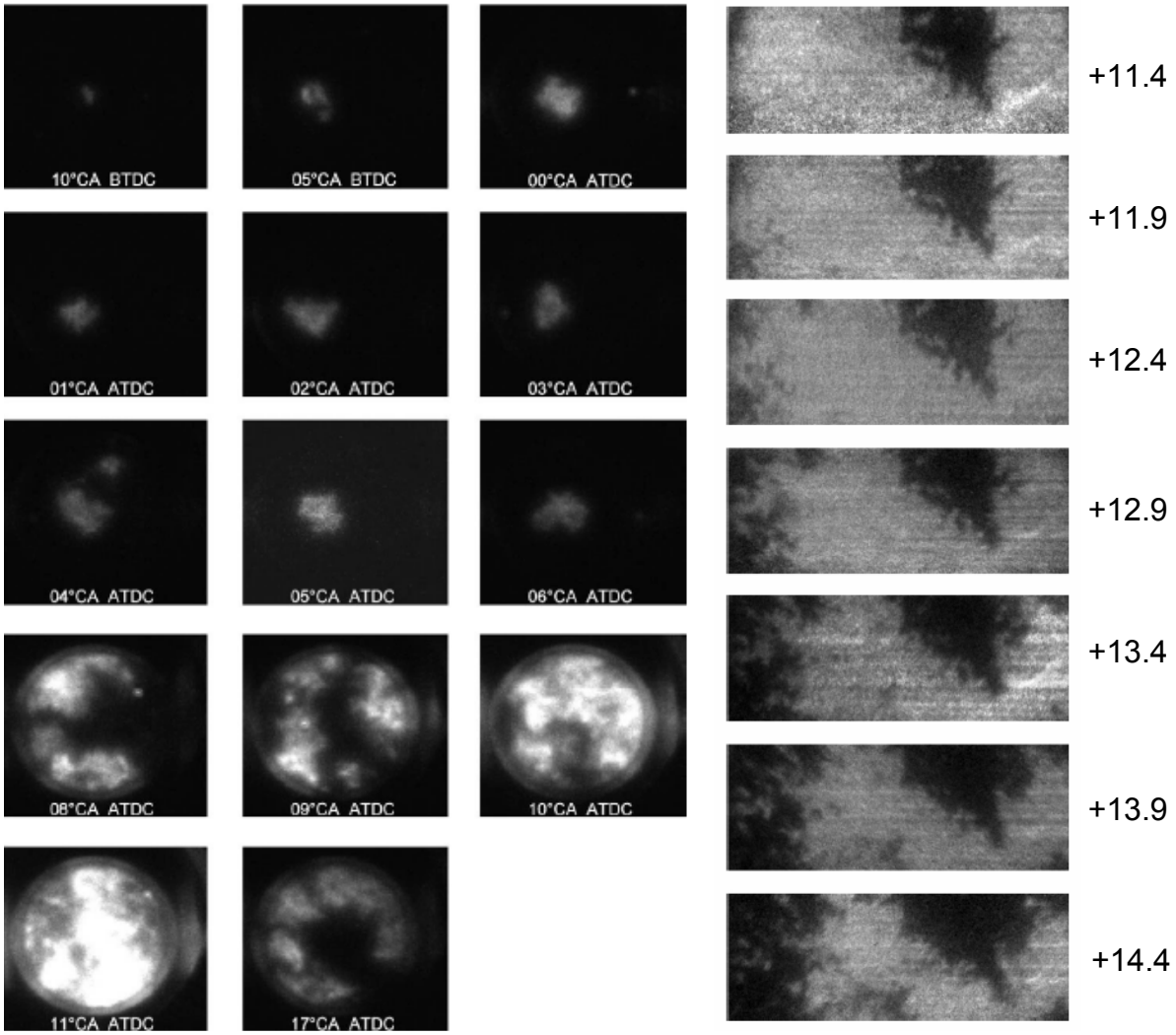

Figure 43: Chemiluminescence images (left) and PLIF images (right) for laser assisted HCCI combustion with PRF80 as fuel. The laser ignition timing was set to 25 CAD BTDC. λ was 2.8 and the engine speed was set to 1200 rpm.

5.4.2 Laser Assisted HCCI Combustion with Natural Gas as Fuel

In previous work conducted by *Kopecek* et al. [30], the effect of laser ignition on HCCI combustion was studied in the TD100 metal engine. A mixture of natural gas (90%) with isooctane (10%) was used as fuel and the HCCI combustion phasing could be advanced by the assistance of the laser plasma for fairly lean mixtures, $\lambda = 2.7$. Since the experience of using lean mixtures of PRF80 for the laser ignition experiments were bad, and there still was an interest in visualizing the flame propagation and auto ignition during laser assisted HCCI combustion, it was decided to run optical experiments in the Scania D12 engine again but this time with natural gas as fuel. This fuel is used to extend the lean limit and decrease NOx emissions for lean conditions in big bore SI engines [80, 81]. The compression ratio was set to 18:1 since the auto ignition temperature for natural gas is high and the engine was run at the lean limit for achieving flame propagation with different amounts of EGR. It was found that running the engine with higher amounts of fuel and less EGR improved flame propagation, which was no surprise since burned gases have higher specific heat which decreases the flame

propagation speed. However due to high compression ratio in combination with the selected fuel, flame propagation was seen when using EGR rates up to 40%, which is rather high.

In Figure 44 single shot chemiluminescence images can be seen for laser assisted HCCI combustion. The first image is taken just after the laser plasma discharge, 45 CAD BTDC. The white dot in the lower part of the image shows the ignition point. The rest of the images are taken 2 CAD BTDC when the flame has had time to propagate and the HCCI combustion is about to start. For the cycles corresponding to Image two to five the laser ignition was turned off. In these cycles the start of HCCI combustion is seen in the upper part of the images. The location at which the combustion starts is random from cycle to cycle but probably due to higher temperature and/or a richer mixture the conditions for achieving auto ignition in the upper part of the combustion chamber are better. From Cycle six and onward the laser ignition was turned on. Now, flame propagation, with a typical thin reaction zone, can be seen from the location of the plasma in the lower part of the images. Cycle to cycle variations in the shape of the flame front as well as in how far the flame front has propagated are present. Furthermore, the emitted light from the HCCI combustion is much brighter and the combustion has propagated further through the charge. This is due to the elevated temperatures and pressures caused by the flame front improving the conditions for auto ignition.

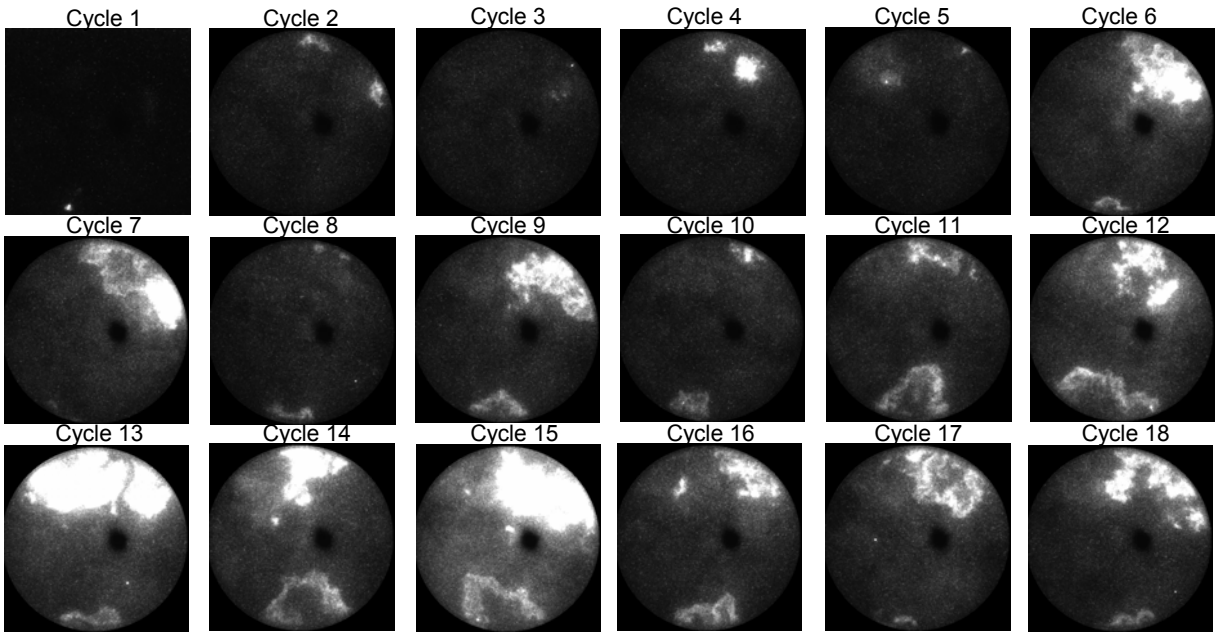

Figure 44: Single shot chemiluminescence images of laser assisted HCCI combustion with natural gas as fuel. White dot on the first image (Cycle 1) denotes the location of the plasma taken shortly after the laser ignition set point of 45 CAD BTDC. The rest of the images are taken 2 CAD ATDC. In Cycle 2 to 5 the laser ignition was turned off and in Cycle 6 and onward the laser ignition was turned on. 1000 rpm, λ = 1.46, EGR = 38%, T_{inlet} = 164 °C and Laser Energy = 19 mJ.

The *Phantom* HSV camera was also used during this study, making it possible to study the entire combustion event from the ignition point of the laser plasma to the end of the HCCI combustion with a high temporal resolution, 4 images per CAD. The high temporal resolution is appropriate for intensity calculations as function of CAD and providing nice high speed videos for presentation purposes. The resulting images for a single cycle are seen in Figure 45, where a limited number of images are selected to show the combustion process. For this single cycle the laser ignition timing was set to 40 CAD BTDC and in the first image, taken

shortly after ignition, the location of the plasma is seen. The ignition delay is quite long, almost 20 CAD, probably due to the high dilution of the charge. Faint flame propagation can be seen from this point onward growing stronger as time passes. The mean flame expansion speed calculated from the crank angle of the first visible light until TDC is roughly 15 m/s. Shortly after TDC the HCCI combustion starts in the upper part of the images just as in the single shot images in Figure 44. Once the auto ignition has started the combustion rate is fast consuming most of the charge in roughly the next 5 CAD. The rate at which the charge is consumed by auto ignition is roughly an order of magnitude faster than the flame expansion speed calculated earlier in the cycle and the expansion speeds for flame propagation found in the literature [5, 71 and 72]. Auto ignition expansion speeds in the range of 100 m/s have been found in HCCI engines by *Hultqvist* et al. [8] and *Dec* et al. [90]. Similar differences in expansion speeds between flame propagation and auto ignition in the same combustion cycle as in the present work were also found by *Persson* et al. [73] in a SACI engine.

The images are scaled so that the highest intensities during auto ignition appear white in order to visualize the faint light from the flame propagation. The reason for the flame front emitting less light than the HCCI combustion is due to the ROHR which is lower from the flame front. ROHR and chemiluminescence intensity are closely related according to [74].

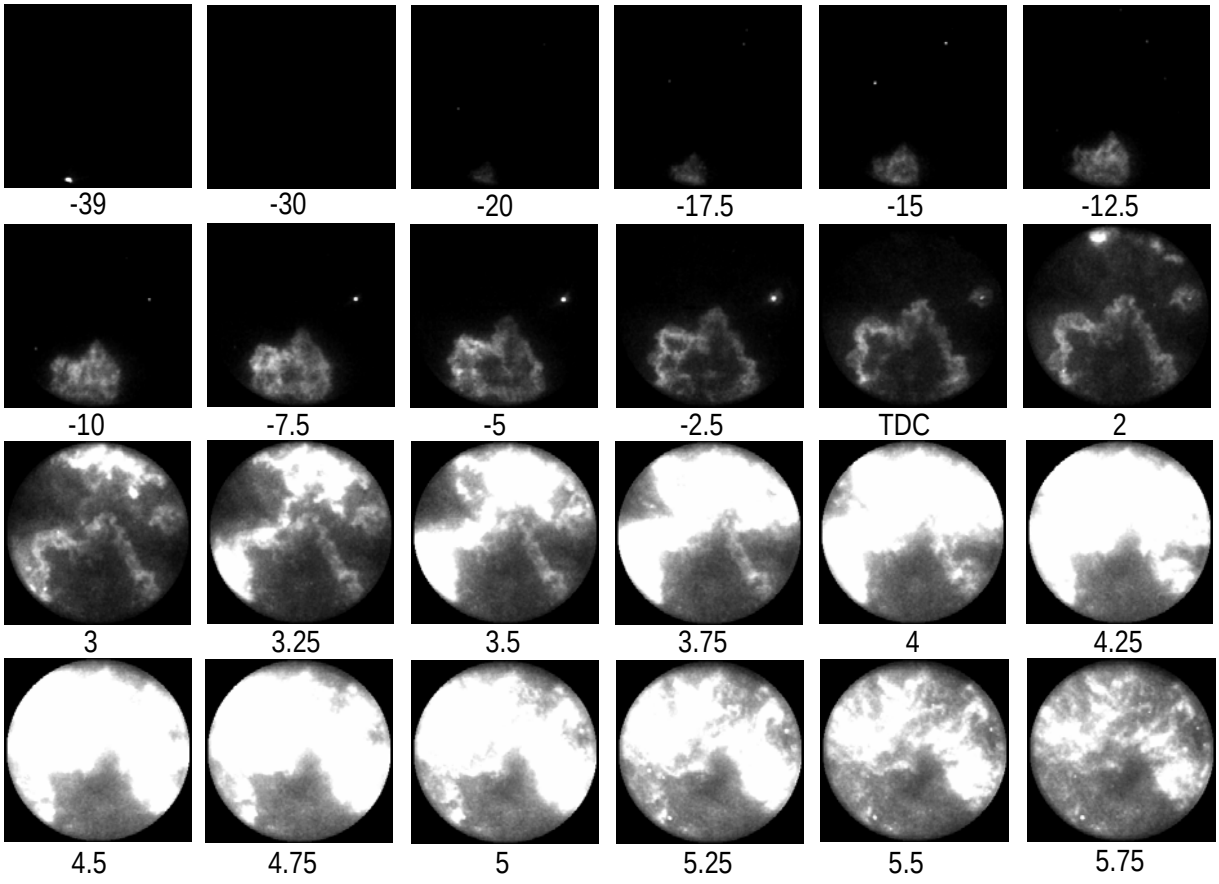

Figure 45: Cycle resolved high speed chemiluminescence imaging of a laser assisted HCCI combustion cycle. Laser ignition timing was set to 40 CAD BTDC. 1000 rpm, λ = 1.9, EGR = 18%, T_{inlet} = 185 °C and Laser Energy = 19 mJ.

The corresponding pressure and heat release traces for the cycle shown in the chemiluminescence images above can be found in Figure 46 (Left). Additionally two pure HCCI combustion cycles with the laser ignition turned off can be seen. The pressure and heat release for the laser assisted cycle starts to deviate from the unassisted cycles about 15 CAD

BTDC when the flame has started to propagate. Shortly after TDC the HCCI combustion starts and the pressure and heat release increases rapidly. The breakpoint, at which the combustion changes from flame propagation to HCCI combustion as described in Section 2.4.2.2, can also be seen in Figure 46. The ISHR fraction was 14.4%. This fairly low amount of flame propagation was enough to advance the HCCI combustion phasing 8 CAD. HCCI cycle number 2 is a case of partial misfire since the total amount of heat released is lower than for the other two cycles.

In Figure 46 (right) the total chemiluminescence intensity in each image as function of CAD are plotted. By performing this calculation it is possible to distinguish the slow flame propagation from the fast auto ignition behaviour of HCCI combustion. As seen previously from the pressure data the combustion is advanced and intensity appears 20 CAD BTDC in contrast to the unassisted HCCI cycles. In the intensity trace of the laser assisted cycle a ringing phenomenon, which might be due to knock, can be seen shortly after the intensity peak. The pressure increase and decrease when a pressure wave traverses the combustion chamber might cause a fluctuation in emission of light. However such an evaluation has not been done to this date and might be difficult due to the relatively low sampling speed of the chemiluminescence images. In the pressure oscillation study the temporal resolution was 10 pressure samples per CAD which is barely sufficient to resolve the oscillation phenomenon.

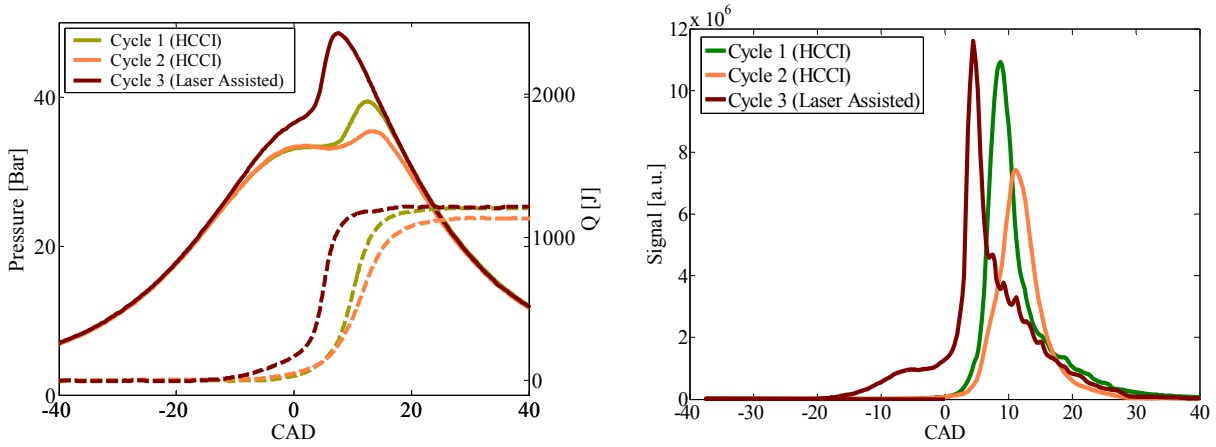

Figure 46: (Left) Pressure and accumulated heat release traces for two HCCI combustion cycles and one laser assisted HCCI combustion cycle. (Right) Summarized chemiluminescence signal intensity over each image as function of CAD.

What can be concluded from the experiments on laser assisted HCCI is that a laser ignition system can successfully be used to sustain HCCI combustion during running conditions that normally would lead to misfire. The laser plasma deployed in the combustion chamber ignites the air/fuel mixture resulting in a flame front which propagates throughout the charge increasing the global pressure and temperature until auto ignition conditions are reached. At this stage multiple auto ignition locations is seen throughout the unburned charge which is consumed in a rapid HCCI manner. The laser assistance has the effect that the combustion is advanced with resulting higher efficiency. By changing the laser ignition timing the HCCI combustion phasing can be controlled. Ignition by means of the laser was achieved running the engine lean and diluted with high amounts of burned gases (EGR).

5.5 Combustion Chamber Geometry Effects on HCCI Operation

Since further studies are necessary to increase the understanding of combustion phenomena when using combustion chambers that provoke turbulence as discussed in Section 2.4.4, it was decided to conduct further experiments but this time in the Scania D12 optical engine instead of the old Volvo TD100 engine. Similar combustion chambers as the ones used in *Christensen's* work [40, 41] were utilized; a Square Bowl in piston and a disc shaped combustion chamber. Drawings of the pistons used can be seen in Figure 47. The pistons were designed in a way that the parameters affecting for example combustion efficiency, should be as similar as possible. Some of the parameters are found in Table 5, as can be seen the compression ratio and topland height are the same for both geometries. The difference in wall area is also seen as well as the different squish heights.

Table 5: Some vital geometrical data of the two combustion chambers investigated.

	Disc	Square Bowl
CR	17.2:1	17.2:1
Squish Distance	8.15 mm	1.75 mm
Topland Height	44.5 mm	44.5 mm
Wall Area at TDC	288 cm^2	333 cm^2

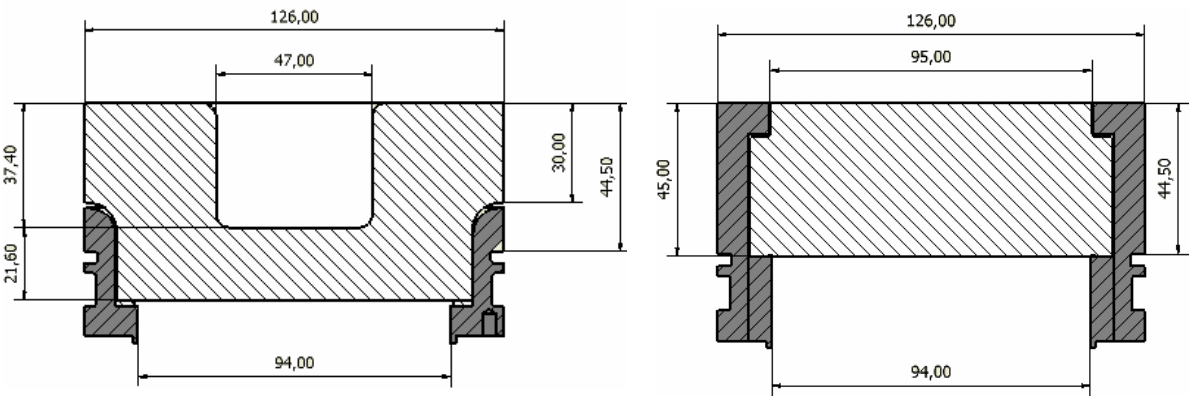

Figure 47: Drawings showing the cross sections of the Square Bowl in piston to the left and the Disc shaped piston to the right. The light grey areas are made of quartz glass while the dark grey areas are made of titanium.

The squish distance in the Volvo TD100 experiments was 1 mm in the bowl case but due to the optical configuration of the Scania D12, with fragile quartz glass parts and a long piston extension, a squish distance of 1.75 mm was used. The squish motion is believed not to be equally strong but enough to create a difference in gas flow between the geometries.

As a first validation to see if the combustion behaves in the same way in the Scania engine as in the Volvo engine, the pressure and heat release were validated. The result can be seen in Figure 48. The amount of fuel injected to the engine was the same for both Disc and bowl, λ was 3.3 and the combustion phasing in terms of CA50 was 8 CAD ATDC. As seen the pressure rise rate and peak pressure are much lower for the bowl case. The lower peak ROHR is also seen for the bowl case. The longer combustion duration is also a fact. The combustion in the bowl case started 10 CAD BTDC while the combustion in the Disc case started closer to TDC. The pressure rise rate in the Disc case was 2.7 bar/CAD while it was only 1 bar/CAD in the bowl. Since the pressure rise rate is the limiting factor for the load range in the HCCI engine this suggests that by using Square Bowl geometry the load can be increased significantly.

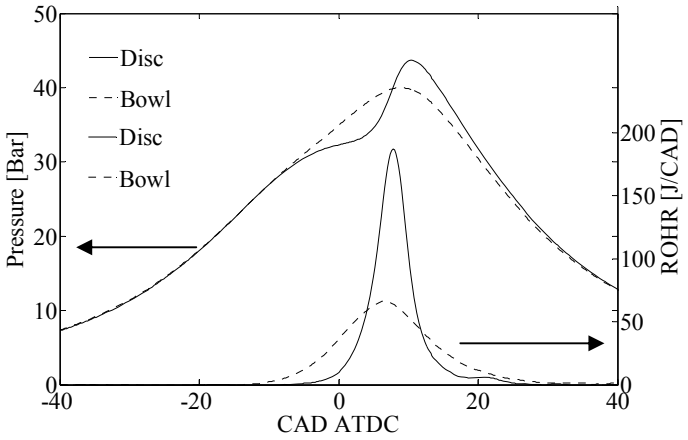

Figure 48: Pressure and ROHR as function of CAD for the Disc piston and the Square Bowl in piston.

Three different studies (Paper 6 – 9) were performed in the optical Scania D12 HCCI engine, chemiluminescence imaging, fuel tracer LIF and lastly the pressure data was used for large eddy simulations (LES). In addition to these optical experiments, metal engine tests were performed in Paper 10 to investigate the difference in behaviour between optical and metal experiments and to validate the combustion chambers at different loads and compare the performance with a standard Diesel bowl combustion chamber.

5.5.1. Chemiluminescence Imaging

Since optical access was enabled in the Scania D12 engine, chemiluminescence imaging was used to study the combustion process with the two combustion chambers. The image resolution was in both cases 288 x 296 pixels. Three images were recorded each CAD corresponding to 21.6 kHz at an engine speed of 1200 rpm. The exposure time was set to 10 μs which corresponds to 0.07 CAD. The field of view is limited by the quartz glass window in the pistons to 51% of the combustion chamber. This means that the outer part of the combustion chamber close to the cylinder walls is not seen, but the bowl and parts of the squish region can be visualized. In this setup the quartz liner was replaced with a steel ring in order to more closely resemble a metal engine regarding heat conductivity. The metal ring was also painted dull-black to reduce scattered light from combustion.

In Figure 49, the chemiluminescence images corresponding to the load case in Figure 48 are seen for the Disc case. The first image shows the location of the valves with respect to the field of view. The number in the lower left corner denotes the CAD at which the images were taken. Each image is scaled in such way that the brightest part is close to white in order to visualize the early and late parts of the combustion process which otherwise would not be seen due to low signal levels. The combustion in the visible area starts close to TDC and can be seen as multiple ignition kernels in the left part of the images. The fuel is gradually oxidized in this area and propagates slowly at first. Around 7 CAD ATDC the reactions speed up and intensity is found around the perimeter of the image and finally the charge in the centre is combusted. Inspecting the images, a lot of structures can be seen with gradients all over the combustion area. This is typical auto ignition behaviour where ignition first occurs in the locations which are hotter and with more fuel. Heat is transferred to the neighbouring locations which are close to auto ignition. The additional heat to these locations starts the chemical reactions. In deflagration flame propagation of SI combustion the reaction zone is much thinner and the propagation is due to diffusive transport of heat and species. The

unburned gas in front of the flame is not close to auto ignition and the diffusive addition of heat and species from the flame front is needed for reactions to occur. Around 14 CAD ATDC the intensity fades away and the combustion process is completed.

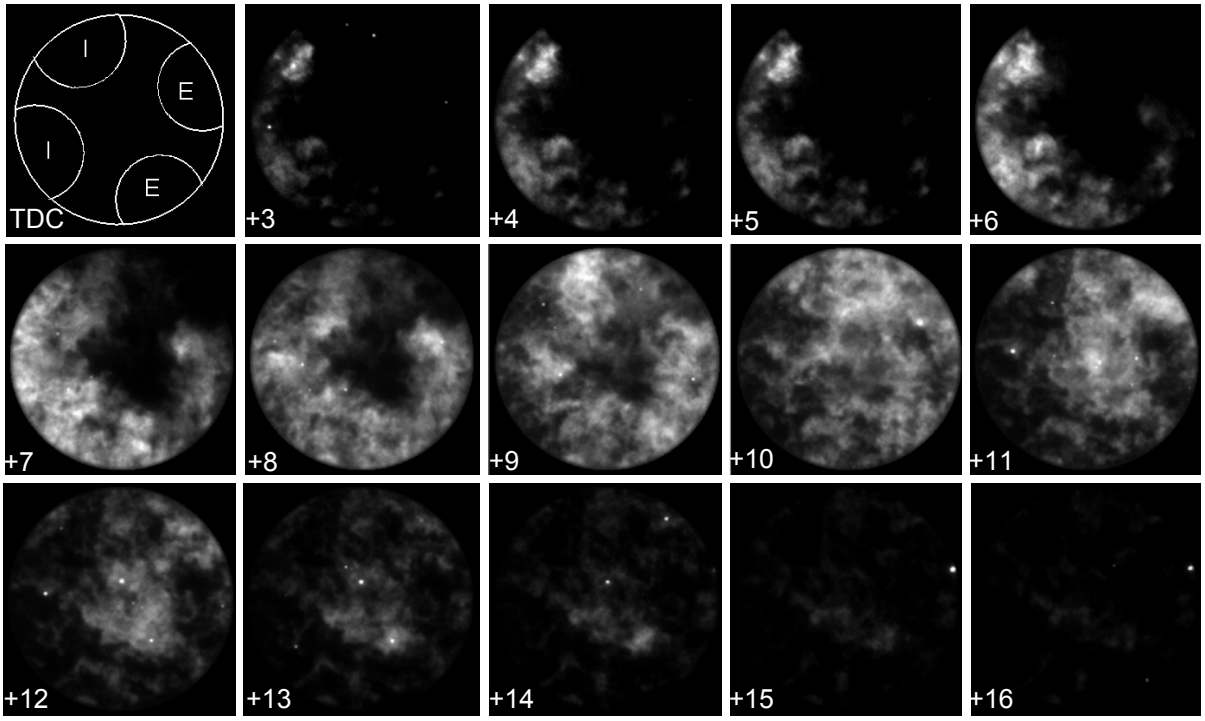

Figure 49: Single cycle chemiluminescence images for the disc case. λ = 3.3, CA50 = 8 CAD ATDC and an engine speed of 1200 rpm.

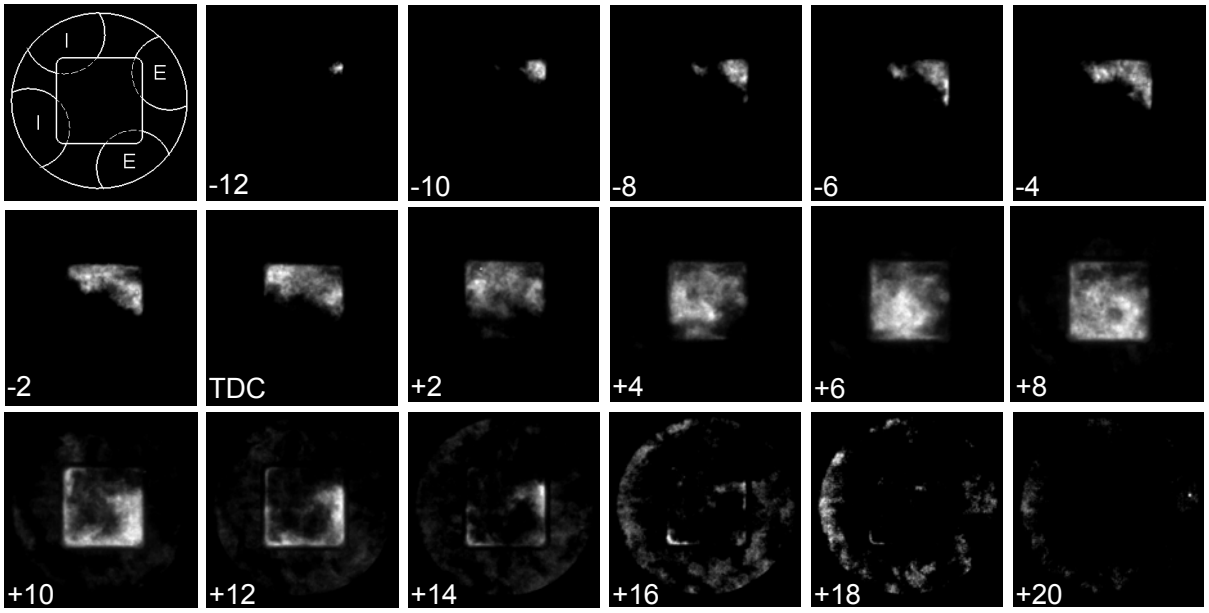

Figure 50: Single cycle chemiluminescence images for the bowl case. λ = 3.3, CA50 = 8 CAD ATDC and an engine speed of 1200 rpm.

In Figure 50, the chemiluminescence images for the bowl case can be seen. In the first image the locations of the valves and the bowl can be found. At 12 CAD BTDC a single ignition kernel can be seen in the upper right corner of the bowl and in the following images the combustion propagates with few small kernels and a sharp gradient between the burned and unburned zones. Unlike the disc case, very few isolated ignition kernels appear. The early combustion in the bowl behaves like a sharp reaction front propagating through the charge. This suggests that the gas in front of the reaction zone has to be far from reaching auto ignition and the heat from the reaction zone only heats up the gas in close proximity. Therefore the combustion rate is slow at first consuming the charge close to the upper wall in the bowl. From the image sequence the average speed of the propagating reaction front along the upper wall was estimated to around 19 m/s. This combustion rate is extremely low and unusual for HCCI operation. However, it should be mentioned that the chemiluminescence intensity is integrated along the line of sight. This means that the reaction front can be present at any depth at different stages through the combustion process inside the Square Bowl. At TDC the combustion rate suddenly speeds up consuming the rest of the charge in the bowl in less than 10 CAD. The combustion of the bulk in the bowl is more globally spread like in the Disc case with more visible structures. This probably means that the bulk charge had to be heated up by the combustion near the upper wall from first ignition 12 CAD BTDC to TDC. And only, when this was completed most of the bulk charge was close to auto ignition conditions, meaning fairly uniform temperature and air/fuel ratio, resulting in a higher burn rate.

At 10 CAD ATDC, combustion in the squish region can be seen, but the signal level is much lower compared to the bowl. Here reactions occur globally over the entire squish volume.
The reason for the combustion in the squish volume to be retarded compared to the bulk combustion in the bowl is probably heat losses caused by the high area to volume ratio in the squish volume. It is not unlikely that at TDC, when the squish distance is around 1.75 mm, the combustion might be quenched due to low temperatures in this volume. As the piston moves down, the temperature and pressure rise from the combustion in the bowl improves the conditions for auto ignition in the squish volume.

It is of interest to compare the mean chemiluminescence signal level with the heat release rate. In Figure 51 (a) the mean chemiluminescence signal level and ROHR are plotted as function of CAD for the Disc geometry. The correlation between the ROHR and the chemiluminescence signal is quite good. The peaks of each trace coincide at 8 CAD ATDC. The ROHR starts to climb around 5 CAD BTDC. Chemiluminescence intensity starts to appear close to TDC.

The reason for the difference between the start of each trace is assumed to be due to the limited field of view. Only 51% of the combustion chamber can be seen through the piston window. As seen from Figure 49 the combustion starts close to the walls. This most likely means that the initial heat release from near liner combustion is not seen. At 20 CAD ATDC the intensity returns to zero, but there is still a long tail of heat release. This tail of heat release is typical for engines with large topland volumes [42]. The fuel trapped in the crevices flows out in the main combustion chamber as the pressure decreases during the expansion stroke. The higher temperature in the main combustion chamber oxidizes the fuel from the topland volume and heat is released. Again, this process is not captured with the limited optical access.

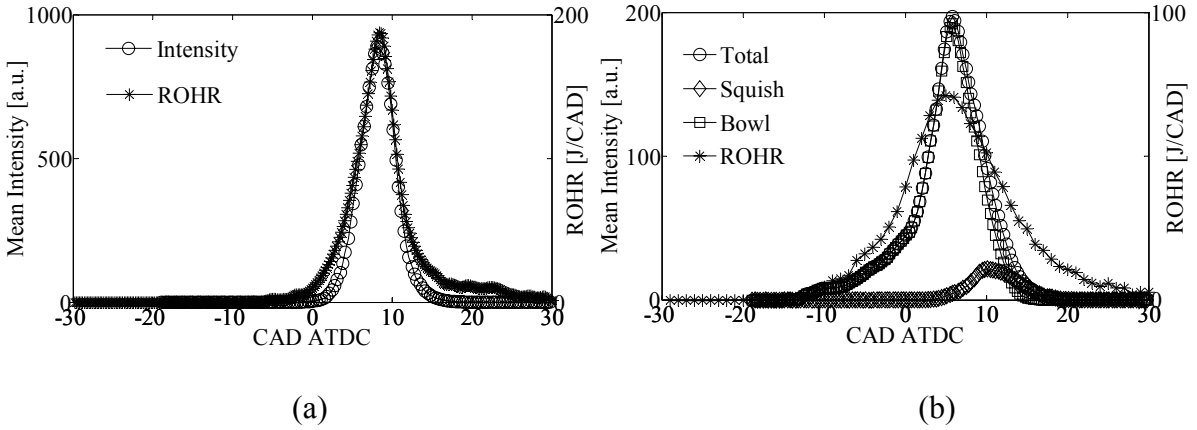

Figure 51: (a) Mean chemiluminescence intensity and ROHR as function of CAD for the Disc case. (b) Mean chemiluminescence intensity and ROHR as function of CAD for the Square Bowl case. The different contributions from the bowl and squish are shown.

In Figure 51 (b), the mean chemiluminescence intensity and ROHR as function of CAD for the bowl case can be found. The intensity trace has been divided into three parts, the squish, bowl and the total signal level. As seen from the previous images, the combustion starts 12 CAD BTDC in a stratified manner. Since the bowl is directly in the field of view the initial heat release during the start of combustion is seen in the intensity. Therefore the starting points of the ROHR and chemiluminescence intensity traces coincide. An additional reason can be that the intensity per unit area is large since the bowl is deep. This makes it easier for the camera to detect it. The intensity trace for the bowl increases in a slow manner until TDC where the signal level increases rapidly. This was also seen as a change in process in the image series. The breakpoint between slow and fast signal increase is where the combustion changes from slow stratified combustion to fast more homogeneous combustion with multiple ignition locations. A similar breakpoint is seen in the heat release but it is not as distinct as in the intensity trace. When comparing ROHR and chemiluminescence intensity it is confirmed that the signal in the squish is retarded compared to the signal appearance in the bowl. The signal in the squish is present from 5 to 20 CAD ATDC. The heat release in the bowl case has a similar tail as the Disc case due to after-oxidation of the fuel from the topland volume.

The chemiluminescence images seen previously are from single cycles. It is of interest to know if the combustion in the bowl is stable from cycle to cycle always starting in the same corner. Also the effect of different mixture compositions may influence the combustion process. In Figure 52 a special procedure for averaging images from 20 engine cycles has been used. Firstly each image has been converted to binary format based on a certain threshold meaning that the signal in each pixel over a certain level in greyscale has been set to 1 and if this criterion has not been fulfilled the value 0 is given. This results in an image with only black and white pixels.

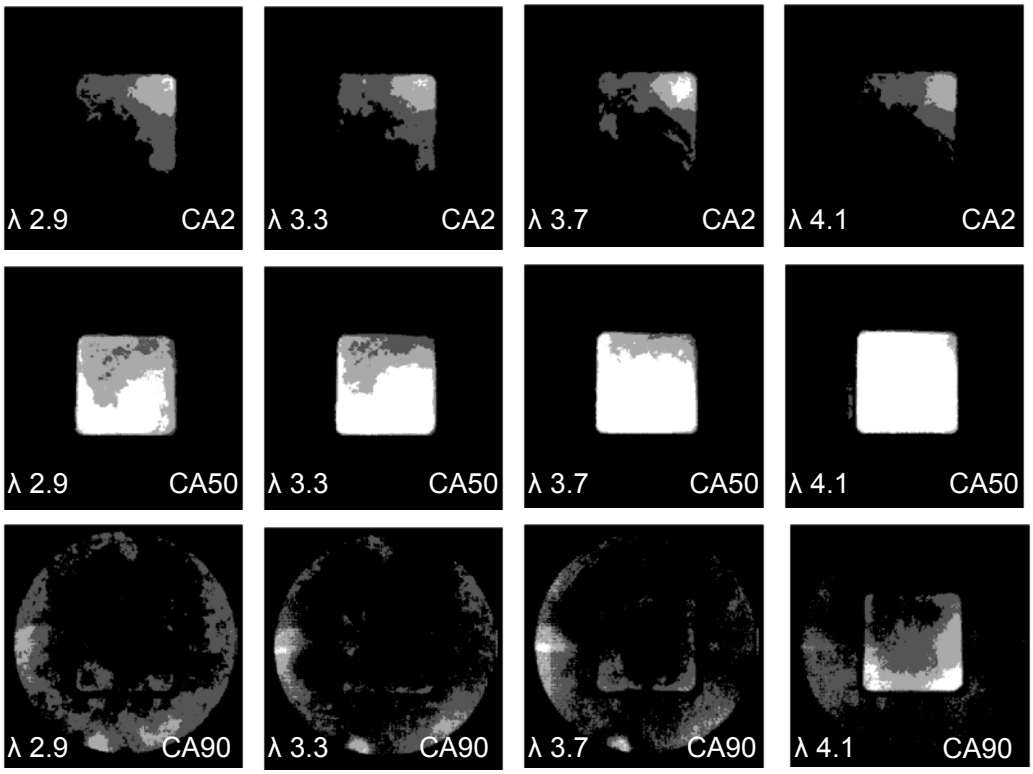

Figure 52: Averaged greyscale images showing four scales of occurrence based on 20 engine cycles. Black: 0-5%, Dark Grey: 5-40%, Light Grey: 40-80% and White; 80-100%. Four different λ-values are shown, 2.9, 3.3, 3.7, 4.1 and three different stages of combustion in terms of crank angle of mass fraction burned, CA2, CA50 and CA90.

Then the images corresponding to a certain crank angle position have been summed up, resulting in pixel values from 0 to 20 (from 20 cycles). A value of 0 means no signal in any of the 20 cycles for that specific pixel. A value of 20 means that signal appears in that pixel in all cycles. Thus a greyscale of 20 tones of grey between black and white is created. In order to simplify the visualization of the occurrence of signal in the images a grouping procedure has been applied. This means that where the images are black 0-5% (≤ 1 cycle) of the 20 cycles have signal. 5-40% (2 – 8 cycles) is dark grey. 40-80% (8 – 16 cycles) is light grey. The white areas show where the probability of signal is 80% or higher. With this method it is easy to see where in the bowl combustion always occurs, and where combustion only occurs sporadically for a certain degree of mass fraction burned. The crank angle of 2% burned is selected since it is an early stage of combustion and by then signal has started to appear in all of the 20 cycles. As seen the combustion always starts in the same corner of the bowl regardless of load. The dark and light grey areas show that there are differences in how far the combustion has progressed. For the case of $\lambda = 4.1$ there are larger cycle to cycle variations in the combustion resulting in a probability of combustion in the same location in the same stage of combustion of less than 80%. When 50% of the heat has been released the higher combustion rate has started and the charge in the bulk of the bowl is being consumed. When 90% of the heat is released the combustion in the squish has started. For the leanest case, $\lambda = 4.1$, combustion in the bowl is still in progress. This probably means that more of the combustion is located in the bowl than in the squish for leaner mixtures, due to quenching in the squish and thus lower combustion efficiency.

5.5.2. Laser Induced Fluorescence

Another diagnostic method for studying inhomogeneities in HCCI combustion is fuel tracer Laser Induced Fluorescence (LIF). In Paper 8 this technique was used to study the slower combustion process while using a Square Bowl in piston combustion chamber compared to a Disc combustion chamber. Acetone was used as fuel tracer for the LIF measurements. The horizontal laser sheet enters through the quartz liner and the fluorescence is captured with CCD cameras through the piston window and the 45 degree mirror. In these experiments there is a slight difference in compression ratio between the two geometries due to a decision to decrease the compression ratio in the bowl experiments which were performed after the Disc experiments. The reason for decreasing the compression ratio in the bowl case was the elongation of the piston extension due to high temperatures and mass forces, especially during gas exchange TDC, which would if luck is not present result in contact between the expensive quartz piston and the valves and would result in instant hardware failure. The squish distance was increased from 1 mm to 1.75 mm which resulted in a decrement in compression ratio from 18:1 to 17.2:1. During heat release analysis it was found that this difference in compression ratio did not affect the combustion duration much but instead the intake air temperature is lower in the Disc case than in the bowl case. In the chemiluminescence experiments the compression ratio was the same for both geometries, 17.2:1, which resulted in lower intake temperatures in the bowl case compared to the Disc case. Comparing the LIF experiments and the chemiluminescence experiments it is noted that the intake temperatures are more representative in the chemiluminescence experiments since the same compression ratio was used with both combustion chamber geometries. The level of intake temperature is important in terms of efficiency since in a real application the power needed to raise the intake temperature to reach auto ignition will affect the thermal efficiency of the engine.

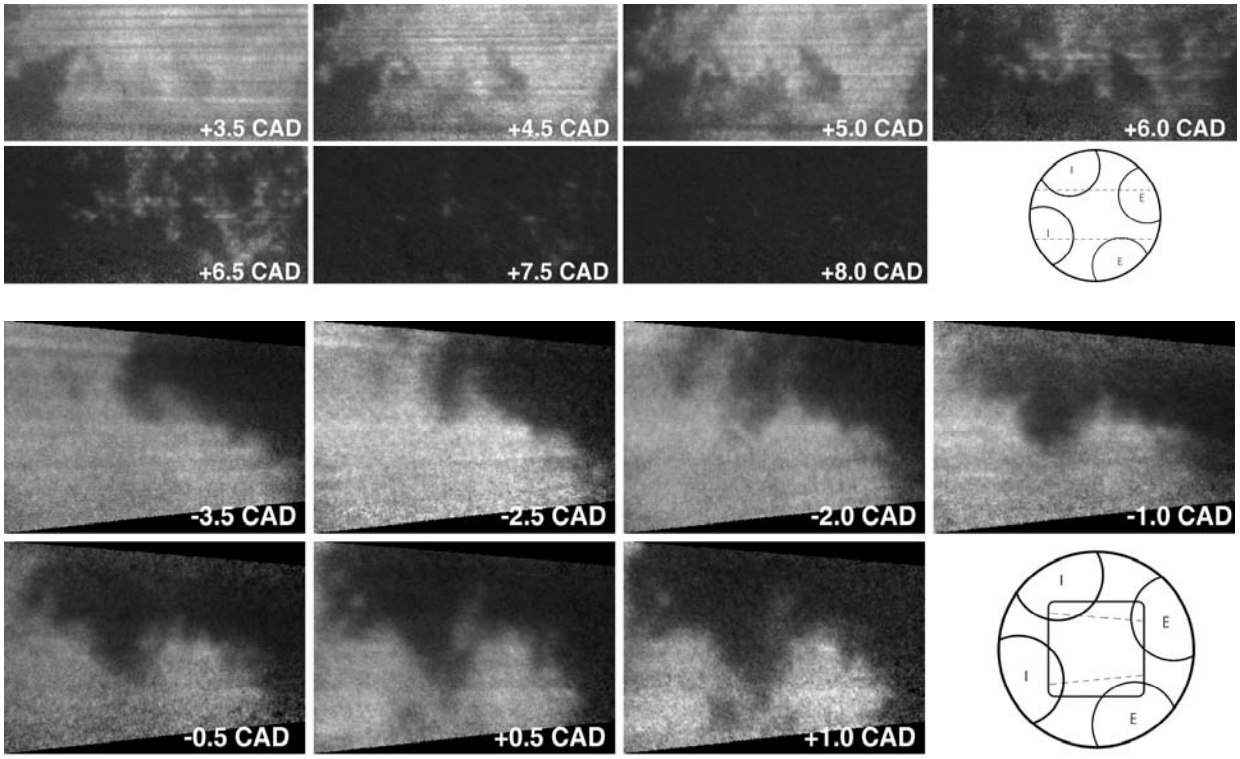

Figure 53. Fuel Tracer LIF images of HCCI combustion in the Disc case (top) and Square Bowl (bottom). The white areas show where fuel is present and the dark areas where fuel is consumed. λ = 3.3, CA50 = 8 CAD ATDC and an engine speed of 1200 rpm.

In Figure 53, acetone fuel tracer LIF images can be found for both geometries, running the engine at 1200 rpm and with an relative air/fuel ratio of 3.3, i.e. the same conditions as in the chemiluminescence images in Figure 49 and Figure 50. From the LIF images of the Disc case it can be seen that there is distributed acetone consumption throughout the entire measurement sheet with a slight preference to the left side of the images. This behaviour of gradual oxidation throughout the charge has been seen in HCCI combustion studies before [8, 46]. In contrast to the gradual oxidation behaviour in the Disc case there are much sharper gradients with finger like structures between the burned and unburned zones in the bowl case. It is probable that the gas corresponding to the upper right hand side of the images is hotter thereby igniting the charge first. The slowly propagating consumption of fuel suggests that the rest of the charge is further away from auto ignition and needs to be heated up by diffusive transport by heat and species from the reacting and post flame zones. Another explanation could be that the fuel distribution in the bowl case is more heterogeneous resulting in rich zones igniting first propagating into the leaner ones. However, the LIF images prior to combustion were found to be equally homogeneous suggesting that the stratification seen is due to a broader temperature distribution. The effect of fuel stratification and thermal stratification has been extensively studied using pressure and optical diagnostics by *Dec* and *Sjöberg* [90, 92 and 93]. They have found that the local relative air/fuel ratio (λ) has little effect on the auto ignition timing for one-stage ignition fuels like isooctane during similar running conditions meaning a heavy duty HCCI engine running lean and premixed using inlet air preheating and high compression ratio as the main ignition source. Instead the naturally occurring thermal stratification due to wall heat transfer and turbulence is the primary source for the inhomogeneities seen in LIF and chemiluminescence image sequences of premixed HCCI combustion. The fuel used in the present study is ethanol which also is a one-stage ignition fuel but other processes like vaporization of the fuel in the inlet could change the fuel distribution if the fuel is not vaporized completely before entering the cylinder. Ethanol has roughly 3 times higher heat of vaporization than isooctane according to [5] meaning that more heat is needed to evaporate ethanol completely.

The results from the chemiluminescence experiments and the fuel tracer LIF experiments show basically the same combustion behaviour, that is much slower combustion with a more stratified character in the bowl case compared to the Disc case where reaction zones are more widely spread throughout the charge gradually oxidizing the bulk.

However it should be noted that the LIF measurement is made in a thin sheet through the bowl and the chemiluminescence measurement is a line of sight method, meaning that the signal level is the integrated sum of light along the distance from the bottom of the bowl to the cylinder head. It is therefore hard to draw any conclusions from the LIF measurements about the total fuel distribution in the cylinder. In the same manner it should be remembered that the light seen in the chemiluminescence images could come from any depth in the bowl. A way of improving the study would be to perform chemiluminescence imaging from the side of the bowl through a quartz liner. Since the bowl is deeper than the height of the quartz liner the reactions in the bottom of the bowl would not be captured but the combustion process starting in the bowl propagating into the squish would be captured. A 3D measurement technique with a rapidly moving mirror could give LIF images at different depths in the bowl and a 3D fuel consumption image could thus be created. Furthermore, a LIF measurement from the side can be performed, but difficulties regarding beam scattering at the edge of the bowl complicates the experiments. Combining the results from these techniques could resolve the combustion process in the bowl better, showing at what depth the combustion starts.

5.5.3. Large Eddy Simulations

Large Eddy Simulations (LES) is a modeling approach to study the effects of turbulence and flows on the temperature field in the cylinder and in turn its effects on chemical kinetics and the combustion process.
The basic principle is to use LES to calculate the local temperature and pressure in each grid location in the cylinder at each time step in the engine cycle. By using a tabulated reaction progress rate obtained from a chemical kinetics model (CHEMKIN) the heat release in each grid location is calculated including the effects of heat and species transport between different locations. Details of this tabulated model are given in Paper 9 and the references therein. By the use of this procedure it is possible to find the cause for temperature stratification due to the turbulent flow field and combustion chamber geometry. Also, since the simulations are coupled to a kinetics model the locations where the combustion starts can be derived and since the local heat release rate is modelled the combustion process both in time and space can be studied.

The models are usually validated against experimental data. In Paper 9 the experimental data from Paper 7, the chemiluminescence measurements, have been used to compare the simulated pressure traces with the experimental ones for both combustion chamber geometries. However, some assumptions have been made which affect the accuracy of the simulations:

- Constant wall temperature and piston temperature both in time and space which affects wall heat transfer and the temperature distribution in the cylinder.
- The topland volume is not included in the model which directly results in overestimated combustion efficiencies.
- The fuel distribution is assumed to be entirely homogeneous.
- The geometry of intake port design is not modelled precisely which affects the flow pattern.

In Figure 54 the pressure traces and heat release traces from the LES can be found along with the pressure traces from the experiments. Both geometries are represented. The LES predicts the behaviour in the two combustion chambers fairly well including the difference in combustion rate as well as the start of combustion between the two combustion chamber geometries. The explanation for the stratified combustion behaviour according to the LES is the temperature distribution in the cylinder during the first parts of intake stroke. Due to increased wall heat transfer and a larger difference in temperature between the burned gases and the fresh charge and differences in the flow field a wider temperature distribution is created in the bowl case. By quantifying the temperature stratification it was found that the temperature inhomogeneity during the intake stroke was almost twice as high in the Square Bowl compared to the Disc. This wide temperature stratification survives all the way through compression to the point of auto ignition. This means that the hotter zones ignite first and propagate into the colder ones which take longer time compared to a less stratified charge where everything ignites more at once.

It can be seen that the peak pressure from LES is higher for both geometries compared to the experiments. A reason for this is the overestimated heat release from LES since the simulations do not take into account that a part of charge is trapped in the topland volume. This means that according to the model the combustion efficiency is calculated from the fuel consumed in the bowl and squish alone. In reality, fuel is trapped in the topland and flows out into the main combustion chamber and subsequently oxidizes during the expansion stroke. This is seen as a tail on the heat release and is typical for engines with large topland volumes,

especially optical engines. Not all of the fuel trapped in the topland is consumed in the post oxidation process due to insufficient heat and thus the topland volume is a major contributor to unburned hydrocarbon emissions. Another source of error could be if one part of the combustion chamber has significantly lower wall temperature, it results in a thicker boundary layer and more quenching close to the walls seen as lower heat release and lower combustion pressure. An improved LES model taking local wall temperature into account would improve this problem. However it is believed that the major contributor to the overestimated heat release is due to the lack of topland in the LES. Even though there are ways of improving the LES the major differences in heat release start and rate between the geometries are captured. To summarise, the early start of combustion and longer combustion duration is captured in the heat release analysis, chemiluminescence imaging, LIF imaging and LES. Since all four techniques show basically the same phenomena there is a solid foundation for the explanation of the lower heat release rate being due to stratification. Then it is left to decide if the inhomogeneities are based on temperature stratification or fuel stratification. A third stratification could be incomplete mixing of residuals and fresh charge which give also stratification in temperature, fuel and diluent distribution.

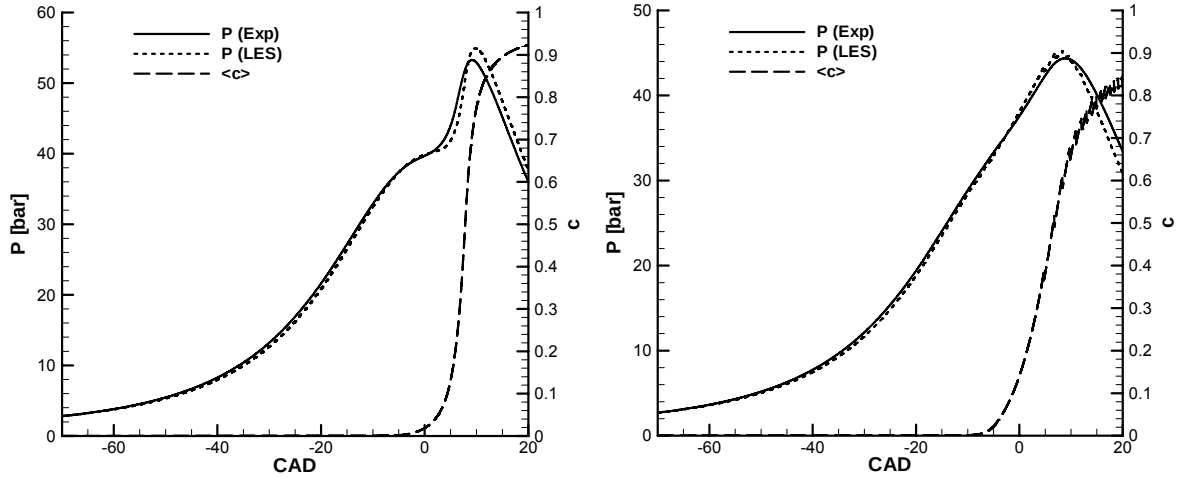

Figure 54. Pressure traces and heat release (c) from LES and experiments. The Disc case is seen to the left and the bowl to the right.

Another feature of the LES is to compare the combustion process in the vertical direction from the bowl into the squish with the chemiluminescence images found in Figure 49 and Figure 50. The temperature field during intake and compression is seen in Figure 55. The instantaneous temperature field is shown along the centre bore axis, between the two intake valves to the right in the images and between the two exhaust valves to the left in the images. Here it is seen that there exists a wider temperature distribution in the bowl case as early as the intake stroke. The reason for this is twofold; the lower intake temperature in the bowl case results in a wider temperature distribution since the burned gas temperatures are assumed to be the same between the geometries. The second reason is the higher wall heat transfer from the bowl. This temperature stratification is fairly constant throughout compression until closer to TDC when the charge autoignites. From Figure 56 the temperature distribution close to TDC can be studied. Note that the temperature scale is not the same as in Figure 55. Here it is clearly visualized that auto ignition appears first in the bottom of the bowl. The higher temperatures due to combustion are not present in the squish until around 10 CAD after TDC. This is consistent with the chemiluminescence signal level calculated for the squish in Figure 51 (b). From the LES the calculated temperatures are between 900 and 1000K for the squish

at TDC. Remember that the peak cylinder pressure (PCP) was overestimated with LES due to the sources of error discussed earlier in this section.

The combustion chamber temperature is calculated from the pressure and thus the peak cylinder temperature is likely also overestimated. This suggests that the temperatures from LES in the squish should be somewhat lower.

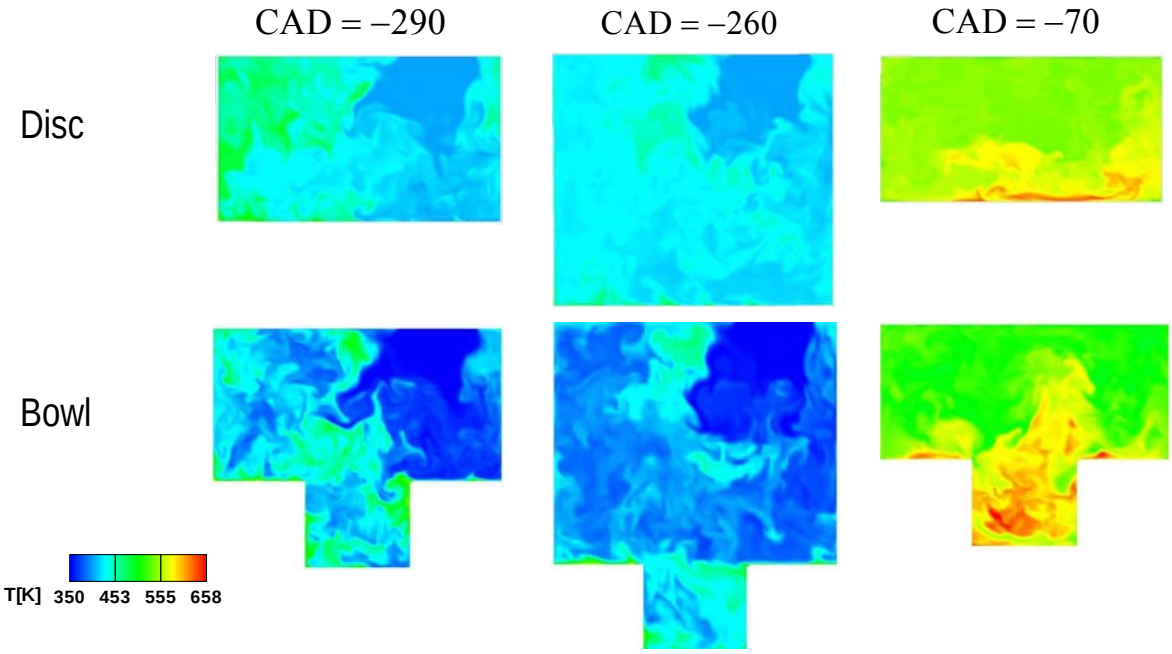

Figure 55: Instantaneous temperature distributions from LES at two CAD positions during intake and one CAD position during compression. Disc and Bowl geometries represented.

Since ethanol autoignites at roughly 950K for this air/fuel ratio calculated from the 1% heat release point in these experiments and according to [42], it is not strange that the reactions are just about to start at this CAD position. Peak cylinder pressure (PCP) is around 10 CAD ATDC which means that between TDC and for the crank angle of PCP the temperature has increased enough to at least partially oxidize the fuel present in the squish. The reason for the temperatures in the squish reaching auto ignition conditions late compared to the bowl is probably higher heat losses due to the high area to volume ratio. The combustion in the bowl increases the global pressure and temperature between TDC and 10 CAD ATDC. Another effect is heat and species transport due to diffusion from the bowl into the unburned zones. These effects together explain the reason for retarded combustion in the squish which also contributes to lower ROHR and longer combustion duration. A counteracting effect to increased combustion duration is quenching which results in advanced end of combustion. The effects of poor combustion in the squish on the engine efficiency and emissions will be discussed in the next section showing results from metal engine experiments.

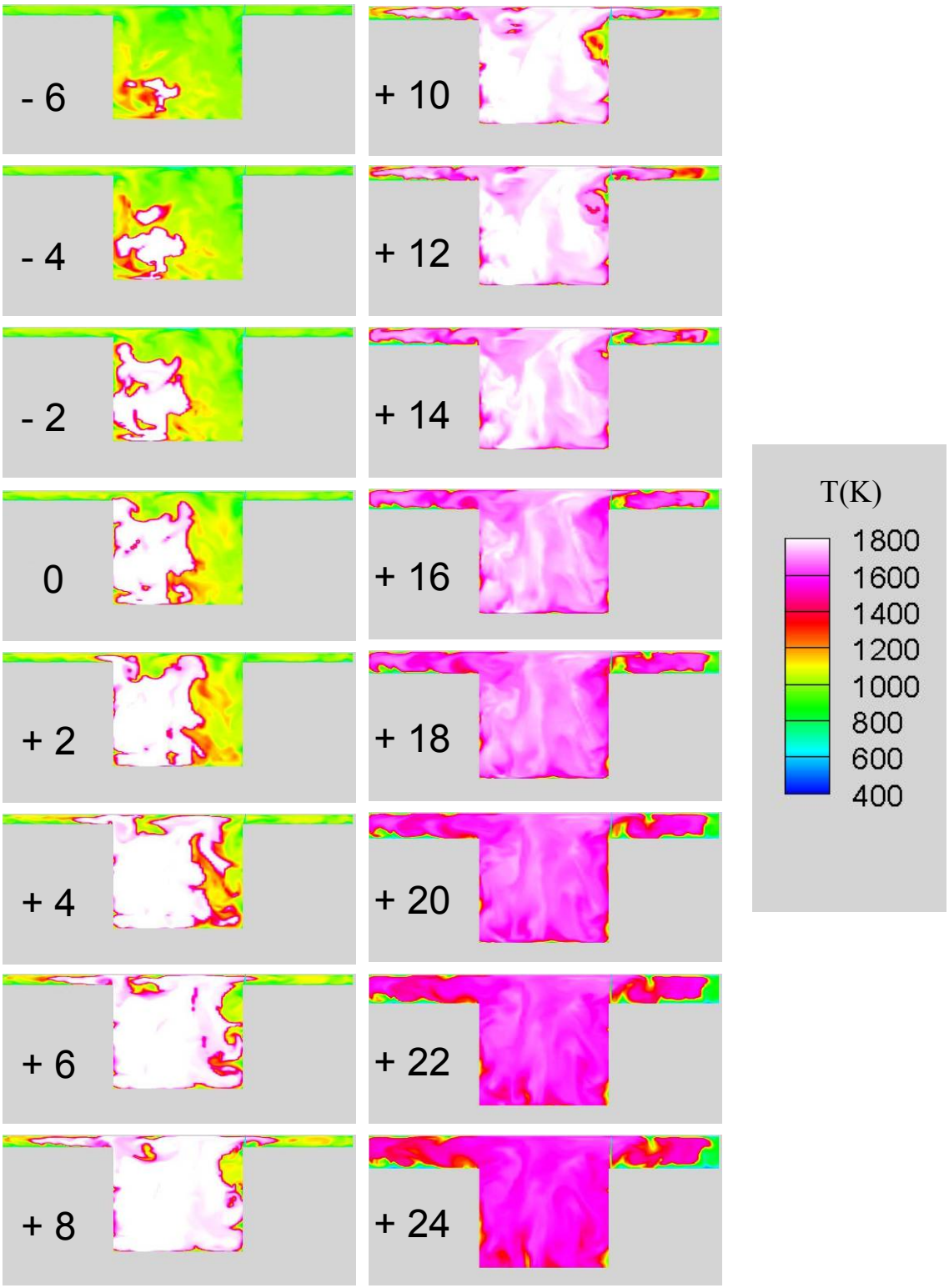

Figure 56: Instantaneous temperature distribution during combustion from LES for the bowl geometry. The numbers denote the corresponding CAD.

5.5.4. Metal Engine Experiments

The aim of the experiments in Paper 10 is to compare the Square Bowl and Disc combustion chambers during more realistic conditions than the optical engine can provide. The drawback of using optical engines is that the crevice volumes are larger which effects the unburned hydrocarbon emissions and engine efficiency. Further, since the quartz glass has much lower heat conductivity the wall temperature is usually higher [82, 83] and the heat losses are less compared to a metal engine [83]. The higher wall temperature will in turn change the temperature distribution in the cylinder. Since HCCI combustion is highly sensitive to wall temperature this is an issue. Optical engines are also limited in engine speed, usually 1200 rpm and also limited in load. The optical Scania engine has never been run with higher loads than approximately 3.5 bar IMEP for extended periods without breaking the gaskets for the piston window. At higher loads knock is a problem and since knock increases the heat transfer to the walls the temperature of the materials increase substantially and eventually the thermal stress limit of the gaskets are reached and they break. Another downside with optical engines is the dry nylon piston rings used to avoid window fouling with oil in the cylinder to be able to conduct optical diagnostics. The lifetime of these piston rings is limited and therefore affects the mass losses and compression pressure when they are worn out. It should also be noted that the long piston extension is affected by mass forces, gas forces and thermal expansion. The mass forces tend to elongate the piston at TDC and are a function of engine speed. The thermal expansion is a function of temperature meaning that the elongation of the piston depends on the heat conductivity of the material used. A counter acting effect to the previous two mentioned effects is the gas forces which compress the piston extension at combustion TDC and is a function of pressure and thus the compression ratio of the engine. These effects together result in different actual compression ratios than the calculated compression ratios from the geometry. This also affects the extent of preheating the inlet air to achieve auto ignition compared to a metal HCCI engine. Lastly, there also exist differences in cooling capacity since the 30 mm high ring placed between the cylinder head and the cylinder liner of the optical engine is not cooled. This ring is either made in quartz glass when optical access is needed from the side of the combustion chamber or it is made of steel if optical access is only needed from below. This suggests that the top 30 mm of the cylinder liner is hotter compared to the metal engine where the cooling water can enter further up the liner through water jackets. The metal engine also uses a cooling oil spray underneath the piston. Since the bottom side of the piston is made of quartz glass in the optical engine and has to be kept clean, an air jet of compressed air is directed towards the piston instead.

In order to investigate the combustion chambers performance regarding emissions and efficiency at different engine speeds and loads it is therefore better to perform the measurements in a metal engine. Another feature is the lower costs of piston crowns in metal rather than quartz glass which enables more geometries to be tested. Such an example is a circular bowl which was tested in order to find the effects of the corners in the Square Bowl on the combustion process. However, due to lack of data only one load point and combustion phasing will be presented from the circular bowl. A standard Scania D12 Diesel piston was also tested since it has a wide and shallow circular bowl. Pictures of the pistons can be seen in Figure 57.

Due to the compact design of the original Diesel piston in the Scania engine, i.e. the distance from the centre of the piston pin to the top of the piston it was not possible to fit the deep Square Bowl without the top of the piston crown protruding above the engine block deck plane. Since a shorter connecting rod was not available the solution was to use a spacer similar to the ones used in the knock and ion current studies between the engine block and the

cylinder head. The downside with using a spacer is that the topland crevice increases since the piston rings must be kept in the original cylinder and not pass the seam between the engine block and spacer which would otherwise instantly lead to hardware failure. However there is still a substantial difference in crevices compared to the optical engine setup. It is suspected that the Diesel bowl will have an advantage in efficiency since the topland height is only 14.3 mm compared to the Disc and bowl geometries with topland heights of 25.7 mm. The topland width in the metal engine experiments has been kept the same. The crevice volume constitutes 8.8 percent of the compression volume at TDC by using this spacer. This has to be kept in mind when comparing the results of the Diesel geometry compared to the Disc and Square Bowl geometries. In an optical setup the topland height of the Disc and Square Bowls are 44.5 mm and the topland width is also larger. Therefore the topland crevice is even larger in the optical experiments compared to the all-metal engine experiments and the total crevices have increased from 8.8% to 13.6% of the compression volume at TDC. In the next subsection a comparison in performance between the optical and metal engines will be shown.

Figure 57: Pictures showing the different combustion chamber shapes tested in the metal engine experiments. Top left is the Disc, top right is the Square Bowl, down left is the Circular Bowl and down right is the standard Scania Diesel Bowl.

5.5.4.1 Comparison between Optical and Metal Engine Experiments

As described in the previous section there are substantial differences in the behaviour of an optical engine compared to a metal engine. The effects of increased crevices, wall temperatures and heat losses change the temperature field in the cylinder which is critical for reaching auto ignition conditions. In order to compare the Disc and Square Bowl with the Diesel combustion chamber the compression ratio was set to 18:1 in the metal engine tests

which is the standard compression ratio of the Scania D12 Diesel engine. The standard Diesel piston has 1 mm squish distance and therefore the same was also used in the Square Bowl case. The geometrical data for the different combustion chambers in both optical and metal engine configuration can be found in Table 6. The table shows the compression ratios, squish distances, topland heights, spacer heights, bowl dimensions, total wall area, percentage of the total wall area which is in the squish, percentage of the total volume which is in the squish and lastly the area to volume ratio in the squish. All values are calculated when the piston is at TDC. Three different Square Bowls are represented in the table, SQ1, SQ2 and SQ3, corresponding to different development stages during the experiments to improve the performance of the Square Bowl regarding efficiency. The circular bowl is also shown.

In Table 7 some performance parameters can be found for different geometries both in optical and all-metal configuration. The relative air/fuel ratio (λ) was 3.3 and the engine speed 1200 rpm as in the LIF, LES and chemiluminescence results presented previously. The aim has been to keep constant combustion phasing (CA50), but since the engine was running in open loop control wall heating effects have resulted in overly advanced CA50 with SQ and SQ2. By comparing the Disc in optical and metal configuration it is seen that the net indicated efficiency ($\eta_{i,net}$) is 4% units higher in the optical engine even though the combustion efficiency is better and the compression ratio is higher in the metal engine. The inlet temperature is also higher in the metal engine even though the compression ratio is higher. This can be explained by lower heat losses in the optical engine due to the lower heat conductivity of quarts glass. The crevice losses are higher in the optical engine due to the large topland region, seen as increased UHC emissions and lower combustion efficiency.

The combustion efficiency, net indicated efficiency, CO and UHC emissions of SQ1 show partial misfire conditions. The reason for the partial misfire is believed to be quenching in the squish region due to a high area to volume ratio in combination with higher heat conductivity of steel resulting in increased heat losses and a lower temperature of the gas. The boundary layer thickness is of importance in the squish volume since the axial distance between the cylinder head and the piston is small. The work by Hultqvist et al. [84, 85] suggests that the axial boundary layer thickness is in the range of 1 – 3 mm during HCCI operation and relative air/fuel ratios (λ) of about 3. This conclusion was drawn from chemiluminescence images in the Volvo TD100 engine using PRF35 as fuel and 10:1 as compression ratio. Similar results were found by Persson et al. [86] in a smaller DI HCCI engine during early injection and using PRF50 as fuel. This means that the squish volumes in the Square Bowl combustion chambers mainly consist of boundary layers at TDC since the boundary layer itself is probably thicker than the squish distance. Therefore it is not far fetched that quenching might occur in the squish region. If a portion of the gas in the combustion chamber is quenched the combustion duration is drastically shorter. If high enough temperature would be present in the whole combustion chamber the ROHR would increase due to the self accelerating process of auto ignition. This effect results in shorter combustion duration. A counter acting effect is that fuel is consumed in areas which were previously quenched and this increases the combustion duration. By increasing the squish distance to 3 mm with the same compression ratio (SQ3) the combustion efficiency and net indicated efficiency improved since better conditions for auto ignition were achieved in the squish region. In this case the effect of combustion occurring in regions previously quenched is stronger than the effect of increased ROHR resulting in overall longer combustion duration.

Table 6: Geometrical data of different combustion chambers in both optical and metal engine configuration. SQ = Square Bowl, CB = Circular Bowl, DB = Diesel Bowl, Q = Quartz, T = Titanium, S = Steel.

	Optical Engine		Metal Engine					
Geometry	**Disc**	**SQ**	**Disc**	**SQ1**	**SQ2**	**SQ3**	**CB**	**DB**
CR	17.2:1	17.2:1	18:1	18:1	17.0:1	18:1	18:1	18:1
Squish Distance [mm]	8.15	1.75	8.15	1.00	2.00	3.00	3.00	1.00
Topland Height [mm]	44.5	44.5	25.7	25.7	24.7	25.7	25.7	14.3
Spacer height [mm]	30	30	14	14	14	14	14	0
Bowl Dimensions [mm]	-	47 x 37.5	-	47 x 38	47 x 37	47 x 27	Ø 53.9 x 27	Ø 86
Wall Area [cm^2]	288	333	288	330	332	317	311	~300
Squish Area [%]	-	65.6	-	64.2	65.0	69.3	70.66	~47
Squish Volume [%]	-	15.3	-	9.0	17.1	27.2	27.2	6
Squish Area/Volume ratio	2.8	11.8	2.8	20.4	10.4	7.0	7.0	20.6
Piston Crown Material	Q / T	Q	S	S	S	S	S	S

Table 7: Performance comparison between different combustion chamber geometries in both optical and metal engine configuration at an engine speed of 1200 rpm and λ=3.3. SQ = Square Bowl, CB = Circular Bowl, DB = Diesel Bowl

	Optical Engine		Metal Engine				
Geometry	**Disc**	**SQ**	**Disc**	**SQ1**	**SQ2**	**SQ3**	**CB**
CA10 [CAD]	3.5	-1.2	4.8	3.6	2.5	3.9	3.7
CA50 [CAD]	7.9	6.8	7.8	7.8	5.8	7.7	7.8
CA90 [CAD]	14.4	18	10.6	11.4	11.0	12.8	13.7
CA90-CA10 [CAD]	10.9	19.2	5.8	7.8	8.5	8.9	10.0
UHC [ppm]	3563	5629	2458	7938	3277	2557	3040
CO [ppm]	1368	3330	1476	3460	2209	2659	4001
η_{comb} [%]	90.3	82.9	91.9	76.9	89.3	90.1	87.8
$\eta_{i,net}$ [%]	44.2	35.0	40.2	25.6	35.5	38.9	38.6
T_{inlet} [°C]	127	93	130	99	115	113	113

The Disc combustion chamber has 2,4 percent units higher net indicated efficiency than SQ3 which is an effect of combustion phasing since each geometry has its own optimum phase for maximum net indicated efficiency. This fact will be shown later in the next section.

The circular bowl (CB) has about the same net indicated efficiency and combustion duration as SQ3. However the combustion efficiency for CB is poorer since the UHC and CO emissions are high. This suggests that the thermal efficiency is better with CB probably due to the smaller wall area. In Figure 58, CB and SQ3 have been compared regarding rate of heat release and cumulative heat release. The heat release seems identical from point of ignition to about 60% heat released. After this point the CB combustion rate decreases compared to SQ3. A theory explaining this phenomenon is that the heat losses are higher in SQ3 during the early stages of combustion since the swirling motion has been broken up into turbulence and thus heat losses. This means that there is less energy left in the turbulence and flow when the compression from combustion pushes the unburned gases into the squish compared to the more undisturbed swirling flow motion of CB. If the flow in SQ1 is slower parallel to the piston surface and cylinder head in the squish region this results in lower heat transfer according to *Woschni* [52]. Since the squish region is sensitive to heat losses, the combustion

efficiency will be suffering from the higher flow velocities in CB. This would in such a case be seen as lower heat release rate in the later stage of the combustion process and also increased UHC and CO as seen in Figure 58. A counteracting effect to the higher heat losses inside the square bowl in the early part of the combustion process due to higher turbulence and larger wall area could be more efficient combustion. Recirculation zones are easily achieved in corners when the swirling flow is entering the bowl during the intake stroke. In a corner the local wall area to volume ratio is higher resulting in higher heat transfer to the gas and due to the recirculation phenomenon the hot gases are not transported away from the walls to the same extent as one would suspect with a flat wall. This suggests that the gas temperature close to a corner is higher than the rest of the bowl during compression but some is lost due to increased local heat transfer from higher difference between gas and wall temperature. If the temperature next to the wall is higher also during the combustion process the combustion efficiency could improve. If the increased heat losses due to increased turbulence and larger wall area and improved combustion efficiency due to higher local temperatures are counteracting each other and are equal in size the net result is the same heat release rate in SQ3 as in CB. The discussion above should merely be seen as a hypothesis and not a proof. Further studies are needed to really distinguish the real effects of the corners on the combustion process.

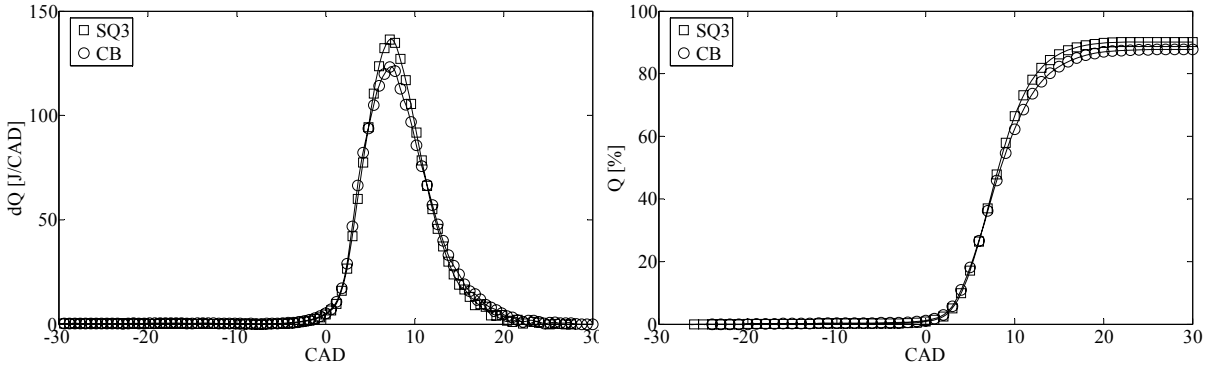

Figure 58: Comparison between SQ3 and the circular bowl for the same fueling rate and 1200 rpm. Rate of heat release (dQ) is seen to the left and the cumulative heat release to the right. The geometrical data can be found in Table 6 and performance figures in Table 7.

What can be concluded from the comparison between the optical and metal engine tests is that the quartz glass changes the temperature distribution in the cylinder acting as an insulator. If the wall temperature is high as it is with quartz glass the heat transfer occurs to a larger extent from the walls to the gas during the intake stroke creating a wider temperature distribution in the cylinder. This is particularly pronounced in the bowl case since the walls in the bowl consist entirely of quartz glass. In the corners of the bowl the local area to volume ratio is high resulting in high local heat transfer. An additional effect could be the swirling flow into the bowl causing recirculation zones in the corners locally heating up the gas. This is probably the reason for the start of combustion always being in one of the corners of the bowl according to the chemiluminescence images seen in Figure 50 and Figure 52. The poor combustion efficiency in the Square Bowl in metal configuration (Table 7) suggests that the walls of the squish region are cooler compared to optical experiments resulting in local quenching. If not all areas in the engine undergo combustion the combustion duration is drastically shorter. Here it is shown that there can be large differences in engine performance for what seems to be similar conditions between an optical and metal engine. This problem is especially important in HCCI engines compared to SI and CI engines since the HCCI combustion process is highly affected by wall temperatures. A way of performing optical

experiments in engines without using large sections of windows is to use an endoscope mounted in the spark plug thread or through a specially made passage to the combustion chamber of a metal engine. Even though the field of view is less compared to an engine using a Bowditch type of optical access the temperature distribution in the cylinder should be more undisturbed resulting in more realistic experiments. Also by using an endoscope the combustion process in the circular bowl could show the effects of the corners in the square bowl. For a more detailed comparison between the optical and metal engine the interested reader is referrer to Paper 10.

5.5.4.2 Metal engine performance with different combustion chambers

Low load case

In this section the performance with the Disc, SQ2, SQ3 and the Diesel combustion chambers will be evaluated. The reason for excluding SQ1 is its extremely poor efficiency which has been shown in the previous section. The geometrical data of the combustion chambers can be found in Table 6. The tests have been performed with the same fuel rating for all running conditions and all combustion chambers corresponding to a FuelMEP of 6.55 bar. Due to different efficiencies depending on combustion chamber used, the load is roughly 2.5 to 3 bar IMEP, similar to the load tested in the optical and LES studies. The engine speed was 1200 rpm and the combustion phasing was altered by changing the inlet air temperature. The results can be found in Figure 59.

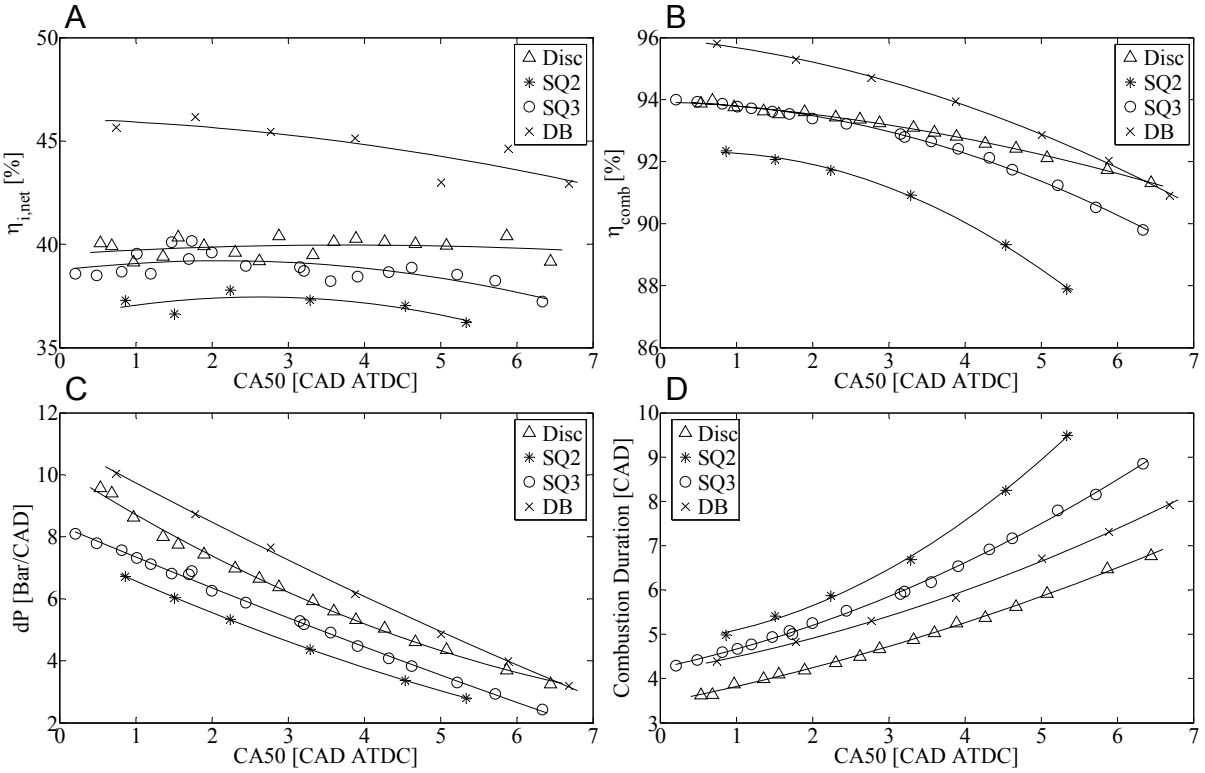

Figure 59: Performance of the Scania D12 HCCI engine as function of CA50 while using different combustion chamber geometries. (A) Net indicated efficiency ($\eta_{i,net}$). (B) Combustion efficiency (η_{comb}). (C) Pressure rise rate (dP). (D) Combustion duration (CA90-CA10) as function of CA50. See Table 6 for geometrical data of the combustion chambers. The engine speed was 1200 rpm and the FuelMEP was 6.55 bar.

The net indicated efficiency ($\eta_{i,net}$) increases with advanced combustion phasing (Figure 59 A), i.e. lower CA50, mainly due to improved combustion efficiency as seen in (B), combustion duration being shorter (E) and closer to TDC. This is true until the heat losses exceeds the previous factors mentioned and the net indicated efficiency decreases for early CA50. Even if the trends are weak, the peak net indicated efficiency for the Square Bowl combustion chambers are around 2.5 CAD ATDC in CA50, while the Diesel combustion chamber seem to have peak net indicated efficiency at overly advanced combustion phasing outside the tested CA50 range. The Disc has a very flat net indicated efficiency profile suggesting that a wider range of CA50s can be used without any major loss in efficiency. For early CA50 the efficiencies of SQ3 and the Disc are quite equal with a small advantage for the Disc. The main reason is that the combustion efficiency improves substantially with SQ3 for early CA50 suggesting that a larger portion of the fuel in the squish is consumed due to higher temperatures and pressures. The Diesel combustion chamber is superior regarding net indicated efficiency, around 5% units higher than the Disc and SQ3 much due to less crevices and smaller squish region. For late CA50 the Disc performs the best due to lack of squish region and less charge is therefore quenched. Regarding pressure rise rate (C), the highest values are found for the Diesel combustion chamber and the Disc. There are two reasons explaining this, one is the higher overall ROHR and the other is less stratified charge resulting in shorter combustion duration. The combustion duration is found in (D) where the Disc combustion chamber has the shortest combustion duration followed by the Diesel, SQ3 and lastly SQ2. In section 5.5.4.1 it was shown that the combustion duration was increased when changing piston from SQ2 and SQ3, the opposite of what was just concluded. An explanation to this might be that the combustion phasing is rather late in the comparison in Table 7 resulting in low combustion temperatures. This is especially pronounced in a combustion chamber with a tight squish region resulting in more heat losses and more quenching. If enough of the charge is quenched the combustion duration is decreased.

To summarize this section the main conclusion is that the net indicated efficiency is similar between the square bowl and the disc for early combustion phasing when there is high enough temperature present to sustain the combustion in the squish volume of the square bowl combustion chamber. In the metal engine, the square bowl results in longer combustion duration and lower pressure rise rate than the Disc combustion chamber. The effect is however not as pronounced as in the optical configuration.

In the experiments by Christensen [40, 41] in a Volvo TD100 HCCI engine the efficiency for the square bowl combustion chamber was found to be equal or better than the disc. In the present study performed in a Scania D12 HCCI engine the efficiency of the square bowl combustion chamber was only equal to the disc for early combustion phasing. A major difference between the previous study in the Volvo TD100 engine and the present study in the Scania D12 engine is the compression ratios used. The Volvo TD100 engine had 11,1:1 in CR resulting in a much higher fraction of the total compression volume in the bowl compared to the Scania D12 engine with 18:1 in compression ratio since the squish distance was the same in both engines, 1mm (SQ1). The width/depth relationship of the square bowl was the same in both studies. A larger bowl results in a smaller squish region and has therefore less quenching problems. This suggests that the square bowl combustion chamber is better than the disc for low compression ratios. Experiments with different compression ratios in the Scania D12 engine could show the effect of compression ratio on the performance of the square bowl and disc combustion chambers.

Load Sweep

The low load case presented previously has shown the characteristics of the combustion processes in the combustion chambers as function of combustion phasing and pressure rise rate. In this section the aim is to show the performance of the engine with different combustion chambers as function of load. For each load point and combustion chamber the combustion phasing was tuned toward maximum indicated efficiency. In Figure 60 the net indicated efficiency (A) and pressure rise rate (B) as function of $IMEP_{net}$ can be found. The overall trend seen in (A) is that $\eta_{i,net}$ increases with higher load up to a limit when the heat losses become dominating due to high temperatures and knock. The major contributor to the poor low load efficiencies are low combustion efficiencies due to lower combustion temperatures especially in the squish regions. The highest efficiencies are found slightly above 4 bar $IMEP_{net}$ for all combustion chambers. The Diesel combustion chamber has a maximum efficiency of 48% and at idle conditions around 1 bar $IMEP_{net}$ the efficiency has decreased to 30%. SQ3 has the same net indicated efficiency of 43% as the Disc at loads around 4.5 bar $IMEP_{net}$, but for lower loads around 2.5 bar $IMEP_{net}$ the Disc has slightly higher efficiency than SQ3. When selecting these measurement points with maximum net indicated efficiency a criterion has been that the pressure rise rate should not exceed 10 bar/CAD due to excessive noise, see (B). A way of improving the low load efficiency with HCCI operation could be to use charge stratification using DI and create richer zones which burn at a higher rate [92, 93]. An alternative is inlet air throttling where a richer uniform mixture is obtained which burns at a higher rate but at the expense of increased throttling losses [35].

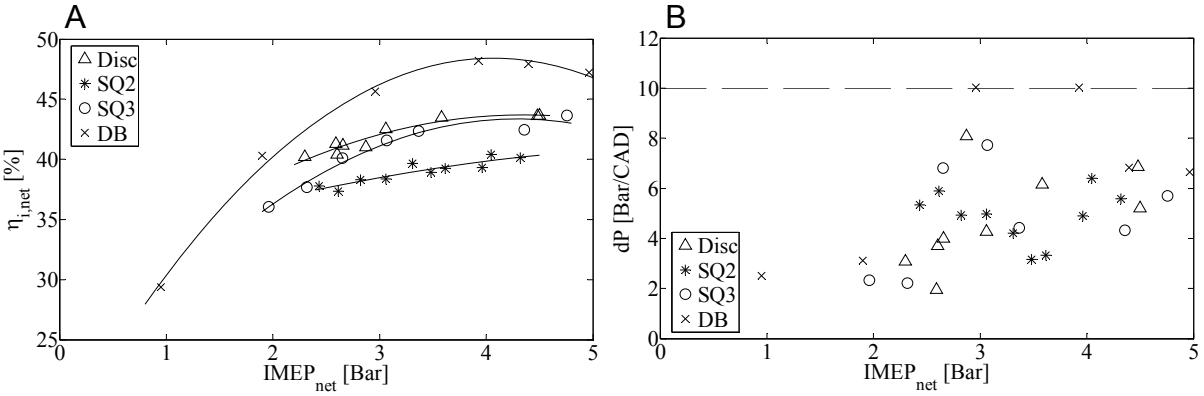

Figure 60: (A) Net indicated efficiency, (B) Pressure rise rate as function of $IMEP_{net}$. The engine speed was 1200 rpm.

The main conclusion that can be drawn from this load sweep is equal net indicated efficiencies for the Square Bowl and the Disc at higher loads. At lower loads quenching is dominant in the combustion chambers with a squish volume which makes the Disc a better choice than the Square Bowl. In this comparison the Diesel combustion chamber has superior efficiency much due to less crevice losses. The results of the Diesel combustion chamber would be more comparative with the other combustion chambers if the topland volumes were similar but this was not possible to achieve within this study.

5.5.5 Discussion on Combustion Chamber Geometry Effects on HCCI Operation

The results presented in this section showed something which was not clarified before, the combustion starts in the bowl and propagates into the squish volume. From the chemiluminescence images it is evident that the combustion starts in the bowl but it is still unclear if the residuals start the combustion or it is due to some other effect. It is thought that the fastest combustion is achieved in a perfectly mixed charge where the relative air/fuel ratio and also temperature is the same all over the combustion chamber. Under these conditions the charge will ignite all at once and the rate of combustion will be very high. If there is a location in the charge with different temperature or different relative air/fuel ratio the combustion duration will be longer since the locations in the charge with the best conditions for auto ignition will burn first and when the pressure and thus temperature is increased globally in the combustion chamber the rest of the charge will burn too. Small stratifications in temperature and air/fuel ratio will always exist in a combustion engine, but the larger stratifications might change the combustion process drastically. The potential of thermal stratification for decreasing pressure rise rates and increasing the maximum load has been studied by other researchers such as for example *Sankaran* et al. [91] and *Sjöberg* et al. [87 - 90] where the effect of different running conditions on the natural thermal stratification was investigated both in experiments and simulations.

However, it should be mentioned that there may exist running conditions where temperature stratification could decrease the combustion duration. When the combustion phasing is too late partial misfire occurs due to bulk quenching when it is too cold in the entire combustion chamber. If a large temperature stratification is introduced into this well mixed charge the combustion would start earlier in the location with the best conditions for auto ignition. This initial heat release will increase the pressure and temperature in the combustion chamber and, if sufficient, start the reactions in the rest of the combustion chamber earlier preventing misfire. The result is advanced combustion similar to the laser assisted experiments in Section 5.4.2 and since the rate of heat release increases the combustion duration decreases.

From the chemiluminescence and LIF images the combustion seems highly stratified and slow during the first 10 CAD of the combustion. The early start of combustion in one of the corners of the bowl could be due to locally high temperature. The higher temperature in this zone could be due to high local area to volume ratio increasing the heat transfer from the walls to the gas during the intake stroke. If a recirculation zone exists in the corner less heat is transported away resulting in larger temperature stratification in the bowl. Since the wall temperature is expected to be higher in the optical engine the local gas heating effect should be higher compared to the metal engine.

The retarded combustion in the squish volume is probably an effect of lower temperature due to quenching at TDC. Since there is a long ignition delay in the squish the combustion duration is long. But the ROHR is low also during the combustion in the bowl. If it is assumed that air and fuel are well mixed, the sharp gradients seen in the images could be due to large temperature stratification. In contradiction to this statement one might argue that the increased turbulence level in the bowl ought to mix the hot and cold zones creating a fairly homogeneous mixture. Another effect of turbulence but earlier in the cycle during the intake stroke is that the turbulence transport hot gases from the hot walls into the cold fresh charge creating temperature stratification, as seen from the LES study in Paper 9.

The initial highly stratified combustion in the bowl is of great interest since it behaves almost like flame propagation, even though no external ignition source has been used. The calculated expansion speed of the reaction front along the upper wall in the Square Bowl was roughly 19 m/s which is similar to the flame expansion speed calculated in the laser assisted HCCI experiments, i.e. 15 m/s. Usually, the expansion speed seen with HCCI combustion is at least 10 times higher. With flame propagation in SI engines the reactions propagate due to diffusive transport of heat and radicals to the neighbouring gas just in front of the flame. The gas further ahead of the flame front is far from auto ignition even if the global pressure and temperature is raised due to the reactions in the flame front and in the post flame. When fairly homogeneous HCCI combustion has started and unburned reaction zones exist, the pressure does not have to be raised much to increase the temperature to reach auto ignition in these zones. Thus the transport of heat is much faster than the transport of radicals needed to start new chemical reactions. However when the surrounding unburned zones have a much lower temperature it takes longer time to increase the temperature to reach auto ignition. Since it takes time to raise the temperature in the unburned charge, the effect of reactive radical transport may play a larger role. In Figure 50 the highly stratified reaction propagation is seen. It is likely that the rest of the charge has a much lower temperature as described previously, thus the gas closest to the reaction zone is the only one reaching auto ignition. However to separate this type of combustion from flame propagation, the reaction zone is much thicker, since the fuel is gradually consumed even though it is in a small volume. The reaction zone in a flame front is much thinner and consumes almost all the fuel quickly at high temperatures as it propagates. This is seen in the experiments with laser ignition, in Figure 45 close to TDC, with a thin reaction zone.

To return to the discussion about the combustion inside the bowl the combustion rate speeds up close to TDC. It is likely that the temperature in the unburned charge has been increased by the slow stratified combustion from 12 CAD BTDC to TDC. The rest of the bulk is consumed at a faster rate, suggesting that the temperature distribution is not as wide, and reaches auto ignition almost simultaneously. Another explanation to the faster combustion rate closer to TDC could be that the turbulence influences the combustion in some way, either by the kinetics directly or through mixing. The measured turbulence level seen in the Volvo TD100 experiments in Figure 4 (a) is increases rapidly close to TDC when the squish motion has started to move the gas. In the optical Scania D12 experiments the squish distance was almost twice as high as in the Volvo engine. It is probable that the squish motion is not as strong in the Scania D12 and maybe closer to TDC. If the squish motion has time to mix the hot and cold zones this can also explain the increased combustion rate during the bulk combustion. To really know if this is the case new turbulence measurements have to be conducted in the Scania D12 engine and at several locations in the bowl, preferably at different depths in the bowl. Also chemiluminescence imaging from the side through the quartz liner could show where inside the bowl the combustion starts and how it propagates. If a well defined flow field can be established in combination with further optical measurements and simulations the knowledge about the effect of combustion chamber geometry on HCCI combustion could improve.

6 Summary and Conclusions

In this thesis different diagnostic methods have been used to study local and global combustion phenomena in the HCCI operating range.

The work started with a study on pressure wave phenomena during rapid HCCI combustion. Eight pressure transducers in the same cylinder were used to distinguish the pressure inhomogeneities during knocking combustion. It was found that the pressure oscillations experienced on the pressure trace during operating conditions that result in high heat release rates correlate well with the acoustic wave theory usually applied to knock in SI engines. Further it was found that changing the combustion chamber geometry from a Disc to a circular bowl in piston suppressed knock during similar running conditions.

Ion current diagnostics were investigated in two HCCI engines. The location of the ion current probe and the effect of using different fuels were evaluated. Since the ion current is depends heavily on the local air/fuel ratio and temperature, it is of high importance to select the right location in the combustion chamber for ion current feedback in an engine control perspective. Higher octane number fuels seem to more easily provoke ion current appearance. Still there is an issue of using ion current for feedback purposes due to lack of signal at low loads close to idle when the mixture is lean and the temperature is low.

Also laser assisted HCCI combustion was studied at running conditions that normally would lead to partial or total misfire with resulting poor efficiency. By the use of a laser ignition system a flame propagates through the charge raising the global pressure and temperature which results in improved conditions for auto ignition. The HCCI combustion is then advanced and the overall efficiency improved. Two different fuels were tried, PRF80 and natural gas. PRF80 provoked cool flames which seemed to suppress the effect of increased pressure and temperature on the main combustion. The experiments while using natural gas as fuel were more successful where the HCCI combustion could be advanced up to 8 CAD during very lean and diluted running conditions. Thus by using laser assistance it is possible to control the HCCI combustion phasing during poor running conditions.

Lastly the effect of combustion chamber geometry was studied using chemiluminescence imaging, fuel tracer LIF, LES and metal engine experiments. Drastically decreased combustion rates were experienced while using a deep Square Bowl in piston geometry compared to a Disc shaped combustion chamber. Similar engine efficiencies in the optical engine open the possibility to increase the load during HCCI operation since the maximum load is limited by excessive combustion rates resulting in knocking combustion and excessive noise. By using chemiluminescence imaging it was found that the combustion was slow and stratified in the bowl geometry and the combustion in the squish region was retarded due to quenching. Fuel tracer LIF showed similar behaviour with sharp wrinkled gradients between the burnt and unburnt gases. LES confirmed the stratified behaviour seen with optical diagnostics and it was found that the slower combustion was due to thermal stratification meaning that hot zones ignite first and propagate into the colder ones. However, in metal engine experiments it was found that the advantage of slower combustion was at the expence of poorer efficiency especially for retarded combustion phasing, one main reason being quenching in the squish region due to the narrow squish distance. Other contributions to poorer efficiency were found in the longer combustion duration and increased heat losses which decreases the thermal efficiency of the engine. If the squish distance was increased the

efficiency was improved up to the same levels as the Disc combustion chamber but the advantage of slower combustion was found to be less with this modification.

7 Future Work

The experiments presented in this thesis have focused on HCCI operation. Since HCCI combustion is limited in load due to rapid heat release in one end and misfire in the other, one suggestion is research on a concept combining classical HCCI with PPC in a heavy duty diesel engine using common rail direct injection (DI) and VVA. The advantage of using common rail DI is the possibility to inject fuel early resulting in a premixed charge for HCCI operation and later injection for running PPC or even later injection for classical CI operation if the load range of PPC is found to be insufficient. To suppress NO_x EGR can be used to decrease the combustion temperature in PPC and CI mode. A low cetane number fuel can be used to increase the ignition delay and increase premixing when running in HCCI or PPC mode. The fuel could still be feasible for CI operation while using the VVA system to increase the effective compression ratio and decrease the ignition delay if necessary. At idle conditions running the engine in HCCI mode throttling of the intake air can be used to increase the mixture strength without loosing efficiency. The richer mixtures also open the possibility to use ion current sensing using the DI injector tip as sensor for combustion control in HCCI mode and to some extent in PPC mode. A tool for controlling the combustion phasing could be the VVA system by changing the effective compression ratio by IVC and/or residual gas trapping. Since the combustion efficiency is improved and exhaust temperature is increased it would be easier to utilize an oxidation catalyst for reducing UHC and CO emissions during HCCI and PPC operation. If it could be possible to run the engine up to 20-22 bar BMEP in PPC mode the result is an engine with similar efficiency as a diesel engine but run with LTC in the full load range and thus low emissions.

Another challenge would be to develop an optical engine with less quartz glass parts and higher mechanical strength making it more similar to a metal engine which is particularly important in HCCI operation since the combustion process is sensitive to the wall temperature. In order to minimize the difference in heat transfer between the remaining optical parts and the metal parts sapphire glass can be used since it has higher heat conductivity. However the sapphire glass is much more expensive than quartz and is also harder to machine.

8 References

1. International Energy Agency, *"World Energy Outlook 2006"*, ISBN 92-64-10989-7, 2006

2. Global Warming Fact Sheets Series Key Stage 3, Atmosphere, Climate and Environment (ACE) Information Recourses (ARIC), Manchester Metropolitan University 2002.

3. Richard von Basshuysen and Fred Schäfer, *"Internal Combustion Engine Handbook – Basics, Components, Systems and Perspectives"*, ISBN 0-7680-1139-6, SAE International, Canada 2004

4. Air Pollution and Acid Rain Fact Sheets Series Key Stage 4, Atmosphere, Climate and Environment (ACE) Information Programme (ARIC), Manchester Metropolitan University 2002.

5. John B. Heywood. "*Internal Combustion Engine Fundamentals"*, McGraw-Hill, Inc, 1988

6. Per Amnéus, Fabian Mauss, Marcus Kraft, Andreas Vressner and Bengt Johansson, *"NO_x and N_2O Formation in HCCI Engines"*, SAE Technical Paper 2005-01-0126

7. California Air Recourses Board (ARB), http://www.arb.ca.gov/html/brochure/history.htm

8. Anders Hultqvist, Magnus Christensen, Bengt Johansson, Mattias Richter, Jenny Nygren, Johan Hult and Marcus Aldén., *"The HCCI Combustion Process in a Single Cycle – High Speed Fuel Tracer LIF and Chemiluminescence Imaging"*, SAE Technical Paper 2002-01-0424

9. Magnus Christensen, Bengt Johansson, Per Amnéus and Fabian Mauss, *"Supercharged Homogeneous Charge Compression Ignition"*, SAE Technical Paper 980787

10. Magnus Christensen, Patrik Einewall and Bengt Johansson, *"Homogeneous Charge Compression Ignition (HCCI) using Iso-octane, Ethanol and Natural Gas- A Comparison with Spark Ignition"*, SAE Technical Paper 972874

11. Göran Haraldsson, Per Tunestål, Bengt Johansson and Jari Hyvönen, *"HCCI Closed-Loop Combustion Control using Fast Thermal Management"*, SAE Technical Paper 2004-01-0943

12. J. Martinez-Frias, S. Aceves, D. Flowers, R. Smith and R. Dibble, *"HCCI Engine Control using Fast Thermal Management"*, SAE Technical Paper 2000-01-2869

13. Göran Haraldsson, Per Tunestål, Bengt Johansson and Jari Hyvönen, *"HCCI Combustion Phasing with Closed-Loop Combustion Control using Variable Compression Ratio in a Multi Cylinder Engine"*, SAE Technical Paper 2003-01-1830

14. Jan-Ola Olsson, Per Tunestål, Göran Haraldsson and Bengt Johansson, *"A Turbocharged Dual Fuel HCCI Engine"*, SAE Technical Paper 2001-01-1896

15. Håkan Persson, *"Spark Assisted Compression Ignition (SACI) – Trapped Residuals and Optical Experiments"*, Thesis for the degree of Licentiate in Engineering, ISRN LUTMDN/TMHP-06/7041-SE, Lund Institute of Technology, Lund, Sweden, 2006

16. Shigeru Onishi, Souk Hong Jo, Katsuji Shoda, Pan Do Jo and Satoshi Kato,*"Active Thermo-Atmosphere Combustion (ATAC) – A New Combustion Process for Internal Combustion Engines"*, SAE Technical Paper 790501

17. Masaaki Noguchi, Yukiyasu Tanaka, Tar Tanaka and Yukihisa Takeuchi, *"A Study on Gasoline Engine Combustion by Observation of Intermediate Reactive Products during Combustion"*, SAE Technical Paper 790840

18. Paul M. Najt and David E. Foster, *"Compression-Ignited Homogeneous Charge Combustion"*, SAE Technical Paper 830264

19. R. H. Thring, *"Homogeneous Charge Compression Ignition (HCCI) Engines"*, SAE Technical Paper 892068

20. Leif Hildingsson, *"Laser Diagnostics of HCCI and Partially Premixed Combustion"*, Doctoral Thesis, LUTMDN/TMHP--06/1041--SE, ISBN 91-628-6849-7, Lund Institute of Technology, Lund, Sweden , 2006

21. Christof Nöhre, *"Characterization of Partially Premixed Combustion"*, Master Thesis, LUTMDN/TMHP—05/5076—SE

22. S. Kimura, O. Aoki, H. Ogawa, S. Muranaka, *"New Combustion Concept for Ultra-Lean and High Efficiency Small DI Diesel Engines"*, SAE Technical Paper 1999-01-3681

23. H. Suzuki, N. Koike, M. Odaka, *"Combustion Control Method of Homogeneous Charge Diesel Combustion",* SAE Technical Paper 980509

24. M. Odaka, H. Suzuki, N. Koike, H. Ishii, *"Search for Optimization Control Method of Homogeneous Charge Diesel Combustion "*, SAE Technical Paper 1999-01-0184

25. R. Hasegawa, H. Yanagihara, *"HCCI Combustion in a DI Diesel Engine"*, SAE Technical Paper 2003-01-0745

26. R. Hasegawa, I. Sakata, T. Koyama, H. Yanagihara, *"Numerical Analysis of Ignition Control in HCCI Engine"*, SAE Technical Paper 2003-01-1817

27. N. Shimazaki, H. Akagawa, K. Tsujimura, *"An Experimental Study of Premixed Lean Diesel Combustion "*, SAE Technical Paper 1999-01-0181

28. Y. Iwabuchi, K. Kawai, T. Shoji, Y. Takeda, *"Trial of a new Diesel Engine System – Premixed-Compression-Ignited Combustion"*, SAE Technical Paper 1999- 01-0185

29. Jari Hyvönen, *"The Performance of a Multi Cylinder HCCI Engine using Variable Compression Ratio and Fast Thermal Management"*, Doctoral Thesis, ISRN LUTMDN/TMHP-05/1034-SE, ISBN 91-628-6681-8, Lund Institute of Technology, Lund, Sweden, 2005

30. Kopecek, H., Wintner E., Lackner, M., Winter, F., Hultqvist, A., *"Laser Stimulated Ignition in a Homogeneous Charge Compression Ignition Engine",* SAE paper 2004-01-0937, 2004

31. Ronney, P.D., *"Laser versus Conventional Ignition of Flames",* Opt. Eng. 33 (2), p510-521, 1994

32. Weinberg, F.J., *Wilson, J.R., "A preliminary Investigation of the Use of Focused Laser Beams for Minimum Ignition Energy Studies",* Proc. Roy. Soc. London, A321, p41-52, 1971

33. Kopecek, H., Maier, H., Reiser, G., Winter, F., Winter, E., *"Laser Ignition of Methane-Air Mixtures at High Pressures",* Experimental Thermal and Fluid Science 27, p499-503, 2003

34. Weinrotter, M., Kopecek, H., Tesch, M., Lackner, M., Wintner, F., Winter, E., *"Laser Ignition of Ultra-Lean Methane/Hydrogen/Air Mixtures at High Temperature and Pressure",* Experimental Thermal and Fluid Science, vol.29/5, p569-577. *2005*

35. Jari Hyvönen, Göran Haraldsson and Bengt Johansson*"Supercharging HCCI to Extend the Operating Range in a Multi-Cylinder VCR-HCCI Engine",* SAE Technical Paper 2003-01-3214

36. Jan-Ola Olsson, *"The HCCI Engine – High Load Performance and Control Aspects",* Doctoral Thesis, ISRN LUTMDN/TMHP-04/1019-SE, ,Lund Institute of Technology, Lund, Sweden, 2004

37. Carl Wilhelmsson, Per Tunestål and Bengt Johansson, *"Operation Strategy of a Dual Fuel HCCI Engine with VGT"*, SAE Technical Paper 2007-01-1855

38. Timothy Jacobs, Alexander Knafl, Stanislav V. Bohac, Dennis N. Assanis and Patrick G. Szymkowicz, *"The Development of Throttled and UnThrottled PCI Combustion in a Light-Duty Diesel Engine"*, SAE Technical Paper 2006-01-0202

39. D. Yap, A. Megaritis, M.L. Wyszynski, Hongming Xu, *"Effect of Inlet Valve Timing on Boosted Gasoline HCCI with Residual Gas Trapping"*, SAE Technical Paper 2005-01-2136

40. Magnus Christensen, Bengt Johansson and Anders Hultqvist, *"The Effect of Combustion Chamber Geometry on HCCI Operation"*, SAE Technical Paper 2002-01-0425

41. Magnus Christensen and Bengt Johansson, *"The Effect of In-Cylinder Flow and Turbulence on HCCI Operation"*, SAE Technical Paper 2002-01-2864

42. Magnus Christensen, *"HCCI Combustion – Engine Operation and Emission Characteristics"*, Doctoral Thesis, ISRN LUTMDN/TMHP-02/1006-SE, ISBN 91-628-5424-0, Lund Institute of Technology, Lund, Sweden, 2002

43. S.C. Kong, R.D. Reitz, M. Christensen, B Johansson, *Modeling the Effects of Geometry Generated Turbulence on HCCI Engine Combustion",* SAE Technical Paper 2003-01-1088

44. Salvador M. Aceves, Daniel L. Flowers, Joel Martinez-Frias, Fransisco Espinosa-Loza, Magnus Christensen, Bengt Johansson and Randy P. Hessel, *"Analysis of the Effect of Geometry Generated Turbulence on HCCI Combustion by Multi-Zone Modeling"*, SAE Technical Paper 2005-01-2134

45. Randy P. Hessel, Salvador M. Aceves and Daniel L. Flowers, *"A Comparison of the Effect of Combustion Surface Area and In-Cylinder Turbulence on the Evolution of Gas Temperature Distribution from IVC to SOC: A Numerical and Fundamental Study"*, SAE Technical Paper 2006-01-0869

46. Jimmy Olofsson, Hans Seyfried, Mattias Richter, Marcus Aldén, Andreas Vressner, Anders Hultqvist, Bengt Johansson & Karine Lombaert, *"High-Speed LIF Imaging for Cycle-Resolved Formaldehyde Visualization in HCCI Combustion"*, SAE Technical Paper 2005-01-0641

47. Gustaf Särner, Mattias Richter and Marcus Aldén, Andreas Vressner & Bengt Johansson, *"Cycle Resolved Wall Temperature Measurements Using Laser Induced Phosphorescence in an HCCI Engine"*, SAE Technical Paper 2005-01-3870

48. Carl Wilhelmsson, Andreas Vressner, Per Tunestål, Bengt Johansson Gustaf Särner, Marcus Aldén, *"Combustion Chamber Wall Temperature Measurements and Modeling during Transient HCCI Operation"*, SAE Technical Paper 2005-01-3731

49. Fred W Bowditch, *"A New Tool for Combustion Research – A Quartz Piston Engine"*, SAE Technical Paper 610002

50. Lyle Cummins, *"Internal Fire"*, Third Revised Edition, dba Carnot Press 2000

51. Sasa Trajkovic, Alexandar Milosavljevic, Per Tunestål and Bengt Johansson, *" FPGA Controlled Pneumatic Variable Valve Actuation"*, 2006-01-0041

52. G. Woschni, *"A Universally Applicable Equation for the Instantaneous Heat Transfer Coefficient in the Internal Combustion Engine",* SAE Technical Paper 670931

53. Michael F.J. Brunt, Christopher R. Pond and John Biundo, "*Gasoline Engine Knock Analysis using Cylinder Pressure Data"*, SAE Technical Paper 980896

54. Richard Stone. "*Introduction to Internal Combustion Engines, Second Edition".* Macmillan, 1992

55. C.G.W. Sheppard, S. Tolegano and R. Woolley, "*On the Nature of Autoignition leading to Knock in HCCI Engines"*, SAE Technical Paper 2002-01-2831

56. C.S. Draper, *"Pressure waves accompanying detonation in engines",* J. Aeronaut. Sci., 5(6), pp. 219–226.

57. Donald F. Young, Bruce R. Munson and Theodore H. Okiishi, **"***A Brief Introduction to Fluid Mechanics"*, John Wiley & sons, Inc. 1997

58. R. M. Clements, *"The variation of ionization with air/fuel ratio for a spark ignition engine"*, Journal of Applied Physics, Volume 47(2), 1976

59. Nick Collings, Steve Dinsdale, Derek Eade, *"Knock Detection by Means of the Spark Plug"*, SAE Technical Paper 860635, 1986

60. Yuichi Shimasaki, Masaki Kanehiro, Shigeki Baba, Shigeru Maruyama, Takashi Hisaki, Shigeru Miyata, *"Spark Plug Voltage Analysis for Monitoring Combustion in An Internal Combustion Engine"*, SAE Technical Paper 930461, 1993

61. John Auzins, Hasse Johansson, Jan Nytomt. "*Ion-Gap Sense in Misfire Detection, Knock and Engine Control*", SAE Technical Paper 950004, 1995

62. Jürgen Förster, Achim Günther, Markus Ketterer and Klaus-Jürgen Wald. "*Ion Current Sensing for Spark Ignition Engines",* SAE Technical Paper 1999-01-0204

63. H.F. Calcote, "*Ion production and recombination in flames"*, Eigth (International) Symposium of Combustion, p. 184, 1962.

64. J. A. Green, T. M. Sugden, *"Some observations on the mechanism of ionization in flames containing hydrocarbons"*, Ninth (International) Symposium of Combustion, p. 607, 1963.

65. Raymond Reinmann, *"Theoretical and Experimental Studies of the formation of Ionized Gases in Spark Ignition Engines"*, SAE Technical Paper 980161, 1998

66. Axel Franke, *"Characterization of an Electrical Sensor for Combustion Diagnostics."*, Doctoral Thesis, TFCP-80-SE, Lund Institute of Technology, Lund, Sweden , 2002

67. Raymond Reinmann, *" Theoretical and Experimental Studies of the Formation of Ionized Gases in Spark Ignition Engines"*, Doctoral Thesis, TFCP-37-SE, ISBN 91-628-2985-8, Lund Institute of Technology, Lund, Sweden , 1998

68. Petter Strandh, Magnus Christensen, Johan Bengtsson, Rolf Johansson, Andreas Vressner, Per Tunestål and Bengt Johansson*, "Ion Current Sensing for HCCI Combustion Feedback"*, SAE Technical Paper 2003-01-3216

69. Petter Strandh, Johan Bengtsson, Rolf Johansson, Per Tunestål and Bengt Johansson, *"Cycle-to-cycle Control of a Dual-Fuel HCCI Engine"*, SAE Technical Paper 2004-01-0941

70. Hans Aulin, Pascal Bentioulis, Per Tunestål, Jari Hyvönen, Bengt Johansson *"Improving Ion Current Feedback for HCCI Engine Control",* SAE Technical Paper 2007-01-4053

71. Irvin Glassman, *"Combustion"*, Third Edition, Academic Press 1996.

72. Stephen R. Turns, *"An Introduction to Combustion – Concepts and Applications"*, Second Edition, International Editions 2000

73. Håkan Persson, Anders Hultqvist, Bengt Johansson and Alfredo Remón, *"Investigation of the Early Flame Development in Spark Assisted HCCI Combustion using High Speed Chemiluminescence Imaging"*, SAE Technical Paper 2007-01-0212

74. Habib N. Najm, Phillip H. Paul, Charles J. Mueller, and Peter S. Wyckoff, *"On the Adequacy Certain Experimental Observables as Measurements of Flame Burning Rate"* , Combustion and Flame, 113:312-332, 1998

75. Jimmy Olofsson, *"Laser Diagnostics Techniques with Ultra-High Repetition Rate for Studies in Combustion Environments",* Doctoral Thesis, ISRN LUTFD2/TFCP--07/117-SE, ISBN 978-91-628-7107-9, Lund University, Lund, Sweden, 2007

76. Hans Seyfried, *"Laser Spectroscopic Techniques for Combustion Diagnostics Directed Towards Industrial Applications"*, Doctoral Thesis, ISRN LUTFD2/TFCP--123-SE, ISBN 978-91-628-7310-3, Lund University, Lund, Sweden, 2007

77. J.A. Eng, *"Characterization of Pressure Waves in HCCI Combustion"*, SAE Technical Paper 2002-01-2859

78. Morgan M. Andreae, Wai K. Cheng, Thomas Kenney and Jialin Yang, *"On Hcci Engine Knock"*, SAE Technical Paper 2007-01-1858

79. Yiqun Huang and Darius Mehta, *"Investigation of an In-Cylinder Ion Sensing Assisted HCCI Control Strategy"*, SAE Technical Paper 2005-01-0068

80. A. Manivannan, P. Tamil Porai, S. Chandrasekaran and R. Ramprabhu, *"Lean Burn Natural Gas Spark Ignition Engine – An Overview",* SAE Technical Paper 2003-01-0638

81. Patrik Einewall, *"Study and Development of Techniques to Improve Engine Stability and Reduce Emissions from Natural Gas Engines"*, Doctoral Thesis, ISRN LUTMDN/TMHP-2003/1017-SE, ISBN 91-628-5885-8, Lund Institute of Technology, Lund, Sweden, 2003

82. Richard R. Steeper and Eric J. Stevens, *"Characterization of Combustion, Piston Temperatures, Fuel Sprays, and Fuel-Air Mixing in a DISI Optical Engine"*, SAE Technical Paper 2000-01-2900

83. Ulf Aronsson, Clement Chartier, Uwe Horn, Öivind Andersson, Bengt Johansson and Rolf Egnell, *"Heat Release Comparison between Optical and Ordinary HSDI Diesel Engines"*, SAE Technical Paper 08PFL-157, to be published and presented at the 2008 SAE World Congress.

84. Anders Hultqvist, Magnus Christensen, Bengt Johansson, Axel Franke, Mattias Richter and Marcus Aldén, *"A Study of the Homogeneous Charge Compression Ignition Process by Chemiluminescene Imaging"*, SAE Technical Paper 1999-01-3680

85. Anders Hultqvist, Bengt Johansson,Magnus Christensen, Mattias Richter, Johan Engström and Axel Franke *"Near Wall Combustion in a Homogeneous Charge Compression Ignition (HCCI) Engine"*, Proceedings from the 4th International Symposium on Internal Combustion Diagnostics, pp 83-90, Baden-Baden, 18-19 May, 2000.

86. Håkan Persson, Leif Hildingsson, Anders Hultqvist, Bengt Johansson and Jochen Ruebel, *"Investigation of the Boundary Layer Behaviour in HCCI Combustion using Chemiluminescence Imaging"*, SAE Technical Paper 2005-01-3729

87. Magnus Sjöberg, John E. Dec, Aristotelis Babajimopoulos and Dennis Assanis, *"Comparing Enhanced Natural Thermal Stratification Against Retarded Combustion Phasing for Smoothing of HCCI Heat-Release Rates"*, SAE Technical Paper 2004-01-2994

88. Magnus Sjöberg, John E. Dec and Nicholas P. Cernansky *"Potential of Thermal Stratification and Combustion Retard for Reducing Pressure Rise Rates in HCCI Engines, Based on Multi-Zone Modeling and Experiments"*, SAE Technical Paper 2004-01-2994

89. Magnus Sjöberg, John E. Dec, *"Effects of Engine Speed, Fuel Rating, and Combustion Phasing on the Thermal Stratification Required to Limit HCCI Knocking Intensity"*, SAE Technical Paper 2005-01-2125

90. John E. Dec, Wontae Hwang and Magnus Sjöberg, *"An Investigation of Thermal Stratification in HCCI Engines Using Chemiluminescence Imaging"*, SAE Technical Paper 2006-01-1518

91. Ramanan Sankaran, Hong G. Im, Evatt R. Hawkes and Jacqueline H. Chen, Sankaran, R., Im, H. G., Hawkes, E. R., Chen, J. H., *"The Effect of Non-Uniform Temperature Distribution on the Ignition of a Lean Homogeneous Hydrogen-Air Mixture "*, 30th Symposium (International) of Combustion, 2004.

92. John E. Dec and Magnus Sjöberg, *"Isolating the Effects of Fuel Chemistry on Combustion Phasing in an HCCI Engine and the Potential of Fuel Stratification for Ignition Control"*, SAE Technical Paper 2004-01-0557

93. Magnus Sjöberg and John E. Dec, *"Smoothing HCCI Heat-Release Rates using Partial Fuel Stratification with Two-Stage Ignition Fuels"*, SAE Technical Paper 2006-01-0629

9 Summary of Papers

Paper 1.

Pressure Oscillations During Rapid HCCI Combustion
SAE Technical Paper 2003-01-3217
By Andreas Vressner, Andreas Lundin, Magnus Christensen, Per Tunestål & Bengt Johansson

Presented by Andreas Vressner at the SAE Powertrain & Fluid Systems Conference & Exhibition, Pittsburgh, PA ,USA, October 2003
Approved for SAE Transactions in 2003

In this paper the work was focused on studying the in-cylinder pressure fluctuations caused by rapid HCCI combustion and to determine what they consist of. Inhomogeneous auto ignition sets up pressure waves traversing the combustion chamber. These pressure waves induce high gas velocities which cause increased heat transfer to the walls or in worst case engine damage. Eight pressure transducers where used in the same cylinder to measure these pressure fluctuations simultaneously. It was found that pressure experienced during rapid HCCI combustion is inhomogeneous. The pressure waves were found to be similar of those experienced with knock in SI engines and showed good accordance to vibration mode shapes and frequencies suggested by acoustic vibration theory.

The author ran the experiments and evaluated the data together with Andreas Lundin. The author wrote the paper.

Paper 2.

Ion Current Sensing for HCCI Combustion Feedback
SAE Technical Paper 2003-01-3216
By Petter Strandh, Magnus Christensen, Johan Bengtsson, Rolf Johansson, Andreas Vressner, Per Tunestål & Bengt Johansson

Presented by Petter Strandh at the SAE Powertrain & Fluid Systems Conference & Exhibition, Pittsburgh, PA, USA, October 2003

This paper deals with ion current measurements in an HCCI engine with the purpose of using a spark plug as sensor for combustion feedback controls. It was found that only one ion current peak appears in HCCI combustion compared to two peaks in an SI engine which probably is due to the low temperature nature of HCCI combustion. Further it was found that the ion current signal level is strongly dependant on engine load and combustion phasing. This means that ion current can be used for feedback control purposes at higher loads with sufficiently high accuracy of combustion phasing and knock estimations. Due to the steep nature of the leading edge of the ion current trace it was found that the ion current is a local measurement inside the combustion chamber compared to in-cylinder pressure measurements which are of a more global type. Lastly 2 different spark plugs where investigated. One standard production type of spark plug and one modified with the side electrode removed. It

was found that the modified one gave better ion current signal levels and more accurately predicted the HCCI combustion phasing.

The author assisted in the experiments, evaluation of data and writing the paper.

Paper 3.

Multiple Point Ion Current Diagnostics in an HCCI Engine
SAE Technical Paper 2004-01-0934
By Andreas Vressner, Petter Strandh, Anders Hultqvist, Per Tunestål & Bengt Johansson

Presented by Andreas Vressner at the SAE World Congress, Detroit, MI, USA, March 2004
Approved for SAE Transactions in 2004

This paper is a continuation of the previous ion current study performed by Petter Strandh in paper 2, where it was found that the ion current in HCCI combustion seemed to be a local phenomenon compared to in-cylinder pressure which is a more global phenomenon. Therefore the setup from the pressure wave experiments was used that enabled seven spark plugs to be mounted in the same combustion chamber. Ion current was measured simultaneously at all seven locations and the appearance of the signal was compared to the pressure history. It was found that there were differences in both ion current signal strength and timing depending on measuring location. This is of great importance for combustion feedback and closed loop combustion control, which means that there seem to be a certain location in the combustion chamber where it is optimal to place ion current sensors.

The author carried out all experiments, evaluation of data and wrote the paper.

Paper 4.
Fuel Effects on Ion Current in an HCCI Engine
SAE Technical Paper 2005-01-2093
By Andreas Vressner, Anders Hultqvist, Per Tunestål, Bengt Johansson &
Ryo Hasegawa

Presented by Andreas Vressner at the SAE Brasil Fuels & Lubricants Meeting, Rio De Janeiro, Brazil, May 2005
Approved for SAE Transactions in 2005

In earlier studies by the author it has been found that the ion current signal strength in HCCI engines is highly dependant on load. Different fuels will provoke ion current differently, meaning that there could be a more appropriate fuel for ion current measurements in HCCI engines, thus enabling closed loop combustion control of HCCI even at low load. In this paper seven fuels were tested in the Scania D12 HCCI engine with the possibility to measure ion current at seven locations simultaneously. A correlation between the appearance of ion current at different locations and the fact that combustion starts at the walls and propagates towards the centre of the combustion chamber in this particular engine was of interest. Fuels with higher octane number seemed to provoke ion current more easily. However it was found that the different fuels provoked ion current differently also depending on ion current measuring position and the presence of EGR. It was also found that fuels provoking low temperature

reactions were not appropriate fuels for ion current measurements since the signal did only appear until close to stoichiometric conditions.

The author ran the experiments, evaluated all data and wrote the paper.

Paper 5.
Optical Diagnostics of Laser-Induced and Spark Plug-Assisted HCCI Combustion
SAE Technical Paper 2005-01-0129
By Martin Weinrotter, Ernst Wintner, Kurt Iskra and Theo Neger, Jimmy Olofsson, Hans Seyfried, Marcus Aldén, Max Lackner, Franz Winter, Andreas Vressner, Anders Hultqvist & Bengt Johansson

Presented by Martin Weinrotter at the SAE World Congress, Detroit, MI, USA, April 2005
Approved for SAE Transactions in 2005

The load range of HCCI combustion is limited by high combustion rates in one end and misfire in the other end. In the latter case the load range can be extended when the in-cylinder temperature is too low to maintain a reasonable combustion phasing with the use of spark ignition or laser plasma ignition. In these two cases a flame front develops from the ignition source which causes a temperature increase in the yet unburned gas which eventually ignites at several locations simultaneously, i.e. HCCI combustion starts. Advancement in combustion phasing can thus be achieved with resulting improved efficiency and decreased cycle to cycle variations. In this study spark plug assisted HCCI combustion was compared to laser assisted HCCI combustion as well as traditional HCCI combustion. Optical diagnostics methods as schlieren, chemiluminescence imaging and formaldehyde visualization were used in order to investigate these phenomena. However it was found that the effect of both assistance methods were suppressed by lean mixtures used.

The author was responsible for running the engine and conducting heat release analysis. The laser ignition, schlieren photography and chemiluminescence imaging were conducted by Martin Weinrotter and Kurt Iskra. Jimmy Olofsson and Hans Seyfried carried out the PLIF experiments. The author assisted in writing the paper.

Paper 6.
Visualization of Laser Assisted HCCI Combustion With
Natural Gas as Fuel
Fisita/JSAE Technical Paper F2006P206
By Andreas Vressner, Anders Hultqvist, Bengt Johansson, Martin Weinrotter, Ernst Wintner, Kurt Iskra & Theo Neger.

Presented by Andreas Vressner at the FISITA World Automotive Congress, Yokohama, Japan, October 2006

In this paper laser ignition was applied on HCCI combustion during operating conditions that normally would lead to partial or full misfire. It was found that flame propagation was present from the location of the laser plasma in the cylinder. As the global temperature and pressure were increased due to the propagating flame, the auto ignition timing was advanced compared to unassisted HCCI combustion. Fraction of Initial Slow Heat Release was used as a tool to

find how much of the heat release which was due to flame propagation and how much was due to auto ignition. By chemiluminescence imaging the different types of combustion modes were studied. The lean limit for achieving flame propagation was found to be around λ 2.6. Combustion phasing in terms of CA50 could be advanced up to 8 CAD by the use of laser assistance. It was also found that the laser ignition timing was crucial for achieving the desired effect on HCCI combustion.

The author was responsible for running the engine and conducting heat release analysis, Martin Weinrotter and Kurt Iskra were responsible for the ignition laser and chemiluminescence imaging. The author wrote the paper with the help from the co-authors.

Paper 7.
Study on Combustion Chamber Geometry Effects in an HCCI Engine using High-Speed Cycle-Resolved Chemiluminescence Imaging
SAE Technical Paper 2007-01-0217
By Andreas Vressner, Anders Hultqvist & Bengt Johansson

Presented by Andreas Vressner at the SAE World Congress, Detroit, MI, USA, April 2007
Reprinted in this thesis with permission from SAE International, © 2007

Two combustion chamber geometries were studied in this paper, one with a Square Bowl and one Disc shaped combustion chamber. The flat Disc combustion chamber is normally used in the optical engine setup. By using the Square Bowl in piston chamber the rate of heat release and pressure rise rate could be decreased by half due to a longer and slower combustion process. This means that the maximum load, limit by too fast combustion could be increased. The reason for the slower combustion process was found in more stratified combustion behaviour probably due to temperature or fuel inhomogeneities, meaning that a hotter or richer zones ignites first and propagates into the colder or leaner ones. This takes longer time compared to a perfectly mixed charge where all ignites at once. Chemiluminescence imaging was used to study the combustion processes. In the bowl case the combustion started in the corners and propagated through the bowl and in the early stages of the expansion stroke the charge in the top land volume was also consumed.

The author was responsible for all of the work in this paper, including experiments, evaluation of data and writing the paper.

Paper 8.
High-Speed PLIF Imaging for Investigation of Turbulence Effects on Heat Release Rates in HCCI Combustion
SAE Technical Paper 2007-01-0213
By Hans Seyfried, Jimmy Olofsson, Johan Sjöholm, Mattias Richter, Marcus Aldén, Andreas Vressner, Anders Hultqvist & Bengt Johansson

Presented by Johan Sjöholm at the SAE World Congress, Detroit, MI, USA, April 2007
Reprinted in this thesis with permission from SAE International, © 2007

The work with the combustion chamber geometries continues in this paper, but this time fuel tracer LIF was used instead to study the combustion process. As tracer acetone was used. Due to limited optical access only the combustion inside the bowl was studied from beneath. The

LIF images showed a fairly homogeneous fuel charge but the combustion process itself was shown to be highly stratified and wrinkled. This suggests that the charge is stratified mostly in temperature however fuel inhomogeneities might still occur.

The authors work contribution in this paper was limited to engine experiments, heat release analysis and assisting in writing the paper. Hans Seyfried, Jimmy Olofsson and Johan Sjöholm were responsible for the LIF experiments and evaluation of that data.

Paper 9.
Effect of Turbulence on HCCI Combustion
SAE Technical Paper 2007-01-0183
By Rixin Yu, Xue Song Bai, Andreas Vressner, Anders Hultqvist, Bengt Johansson, Hans Seyfried, Jimmy Olofsson, Johan Sjöholm, Mattias Richter & Marcus Aldén,

Presented by Andreas Vressner at the SAE World Congress, Detroit, MI, USA, April 2007

The paper is first and foremost a simulation study where Large Eddy Simulations have been used to study the slower combustion process while using a deep square bowl in piston compared to a Disc shaped combustion chamber. It was found that large temperature stratifications causing the slower rate of heat release in the Square Bowl were formed during the early stages of the intake stroke. The hotter gases were found inside the bowl acting like a recirculation zone and heat transfer from the hot bowl walls played a large role. These temperature stratifications survive the compression stroke and results in start of combustion inside the bowl which propagates out into the squish volume. Due to theses phenomena the longer combustion duration while using the bowl could be explained and compared to the results found in Paper 7 and 8.

The author was responsible for the engine experiments and providing the chemiluminescence results from paper 7. The LES modeling was conducted by Rixin Yu and Xue Song Bai. They also wrote the paper.

Paper 10.
Combustion Chamber Geometry Effects on the Performance of an Ethanol Fueled HCCI Engine
SAE Technical Paper Draft 08SFL-0290
By Andreas Vressner, Rolf Egnell & Bengt Johansson
To be published at the SAE 2008 International Powertrains, Fuels and Lubricants Congress in Shanghai, China

The last paper of four dealing with combustion chamber geometry effects on HCCI combustion rate. The aim of this paper was to compare a disc shaped combustion chamber with a deep square bowl in piston. The experiments were performed in the Scania D12 HCCI Engine in metal setup which is without optics, the main reason being to compare the combustion chambers during more realistic conditions than the optical engine can provide. The quartz glass parts in the optical engine changes the temperature distribution in the cylinder drastically which also affects the HCCI combustion process. The engine was run at different loads and the combustion phasing was tuned to find the maximum efficiency for each load and combustion chamber geometry. It was found that quenching was a major problem in the metal engine with the square bowl combustion chamber decreasing the

efficiency especially at low loads. Increasing the squish distance results in less local heat losses and the efficiency is improved. For higher loads around 4.5 bar $IMEP_{net}$ the efficiency of the square bowl was equal to the disc.

The author was responsible for all of the work in this paper, including experiments, evaluation of data and writing the paper.